Unsteady Disturbance Structures

in Axial Flow Compressor Stall Inception

by

Han G. Park

B.S. Mechanical Engineering, University of California at Berkeley

(1992)

SUBMITTED IN PARTIAL FULFILLMENT OF THE

REQUIREMENTS FOR THE DEGREE OF

Master of Science in Mechanical Engineering

at the

Massachusetts Institute of Technology

May 1994

Signature of Author_____

Department of Mechanical Engineering
May 18, 1994

Certified by_____

Edward M. Greitzer, Thesis Advisor
H.N. Slater Professor of Aeronautics and Astronautics

Certified by_____

Choon S. Tan, Thesis Advisor
Principal Research Engineer

Certified by_____

Douglas P. Hart, Reader
Professor of Mechanical Engineering

Accepted by_____

Professor Ain. A. Sonin, Chairman
Departmental Graduate Committee

Unsteady Disturbance Structures in Axial Flow Compressor Stall Inception

by

Han G. Park

Submitted to the Department of Mechanical Engineering
on May 18, 1994 in partial fulfillment of the
requirements for the Degree of Master of Science in Mechanical Engineering

ABSTRACT

An experimental study is carried out of the unsteady disturbance structures found in multi-stage axial compressor stall inception. It is shown for the first time that a "precursor" or a warning signal can be associated with short wavelength disturbances (spikes). The precursor can be identified using a detection method based on cross-correlation.

Examples of precursors associated with short wavelength disturbances are shown for both low and high speed compressors. A precursor can be detected on the low speed E^3 compressor up to 350 rotor revolutions prior to stall. Precursors are also detected on the high speed Viper compressor up to 350 and 100 rotor revolutions prior to stall for 81% and 83% of corrected speed, respectively. The precursor is found to be caused by the formation and decay of spikes as the compressor nears stall. For conditions even a small distance away from the stall onset point, the spikes rarely travel beyond 1/2 rotor revolution before decaying. As the compressor approaches closer to stall, the spikes form and decay more frequently, increasing the signal level of the precursor.

To study the operating conditions under which spike type disturbances may develop, experiments were carried out on the MIT Three Stage compressor. While operating under active control (under which long wavelength disturbances are suppressed), no evidence of spike type disturbances was found in the compressor. Instead, an acoustic disturbance is found to grow when the compressor operates on the unstable region of the map.

Finally, experiments are described on stall inception with and without a rotating distortion carried out at the General Electric Low Speed Research Compressor facility. It was observed that compressors which exhibit modal wave disturbance structure in the natural stall inception process can display a peak loss of stability in response to a rotating distortion near 70% of rotor speed. This response is thought to be associated with an excitation of a spike mode.

Thesis Supervisors: Edward M. Greitzer
H. N. Slater Professor of Aeronautics and Astronautics

Choon S. Tan
Principal Research Engineer

Acknowledgments

The author would like to express gratitude to everyone involved in this research. The author especially appreciates the contributions from:

Professor Greitzer for his guidance and support which was invaluable in the completion of this thesis.

Dr. C.S. Tan for providing not only research but personal guidance and support as well.

Dr. Shin for his assistance in setting up instrumentation at GE LSRC and for his personal guidance.

Dr. Wisler for his support which made this work possible.

Dr. Day for his extremely helpful suggestions and guidance without which this work could not have been completed.

Dr. Longley and Professor Cumpsty for their insightful discussions.

Professor Paduano and Joel Haynes for their assistance in bring the MIT Three Stage compressor back to life.

Harold Weigl for his help in conducting experiments on the MIT Three Stage compressor.

Officemates Diego Diaz, Dave Tew, Arif Khalid, Roland Berndt, and all the members of the GTL staff for their kind support and friendship.

Finally, I would like to thank my parents and sister for their patience and infinite support.

This research was supported by the Air Force Office of Scientific Research, Monitor Maj. Daniel Fant, Grant #F49620-93-1-0015, and General Electric Aircraft Engine Corp.

TABLE OF CONTENTS

LIST OF FIGURES

3.8 Cross-correlations of measurements in Figure 3.7 for sequential time intervals up to stall point (t = -0).

3.9 Surface plot of the cross-correlations in Figure 3.8.

3.10 Casing static pressure traces at 1st stage rotor inlet of the Viper compressor at 83% of corrected speed.

3.11 Cross-correlations of measurements in Figure 3.10 for sequential time intervals up to stall point (t = -0).

3.12 Surface plot of the cross-correlations in Figure 3.11.

3.13 Casing static pressure traces at 1st stage rotor inlet of the Viper compressor at 98% of corrected speed.

3.14 Cross-correlations of measurements in Figure 3.13 for sequential time intervals up to stall point (t = -0).

3.15 Illustration of frequent formation and decay of spikes close to stall.

3.16 Illustration of formation and decay of spikes far from stall.

3.17 Illustration of circumferential size and pressure perturbation amplitude of a spike.

3.18 A spike growing larger in amplitude than allowable for compressor stability and growing into a stall cell.

3.19 Casing static pressure traces showing large amplitude spikes propagating around the annulus of a mismatched compressor.

3.20 Example of clarity of the cross-correlation peak associated with a spike precursor for an array of casing static pressure transducers at 1st stage rotor exit.

3.21 Example of clarity of the cross-correlation peak associated with a spike precursor for an array of hot-wire anemometers placed near the blade tip at 1st stage rotor exit.

LIST OF TABLES

NOMENCLATURE

A_m	m'th discrete Fourier transform coefficient (Section 2.2)
B_k	k'th discrete Fourier transform coefficient (Section 2.3.2)
C_k	k'th discrete spatial Fourier transform coeffient (Section 2.2)
Cx	axial velocity
Hz	cycles per second
i	imaginary number
f_{rotor}	rotor frequency
f_s	sampling frequency
j	sampling point (Section 2.3.2)
k	k'th aliasing peak (Section 2.3.3)
M	number of sampling points
N	number of sensors
P_s	static pressure
PSD	power spectral density
P_t	total pressure
s	speed normalized by rotor speed
SHFC	spatial Fourier harmonic coefficients
t	time
U_{tip}	velocity of rotor at tip
Z_j	average cross-correlation function (Section 2.3.2)
z_{nj}	cross-correlation function (Section 2.3.2)

Greek Symbols

Ψ_{S-S}	static to static pressure rise
Ψ_{T-S}	total to static pressure rise
$\frac{\partial \Psi_{T-S}}{\partial \Phi}$	total to static pressure rise slope
Φ	flow coefficient (Cx/U_{tip})
φ	velocity perturbation
θ	circumferential position
ρ	ambient density
τ_d	time scale associated with disturbance duration (Section 2.3.3)
τ_p	time scale associated with disturbance periodicity (Section 2.3.3)

Subscripts

k	k'th spatial harmonic
m	m'th harmonic

CHAPTER ONE

INTRODUCTION

1.1 Introduction

If one reduces the mass flow rate through a multi-stage axial compressor while holding the rotational speed constant, a condition is reached where the compressor experiences a sudden drop in pressure rise, mass flow rate, and efficiency. This drop in performance is generically associated with the term "stall" and is caused by an instability of the compressor flowfield.

In a multi-stage axial flow compressor, there are two types of instabilities, surge and rotating stall. Surge is characterized by large amplitude mass flow oscillations of the entire compression system (Figure 1.1). Rotating stall is characterized by region(s) of low or reversed through-flow velocity fluid (stall cell) which rotate around the compressor annulus at 20% to 50% of the rotor speed. In rotating stall, the overall compression system operating point remains fixed, though the mass flow rate, pressure rise, and efficiency are often substantially below the pre-stall values. There is still no truly predictive capability for stall onset even after many years of study, and stall phenomena are topics of continued interest.

In recent years, the focus of compressor stall research has shifted from compressors operating with an instability (fully developed rotating stall) to compressors in the process of developing an instability (stall inception). This shift has occurred because of recent advances in identifying, modeling, and controlling the unsteady flow disturbance structures which can cause

compressor instability. In particular, it has become possible to extend the operating range of compressors to lower mass flow rates through feedback control suppression of the unsteady disturbance structures which lead to compressor instability. Active control has the potential for higher compressor pressure rise, efficiency, and safety margin.

As part of an overall goal to improve compressor performance through management of fluid dynamics of compressor stall, this thesis presents several experiments conducted to better understand the characteristics of the unsteady disturbance structures observed during stall inception.

1.2 Review of Compressor Stall

1.2.1 Phases of Compressor Stall

The events of compressor stall can be divided into three distinct phases: stall inception, stall, and post-stall. Stall inception phase is defined here as the behavior of the flow in the compressor just prior to the sudden drop in pressure rise and mass flow rate. On a compressor map, stall inception is observed as the unsteady flow in the compressor from operating point A to point B in Figure 1.2. The next phase is stall which is the transition from operating point B to point C in Figure 1.2. During stall, the compressor experiences a sudden drop in pressure rise and mass flow rate. The last phase is post-stall which is the behavior after the compressor has experienced a sudden drop in pressure rise and mass flow rate. The phase which this thesis will concentrate on is the first or the stall inception.

1.2.2 Stall Inception

During the stall inception phase, the flow inside the compressor is unsteady but is found to have clearly identifiable structures. Two different disturbance structures have been identified, a long wavelength type (referred to as a modal wave) and a short wavelength type (referred to as a spike), and these are briefly reviewed below.

1.2.2.1 Long Wavelength Disturbances

One disturbance structure observed during stall inception is essentially two-dimensional and has a length-scale of the order of the compressor annulus. This is referred to as the two-dimensional modal wave and is reasonably well described by the Moore-Greitzer theory [10]. The theory predicts that an initially small amplitude rotating wave, which extends axially all the way through the compressor, will smoothly grow into a rotating stall cell (Figure 1.3). Typically, a modal wave will rotate around the annulus at 20% - 50% of rotor speed.

The original model predicted that all modes associated with a modal wave, which have shapes resembling spatial harmonics, become unstable when the total to static pressure rise slope is zero ($\frac{\partial \Psi_{T-S}}{\partial \Phi} = 0$). Since then Hendricks et al. [13] have shown that some description of the unsteady response of the loss should be included; this has the effect that the lower modes become unstable first. The modes which first become unstable thus have wavelengths comparable to the compressor annulus.

The 2-D modal wave was first detected experimentally by McDougall [11] and was subsequently observed by other experimenters (e.g. Longley [12],

Garnier [3]). The modal wave was detected by McDougall by tracking the phase and amplitude of the spatial Fourier harmonic coefficients using a circumferential array of 6 hot-wires. Garnier later refined the technique of tracking of modal waves by computing the power spectral densities (PSD's) of spatial Fourier harmonic coefficients and was able to detect modal waves in both low and high speed compressors.

1.2.2.2 Short Wavelength Disturbances

Short wavelength disturbances, referred to as spikes, have also been found. The spikes are three-dimensional in nature and are not described by the two-dimensional Moore-Greitzer model. No model currently describes the spikes adequately. Spikes were first observed by Day [2] and are characterized by small circumferential extent (only a few blade pitches in width) and a relatively high propagation rate, typically 50%-70% of rotor speed (Figure 1.4). Day found the short wavelength disturbance to have high growth rate, as evidenced by its transition to a fully developed rotating stall cell in several (say up to 5) rotor revolutions after its first detection (Figure 1.4).

Flow measurements of short wavelength disturbances were also made by Silkowski [12]. The spikes were identified to have a full three-dimensional structure. In the circumferential direction, the spikes were 2-3 blade pitches wide (Figure 1.5). In the radial direction, the spikes were localized to the tip region and characterized by a flow deficit or a flow blockage (Figure 1.6) with a slight flow increase near the hub.

To assess effect of local stability on the formation of spikes, Silkowski also examined a configuration in which the blades of the last 3 stages (of a 4 stage compressor) were restaggered so that the first stage would encounter stall first. For this configuration, Silkowski found that the spikes were localized to the first stage. The pressure rise characteristics of the matched and mismatched compressor are shown in Figures 1.7 - 1.8. When mismatched compressor was throttled down to the matched compressor stall flow coefficient, spikes began to form inside the first stage, but their growth was inhibited by the stabilizing effect of the latter stages. The whole compressor went into full-span rotating stall when the first stage part-span stall cells grew large enough to destabilize the whole compressor (Figure 1.9).

From the set of experiments in [12], spikes are seen to be a local unsteady disturbances in the first stage which may lead to rotating stall if they grow sufficiently large to influence the stability of the whole compressor. In a matched compressor, all the stages will be near their unstable operating points, and local disturbances in the first stage do not have to grow very much to destabilize the whole compressor.

1.3 Objective

The objective of this thesis is to study experimentally the unsteady disturbance structures and their behavior in multi-stage compressors. In particular, the characteristics of a spike and its development are examined. The following specific questions are examined:

Generic Questions:

1) Is there a "precursor" or a warning signal associated with a short wavelength disturbance (spike)?

2) How do local stage pressure rise characteristics (i.e. local stability) affect the formation of the short wavelength disturbance?

3) What is the link between the observed forced response behavior (rotating distortion) and the unsteady disturbance structures present in the natural stall inception of a compressor?

Rig Specific Question:

4) Does the MIT Three Stage compressor go into rotating stall via spike type disturbances while operating under active control?

1.4 Contributions

Some of the contributions of this research are:

1) Development of a new detection scheme based on cross-correlations for the presence of short wavelength disturbances.

2) Presentation of evidence of precursor associated with a spike type stall inception.

3) Observations of new type of compressor behavior when subjected to rotating distortion.

1.5 Organization of Thesis

The present chapter has outlined the problems of stall in axial flow compressors and the stall inception process and presented the objectives of the thesis. In Chapter 2, a method of detecting a modal wave precursor is

reviewed along with a new method of detecting a spike precursor. In Chapter 3, the method of detecting spikes is used to examine previous spike type stall inception data to look for evidence of a precursor. In Chapter 4, two sets of experiments are conducted on the MIT Three Stage compressor to examine the conditions under which spikes may develop. One set of experiments is carried out to increase the relative pressure rise of the first stage in order that spikes may develop. A second set is to determine if the formation of spikes is the cause of stall for an actively controlled compressor. In Chapter 5, observations are made on the link between forced response behavior (rotating distortion) and stall inception behavior of a compressor. In Chapter 6, the conclusions are presented along with recommendations for future experiments regarding axial flow compressor stall inception.

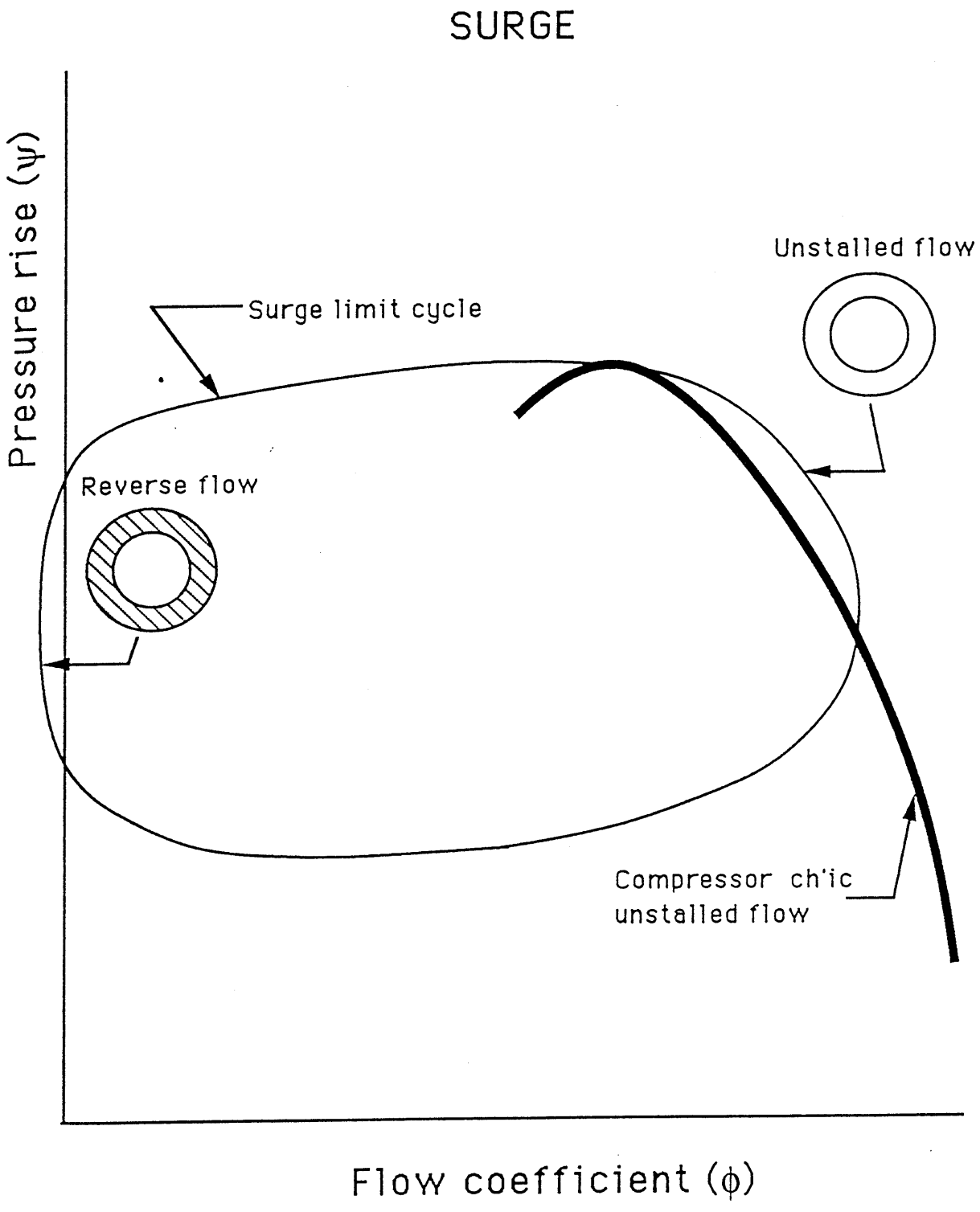

Figure 1.1 Surge limit cycle [3]

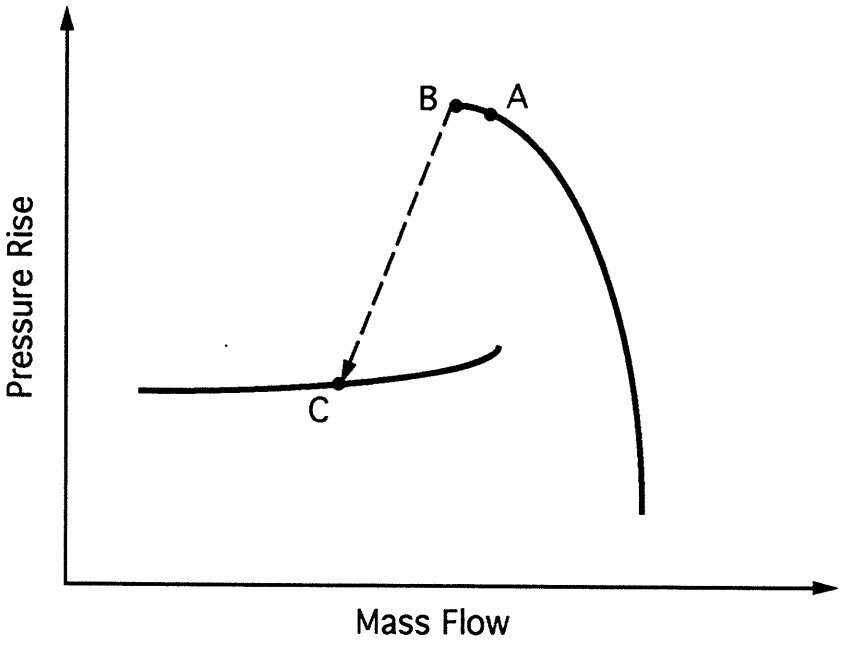

Figure 1.2 Compressor characteristic

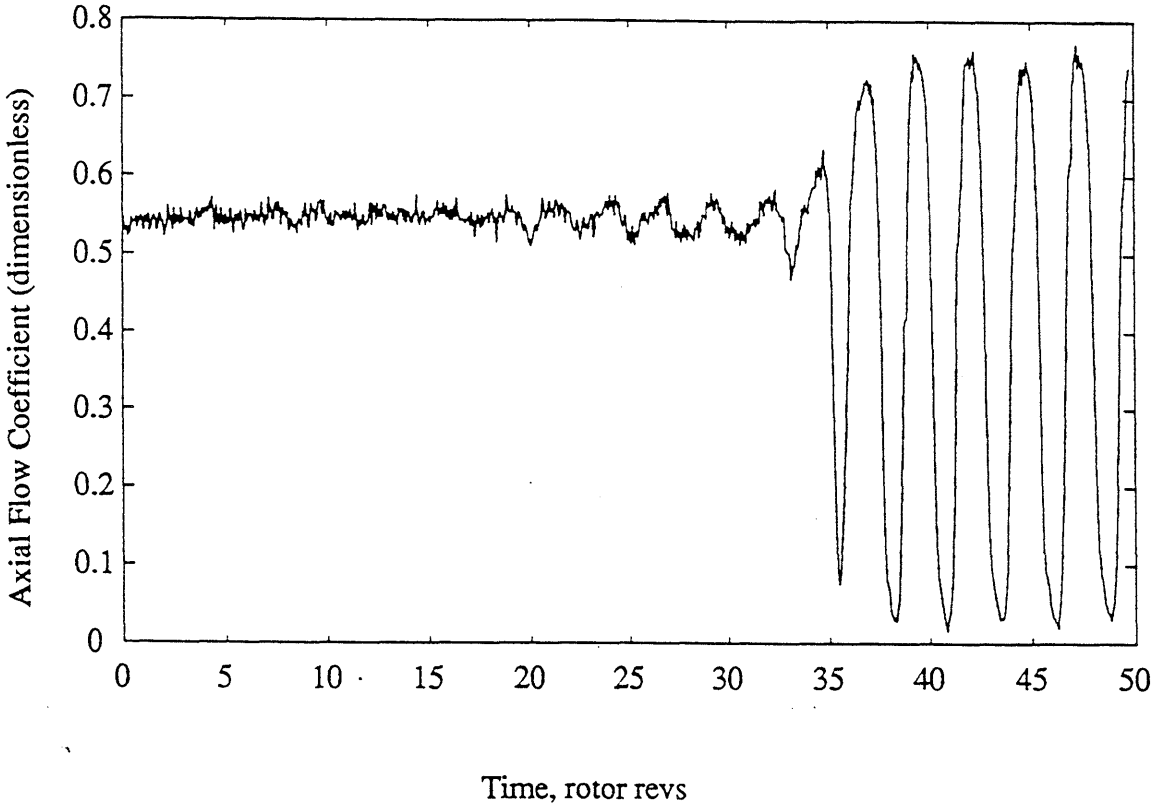

Figure 1.3 Flow transition leading to rotating stall at a single circumferential position. [6]

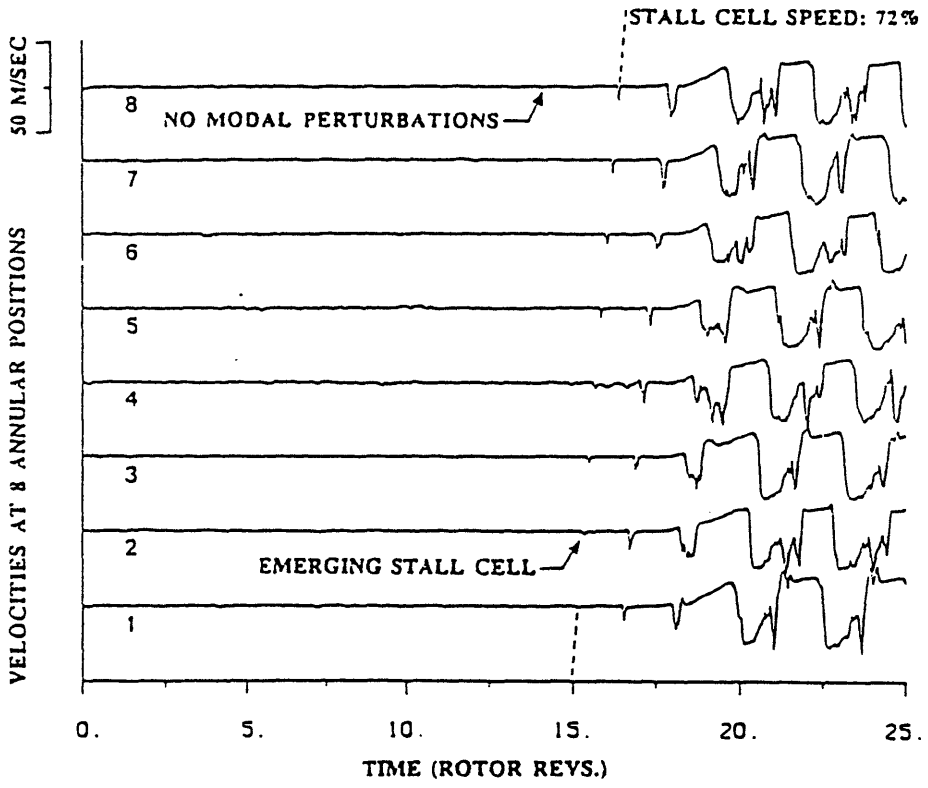

Figure 1.4 Hot-wire velocity traces of a spike type disturbance growing into a stall cell. [2]

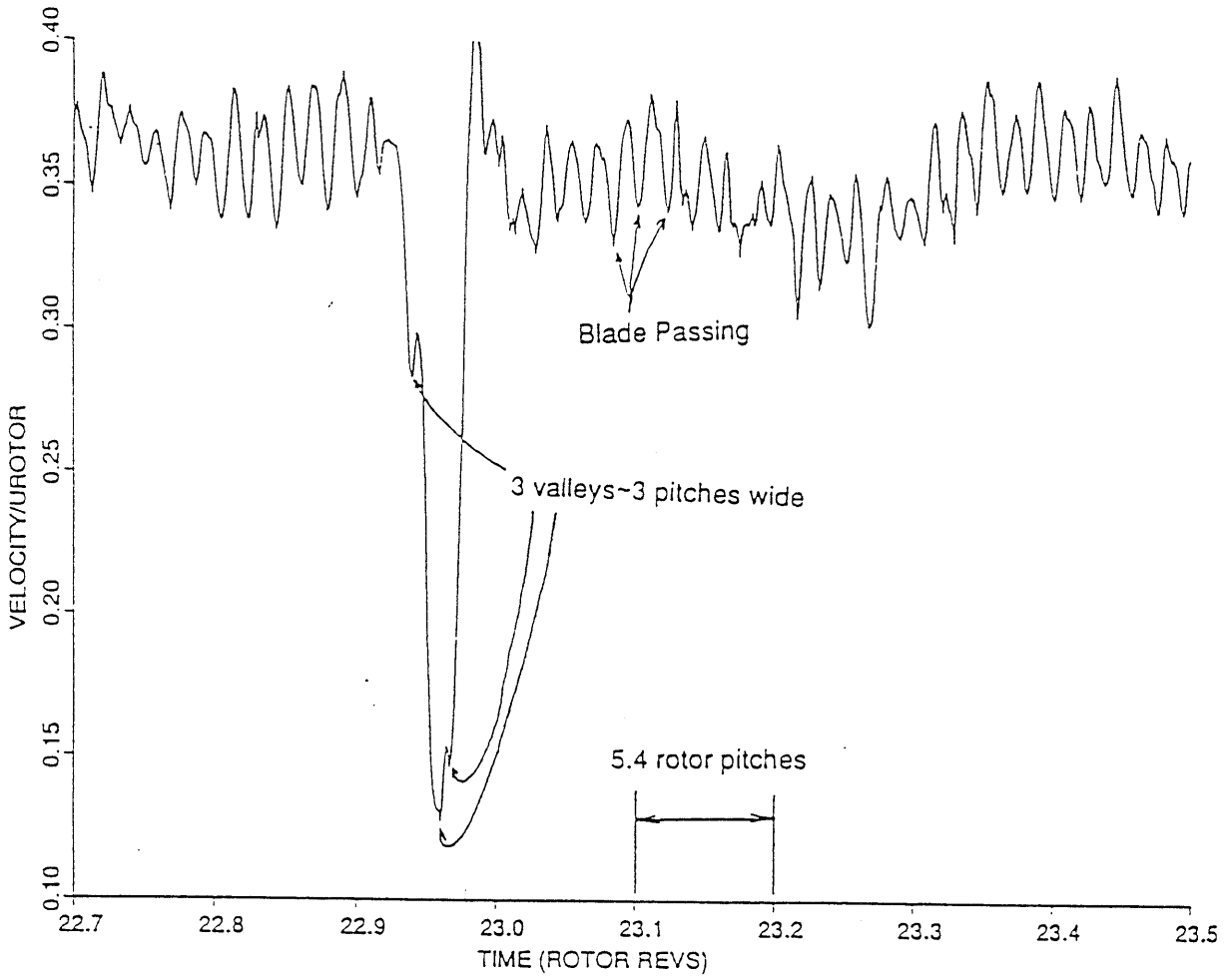

Figure 1.5 Hot-wire velocity trace at 1st stage rotor inlet during stall inception. The spike is roughly 3 blade pitches wide. [12]

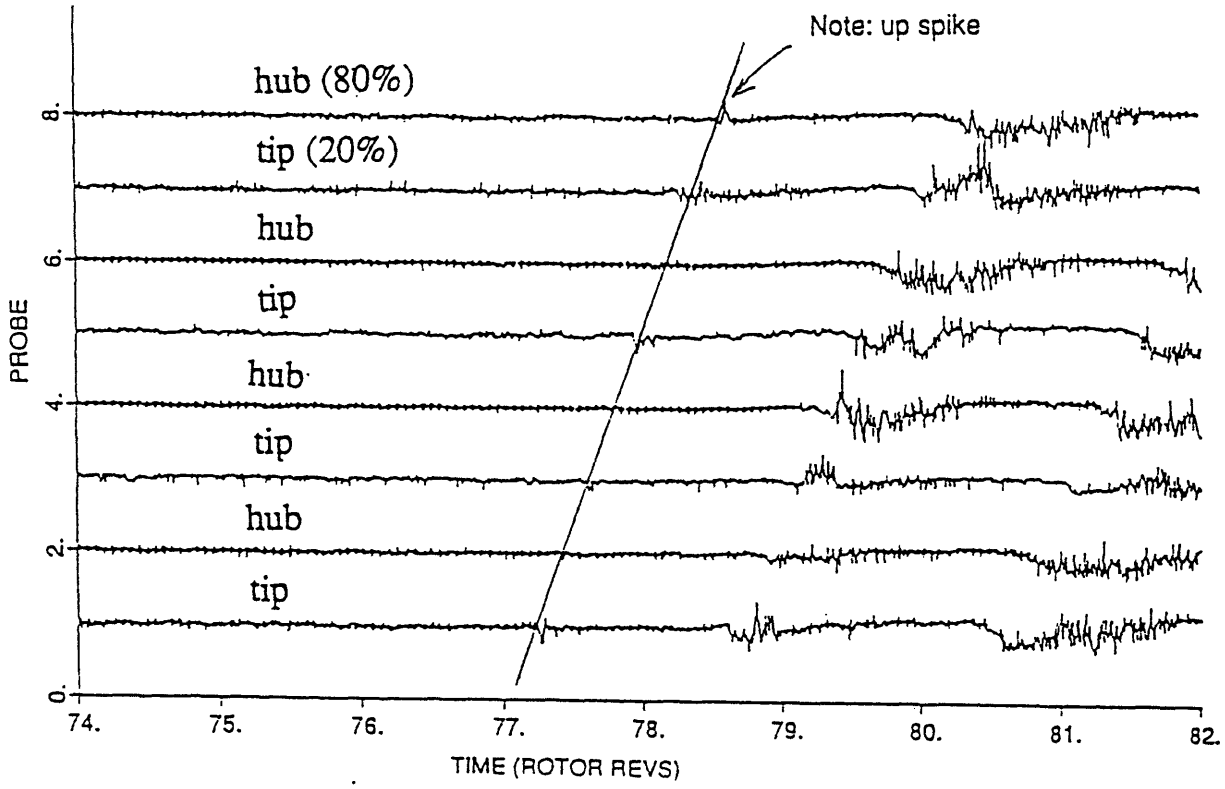

Figure 1.6 Alternating hub-tip hot-wire velocity traces at 1st stage rotor inlet during stall inception. There is a flow velocity deficit at the tip and an increase at the hub. [12]

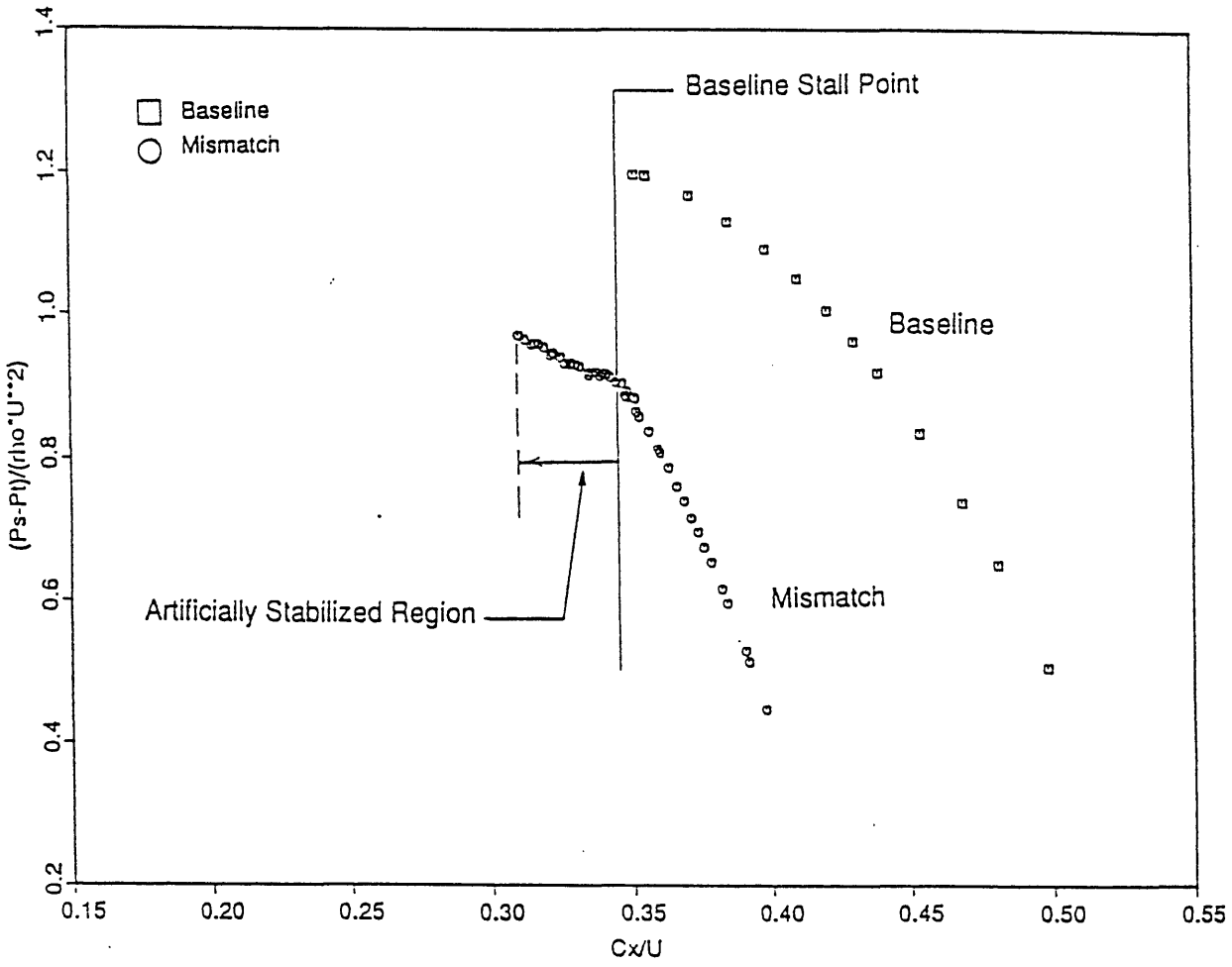

Figure 1.7 Overall total to static pressure rise of matched and mismatched compressor. [12]

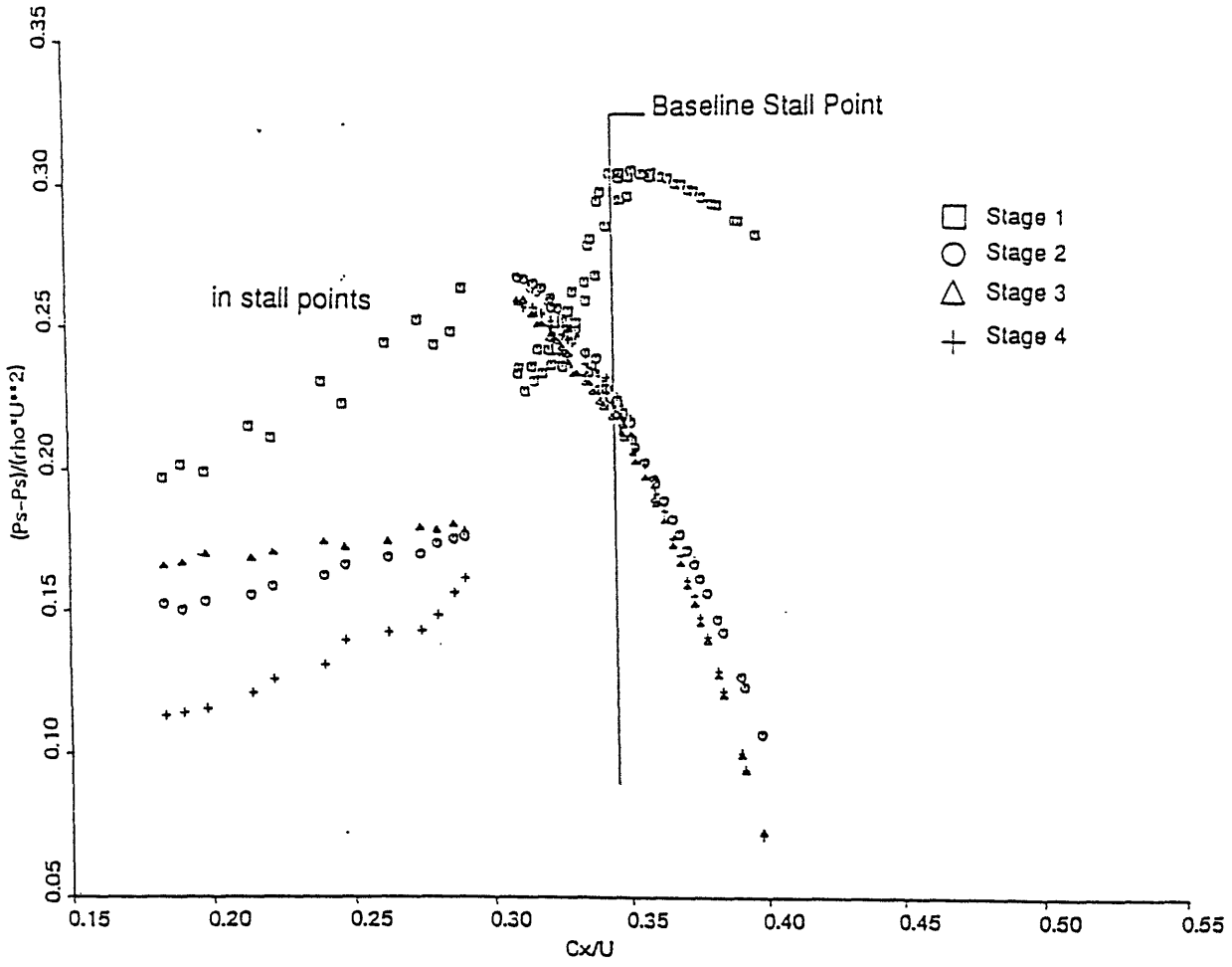

Figure 1.8 Individual static to static pressure rise of the mismatched build. Note the positive pressure rise slope of the 1st stage. [12]

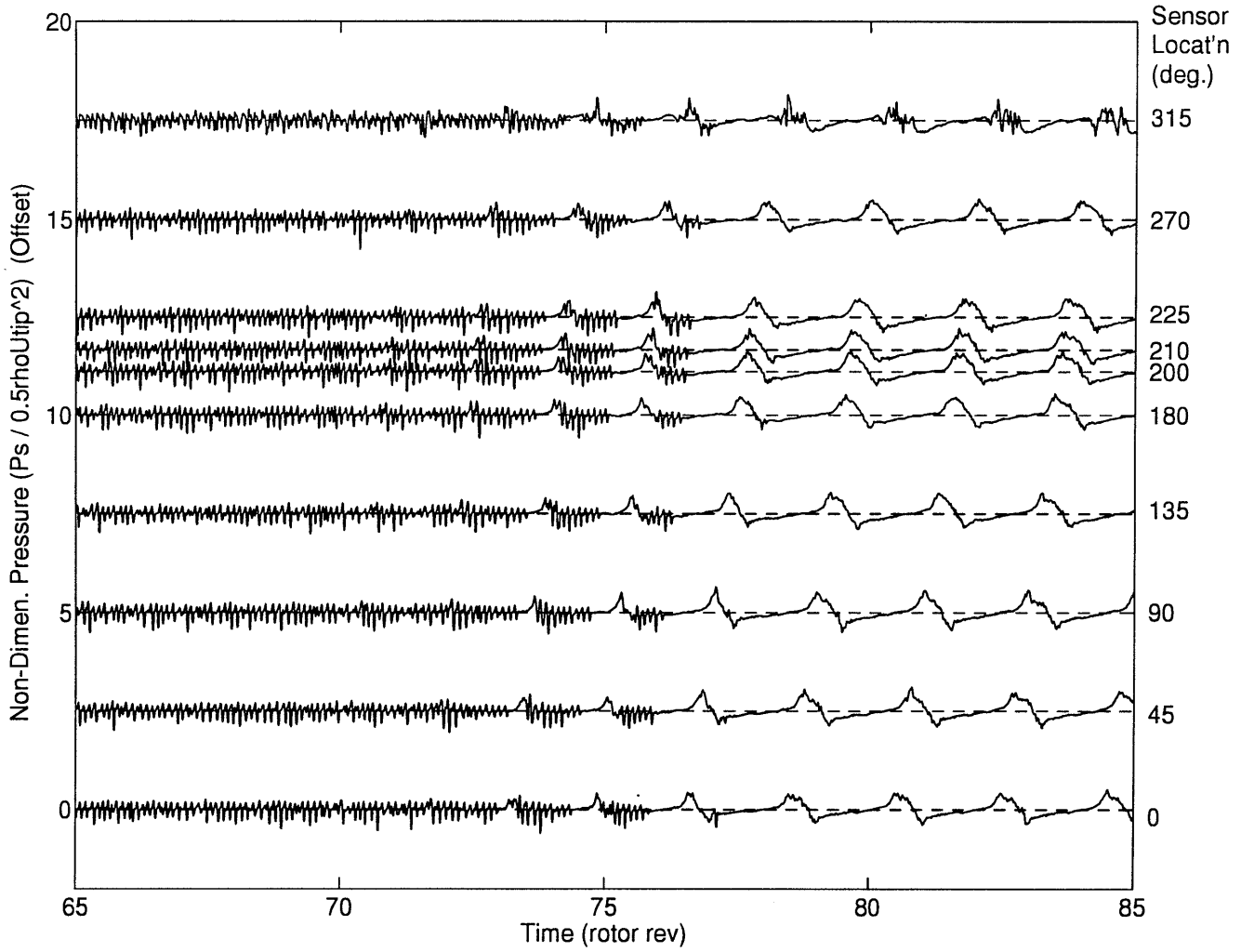

Figure 1.9 Casing static pressure traces of the mismatch build at 1st stage rotor inlet during transition from part-span to full-span rotating stall. Note that 12 part-span stall cells transition into 1 full span stall cell.

CHAPTER TWO

DETECTION OF DISTURBANCE STRUCTURES

2.1 Introduction

In this chapter, two separate data processing techniques are presented. One is better suited for long length scales, and the other is appropriate for short length scales. For detecting long wavelength disturbances, the technique of computing the power spectral density (PSD) of each spatial Fourier harmonic coefficient (SHFC) is used since (as predicted by the Moore-Greitzer model), the disturbance can be spatially decomposed into harmonics. *However, for detecting short wavelength disturbances, the technique of computing the PSDs of SHFC runs into difficulties of spatial aliasing and having to detect a weak signal spread among many spatial harmonics.* A technique using cross-correlations of spatially adjacent sensor signals is thus presented which can avoid these difficulties and facilitate the detection of short wavelength disturbances.

2.2 PSD of Spatial Fourier Harmonic Coefficients

A proven method of detecting long wavelength disturbances is the computation of the power spectral density (PSD) of the spatial Fourier harmonic coefficients (SFHC). It is attractive because the long wavelength disturbance can be decomposed into spatial harmonics as described by the Moore-Greitzer linear model (i.e. modal waves). Including an acoustic type (axisymmetric) disturbance, the velocity (or pressure) is of the form:

$$\tilde{\varphi}(t,\theta) = \sum_{k=-\infty}^{\infty} C_k(t) e^{ik\theta} \qquad (2.1)$$

For N equally spaced sensors around the annulus, the coefficients $C_k(t)$ can be computed at each time instant for spatial harmonics $(-N/2+1) \leq k \leq (N/2)$ by taking the discrete spatial Fourier transform, where:

$$C_k(t)\big|_{t=T} = \frac{1}{N} \sum_{j=0}^{N-1} \tilde{\varphi}(t,\theta)\big|_{t=T} e^{\frac{-2\pi ijk}{N}} \qquad (2.2)$$

The amplitude and the phase speed of each spatial Fourier harmonic can be determined by computing the PSD. $C_k(t)$ can be broken down into:

$$C_k(t) = \sum_{m=-\infty}^{\infty} A_m e^{-imt} \qquad (2.3)$$

For M equally spaced time samples, A_m can be computed for frequencies $(-M/2 + 1) \leq m \leq (M/2)$ by computing the discrete Fourier transform, where:

$$A_m = \frac{1}{M} \sum_{j=0}^{M-1} C_k(t) e^{\frac{-2\pi ijm}{M}} \qquad (2.4)$$

The PSD, or $|A_m|^2$, shows how much wave energy is present at frequency m for the analyzed k'th spatial harmonic.

As an example, Figure 2.1 is a plot of velocities as measured by 8 circumferentially equally spaced hot-wire anemometers at the inlet of the MIT Three Stage compressor during stall inception. The velocity traces clearly show characteristic ripples which are most easily noticed in a modal wave type disturbance. Figure 2.2 shows the PSD's of SFHC computed from the velocity traces in Figure 2.1. The figure shows the PSD's of the 0th to 4th

spatial harmonic for a sampling window time of 0 to 20 rotor revolutions. $C_k(t)$ are analyzed only for $0 \leq k \leq 4$ spatial harmonics since $C_k^*(t) = C_{-k}(t)$ if φ is real. Positive frequency indicates waves traveling in the same direction as the rotor, and negative frequency indicates waves in the opposite direction. The first and second harmonics, which are the first and second modes of the modal waves, are traveling at 28% and 30% of rotor speed, respectively. The second harmonic is physically rotating at 30% of rotor speed, not 60%, as two cycles must pass a stationary observer for the second harmonic to make one complete revolution. The physical rotation speed of the k'th harmonic is thus the PSD frequency divided by k.

2.2.1 Limitations

While the PSD of SFHC is useful in detecting circumferentially long length scale disturbances, it is a poor detector of short wavelength disturbances. A short wavelength disturbance may be idealized as a narrow traveling pulse. The wave energy associated with a narrow pulse is spread over a wide number of spatial Fourier harmonics, and in the limit of zero width, each spatial Fourier harmonic contains infinitesimally small wave energy. In reality, short wavelength disturbances have finite width, and for a typical compressor of 50 to 60 blades, the wave energy will be spread among 20 to 30 spatial harmonics. Roughly 1/20 of the short wavelength disturbance wave energy will be present in the PSD of each SFHC, and this can easily be masked by noise. A more serious difficulty, however, is the need to have an array of 40 to 60 sensors to resolve 20 or so spatial Fourier harmonics to avoid spatial aliasing.

2.3 Cross-Correlation

2.3.1 Introduction

To avoid the above difficulties, a more effective method of detecting a short wavelength disturbance is used: cross-correlation of spatially adjacent sensor signals. It is more effective than PSD of SHFC for two reasons: First, cross-correlation can work effectively with a small array of sensors. Because the time history of a signal, not the instantaneous signal, is used, a large array of sensors is not needed to resolve the spike disturbance at all times. As will be shown in Section 2.3.3, cross-correlation can exhibit aliasing errors if the sensor spacing becomes too large (too few sensors), but the characteristics of short wavelength disturbances are such that aliasing errors can usually be avoided.

Second, cross-correlation is better because there is just one detection band (Zj versus $1/s$) and not many bands (N spatial harmonics), simplifying the detection procedure. A narrow pulse (i.e. short wavelength) disturbance generates a sharp correlation peak which stands out from random correlation noise at the time shift corresponding to the propagation rate (Figure 2.3). Cross-correlation is generally not well suited for accurately detecting long wavelength disturbance because the correlation peak becomes much broader, and it is difficult to locate the peak center (Figure 2.4).

2.3.2 Formulation

The cross-correlation of the n'th sensor signal, φ_n, to the next sensor signal, φ_{n+1}, is defined in the discrete case as:

$$z_{nj} = \sum_{m=0}^{M-1} \tilde{\varphi}_{(n+1)m} \tilde{\varphi}_{n(m-j)} \tag{2.5}$$

where M is the length of the sampling window. The function z_{nj} is an integral measure of the correlation of φ_n to φ_{n+1} if φ_n is shifted j to the right. The computational time for z_{nj} can be considerably reduced by noting:

$$z_{nj} = \sum_{k=0}^{M-1} B_{(n+1)k} B_{nk}^{*} e^{(\frac{2\pi ikj}{M})} \tag{2.6}$$

where B_{nk} and $B_{(n+1)k}$ are the k'th discrete Fourier transform coefficients of φ_n and φ_{n+1}, respectively. Thus, the Fast Fourier Transform (FFT) can be employed to compute z_{nj} quickly.

To minimize noise, an average value of the cross-correlations of measurements taken by pairs of adjacent sensors is computed for an array of N sensors (Figure 2.5). For equally spaced sensors, the average cross-correlation, Z_j, defined as:

$$Z_j = \frac{1}{M}\left(\frac{1}{N}\sum_{n=1}^{N} z_{nj}\right) \tag{2.7}$$

Z_j is the average level of correlation at each sampling point if each of the N sensor signals is shifted to the right by j relative to the next adjacent sensor signal.

Noting that the circumferential distance between sensors is $(\theta_{n+1} - \theta_n)$, and the time for a disturbance to travel between sensors is j/f_S, the speed of the disturbance normalized by rotor speed is given by the following relation:

$$\frac{1}{s} = \left(\frac{2\pi}{\theta_{n+1} - \theta_n} \right) \left(\frac{f_{rotor}}{f_s} \right) j \qquad (2.8)$$

For cross-correlations, the quantity 1/s versus Z_j is normally plotted instead of s versus Zj since Zj is function of j, not 1/j.

An example of using cross-correlations to determine the speed of a short wavelength disturbance is presented in Figures 2.6 and 2.7. Figure 2.6 is a plot of the static pressures as measured by a pressure transducer array at the first stage rotor inlet of the General Electric Low Speed Research Compressor during stall inception. The pressure traces show a propagating short wavelength disturbance at 73% of rotor speed. Figure 2.7, which is the plot of the average cross-correlation of 10 adjacent sensor signals in Figure 2.6, shows a peak at 1/s = 1.37 which corresponds to the short wavelength disturbance traveling at 73% or 1/1.37 of rotor speed.

2.3.3 Aliasing Errors

A possible source of error using cross-correlation to determine speed of a disturbance is aliasing. Aliasing can occur if the sensor spacing is too large. To avoid aliasing, the sensor spacing, $(\theta_{n+1} - \theta_n)$, must meet the condition of:

$$(f_{rotor}\tau_p) \geq \left(\frac{\theta_{n+1} - \theta_n}{2\pi} \right) \qquad (2.9)$$

where τ_p is the time scale associated with the periodicity of a disturbance. To a stationary observer, there are two time scales associated with a disturbance (Figure 2.8). One is the scale associated with the duration of the disturbance, τ_d, and the other with its periodicity, τ_p. For a sinusoidal disturbance such as a modal wave, the two scales, τ_d and τ_p, are equal. For a short wavelength disturbance, the two scales are quite different. Short wavelength disturbances have long τ_p's even though τ_d's are short, so Equation 2.9 is usually well satisfied. The long τ_p's occur because the short wavelength disturbances, which do not have organized patterns and are randomly distributed around the compressor annulus, have an effective τ_p of $1/frotor$ (or $frotor\ \tau_p = 1$) which always satisfies Equation 2.9.

Equation 2.9 only guarantees that the disturbance speed will not be over-estimated by aliasing. Since all rotating disturbances will be periodic, there will be correlation peaks at:

$$\frac{1}{s} = \frac{1}{s}\bigg|_{actual} \pm (f_{rotor}\tau_p)\left(\frac{2\pi}{\theta_{n+1} - \theta_n}\right)k \qquad (2.10)$$

where k = 1, 2, 3... Again, however, the long τ_p's of short wavelength disturbances assure that the periodic correlation peaks (Equation 2.10) will be widely separated, reducing the likelihood of misinterpretation of the cross-correlation.

At times, aliasing cannot be avoided. An example is when disturbances have regular patterns. An illustration of aliasing causing an error in the estimate of the disturbance speed is presented in Figure 2.9 and 2.10. The pressure traces in Figure 2.9 are of 12 equally spaced part-span stall cells rotating about the annulus at 71% rotor speed in the General Electric

Low Speed Research Compressor. Since many of the sensors are spaced wider than the maximum allowable spacing given by Equation 2.9, the average cross-correlation plot in Figure 2.10 shows an aliasing peak at $1/s = 0.47$ or $s = 213\%$ of rotor speed. The reason for the aliasing peak is that the cross-correlation cannot distinguish between one part-span stall cell from another, as illustrated by guidelines in Figure 2.9. In addition, the periodicity of the stall cells generates peaks predicted by Equation 2.10 at locations of $1/s = 1.4 \pm 0.933k$, or $1/s = -1.4, -0.47, 0.47, 1.4$ in Figure 2.10.

2.4 Filtering

Filtering is important since it can greatly accentuate the correlation peak associated with a short wavelength disturbance. This is especially true if the sensors are placed close to a rotor at high sampling rates, as the dominant flow disturbance is due to blade passing. Without filtering blade passing, the short wavelength disturbances can be almost completely masked. To illustrate this, static pressure measurements downstream of the first stage rotor as the General Electric Low Speed Research Compressor is throttled down into stall are shown in Figure 2.11. The measurements were taken with sampling rate of 10kHz, well above the blade passing frequency of 720 Hz. Figure 2.12 is the cross-correlation plot of the data in Figure 2.11 for a sampling window time of 5 to 70 rotor revolutions without filtering out blade passing. Because of aliasing peaks caused by blade passing, it is impossible to extract any information.

Figure 2.13 is the plot of the cross-correlation when blade passing is filtered out using a lowpass filter. There are three distinct correlation peaks at

$1/s = 0, 1, 1.34$, or $s = \infty$, 100%, 75% of rotor speed, respectively. A disturbance which can travel circumferentially at infinite speed is an axisymmetric disturbance. The peak at rotor speed is probably due rotor asymmetry. The interesting peak is the one at 75% rotor speed. Only when blade passing is filtered out, can the cross-correlation pick out the short wavelength disturbances.

The peaks are still somewhat distorted in Figure 2.13. The distortion is caused by noise below rotor frequency which superimposes a broad correlation peak on the sharp correlation peaks produced by short wavelength disturbances. The correlation peaks can be enhanced by filtering out this low frequency noise, and the results are shown in Figure 2.14. The three peaks become much sharper and more separated.

Finally, highpass filtering is necessary when searching for short wavelength disturbances in a compressor which exhibits large amplitude long wavelength disturbances. This is because long wavelength disturbances act like low frequency noise and superimpose a broad correlation peak, distorting the peak associated with a short wavelength disturbance. Therefore, when searching for short wavelength disturbances in compressors which exhibit long wavelength disturbances, all low frequency components associated with long wavelength disturbances are filtered out before cross-correlation is applied.

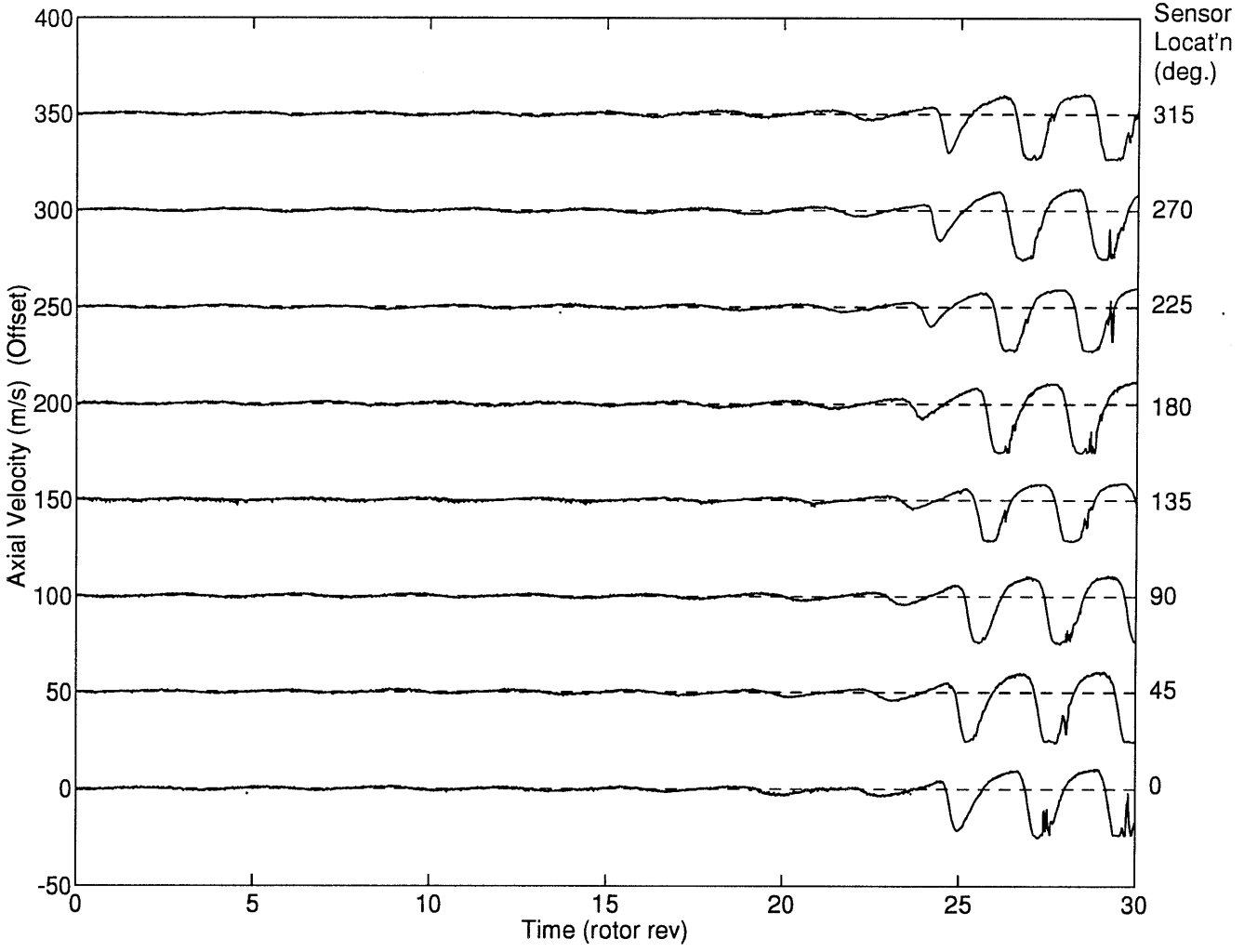

Figure 2.1 Hot-wire velocity traces at IGV inlet during stall inception. Note the characteristic wave-like traces of a modal wave disturbance prior to rotating stall.

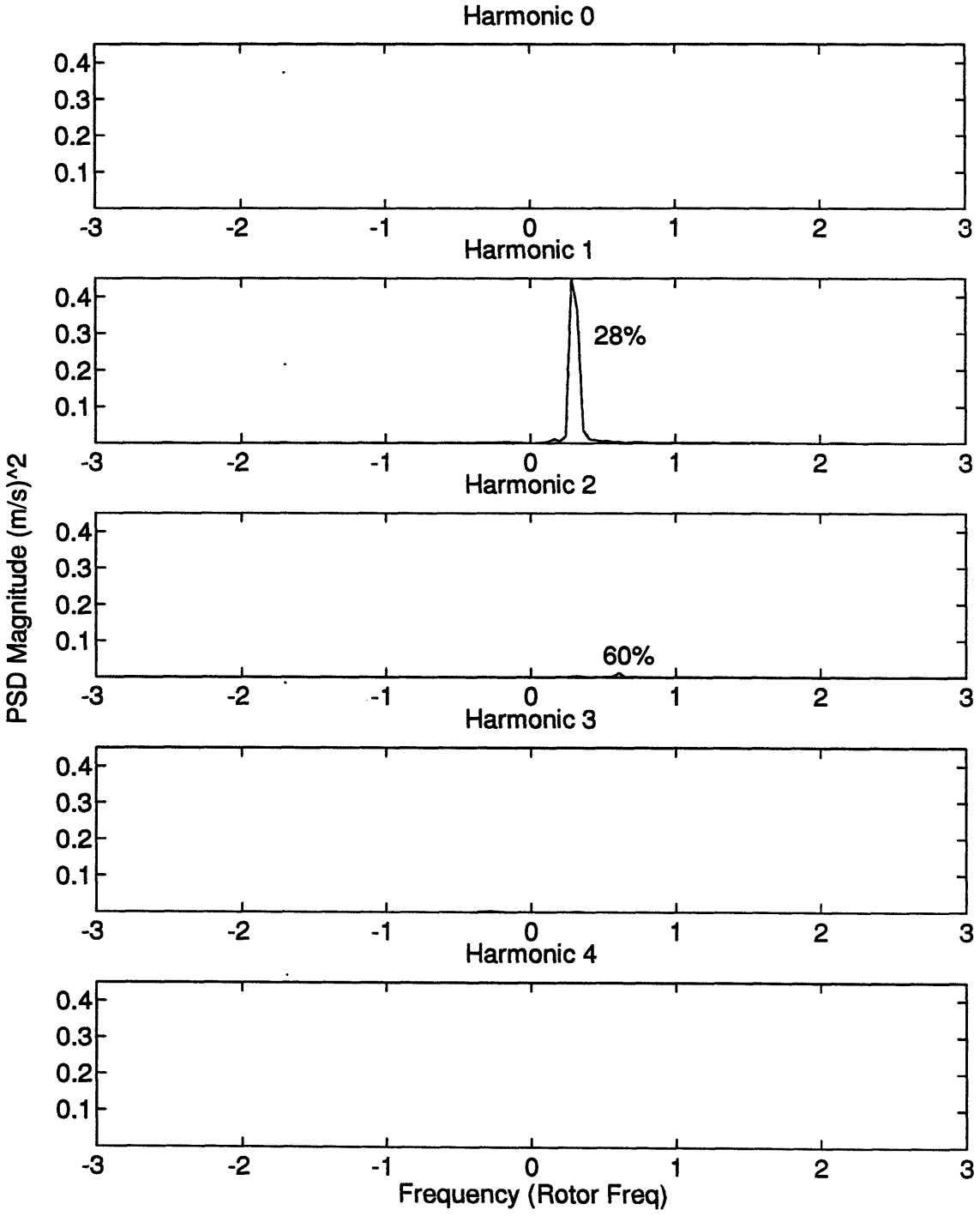

Figure 2.2 PSD's of each SFHC of the velocity measurements in Figure 2.1 for time interval of 0 to 20 rotor revolutions. Note the peak at 28% of rotor speed in the PSD of the 1st spatial harmonic. A small peak at 60% of rotor frequency can also be observed in the PSD of the 2nd spatial harmonic.

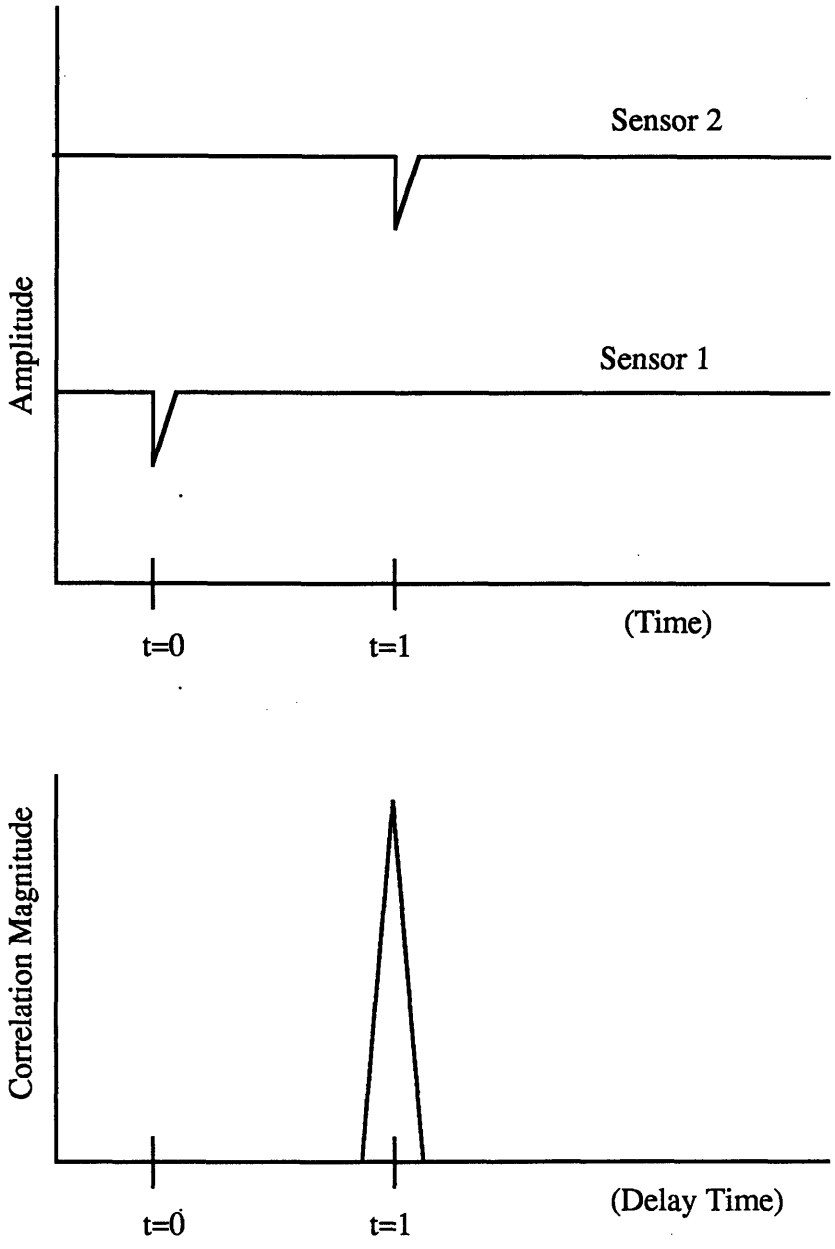

Figure 2.3 Illustration of cross-correlation of a propagating narrow pulse-like disturbance. The lower figure is cross-correlation of measurements from spatially adjacent sensors of a propagating pulse-like disturbance (upper figure). Note the sharpness of the correlation peak.

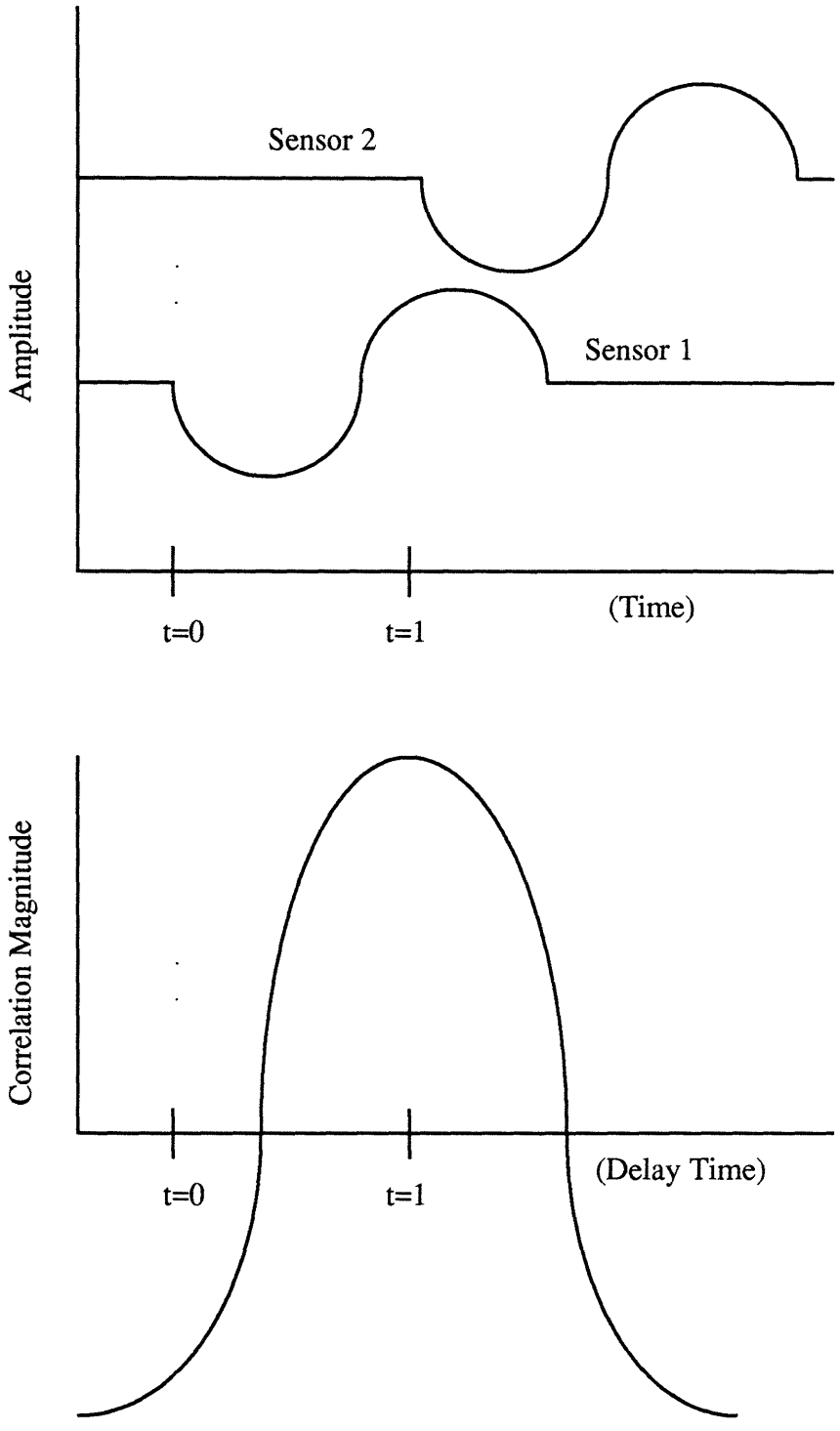

Figure 2.4 Illustration of cross-correlation of a sinusoidal disturbance of a long wavelength. The lower figure is cross-correlation of measurements from spatially adjacent sensors of a propagating long wavelength disturbance. Note the broadness of the correlation peak.

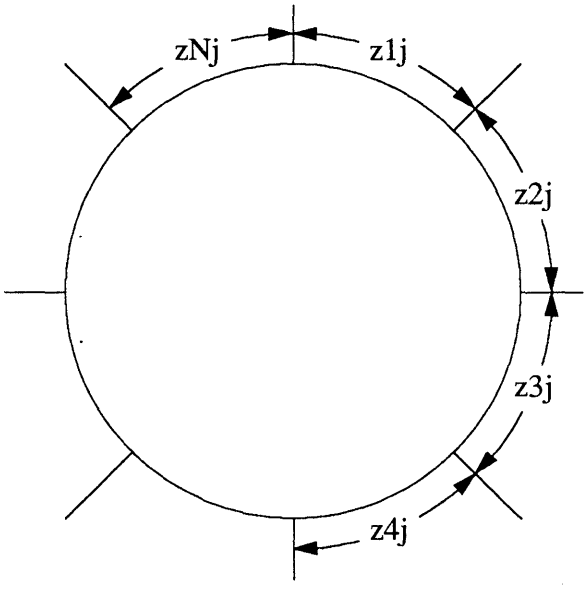

$$Zj = 1/M\ 1/N\ (z1j + z2j + z3j + z4j \ldots + zNj)$$

Figure 2.5 Averaging procedure of cross-correlations of measurements taken by pairs of adjacent sensors.

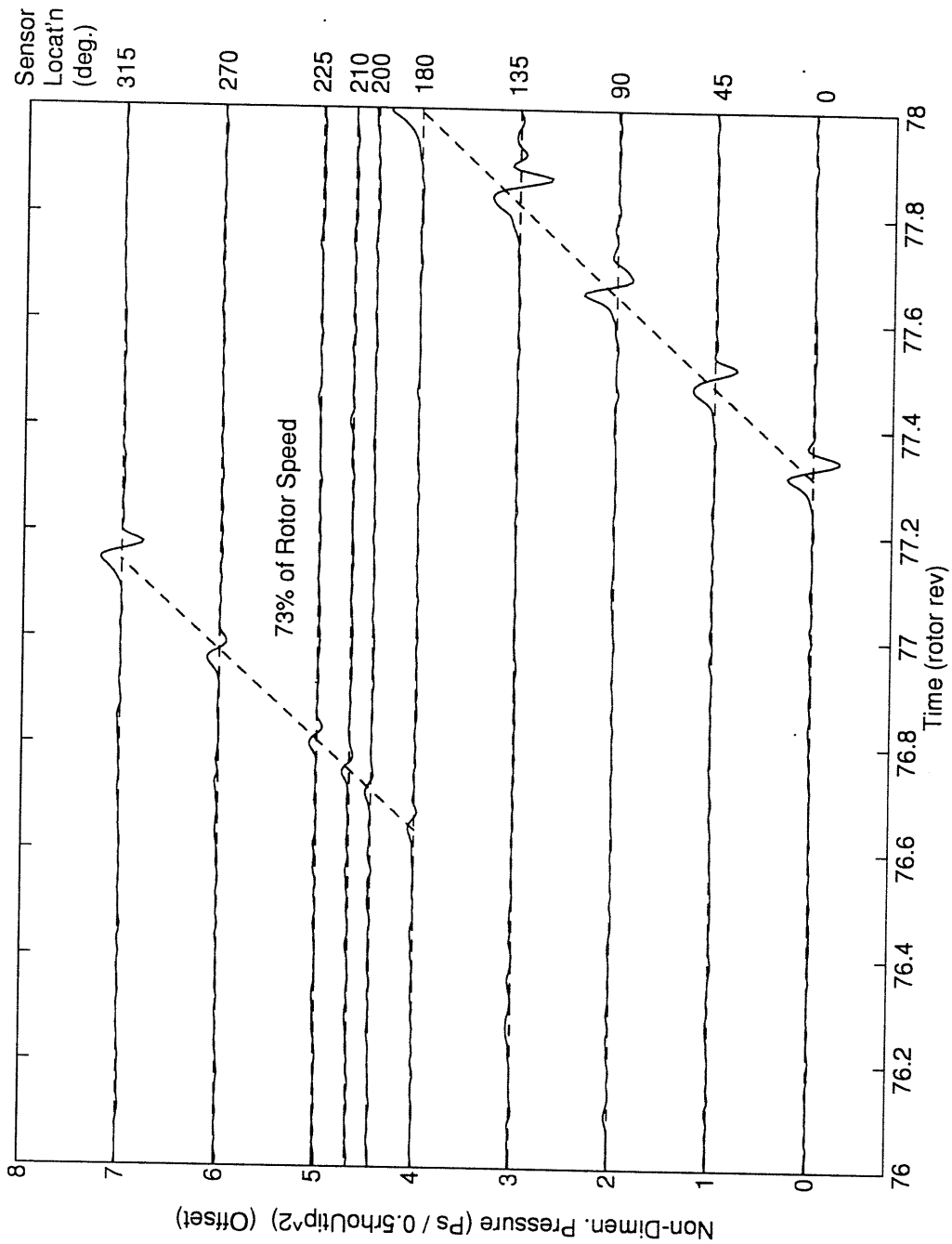

Figure 2.6 Casing static pressure traces at 1st stage rotor inlet of a propagating short wavelength disturbance.

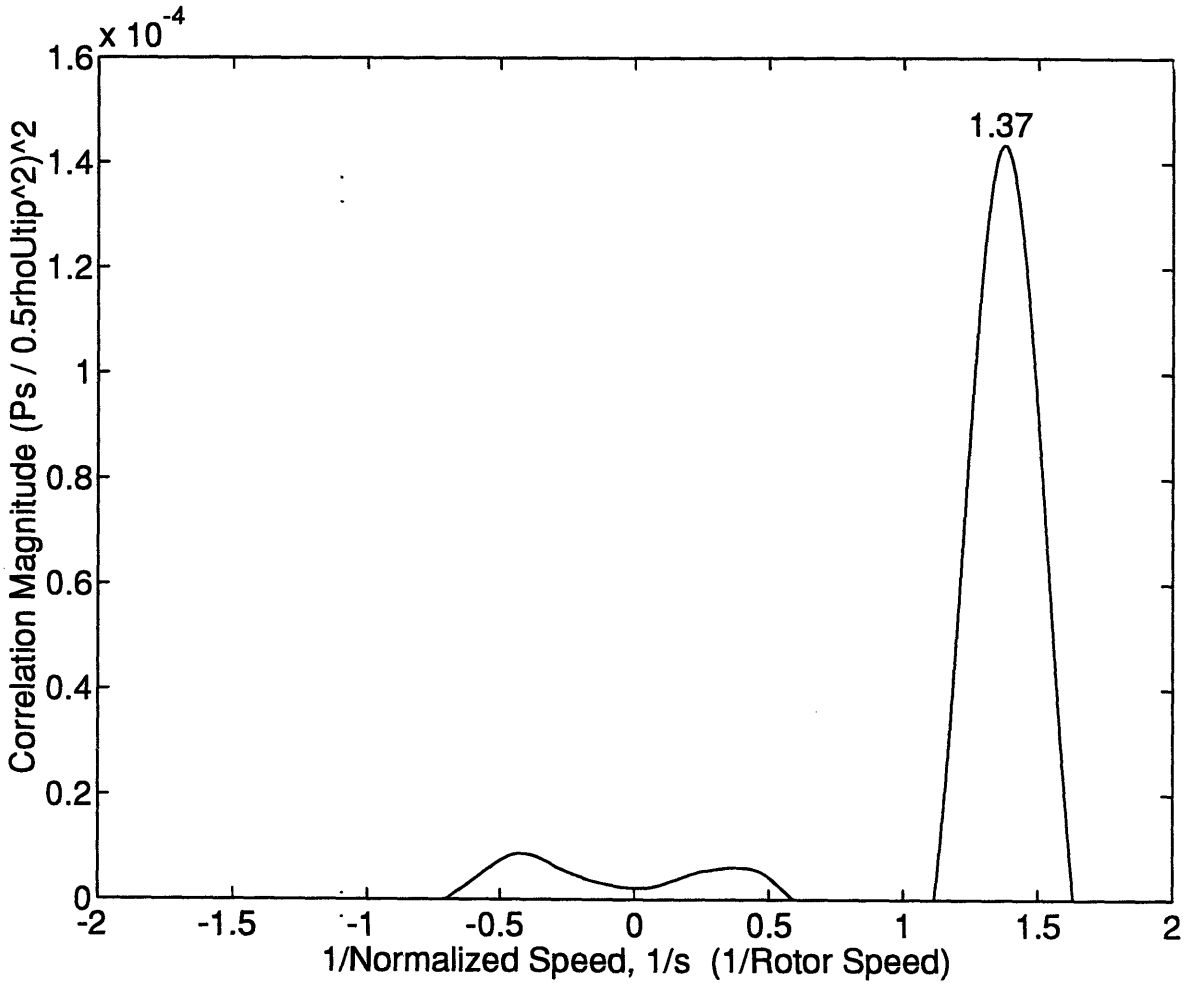

Figure 2.7 Cross-correlation of pressure measurements in Figure 2.6. Note the peak at 1/s = 1.37 or s = 0.73 of rotor speed.

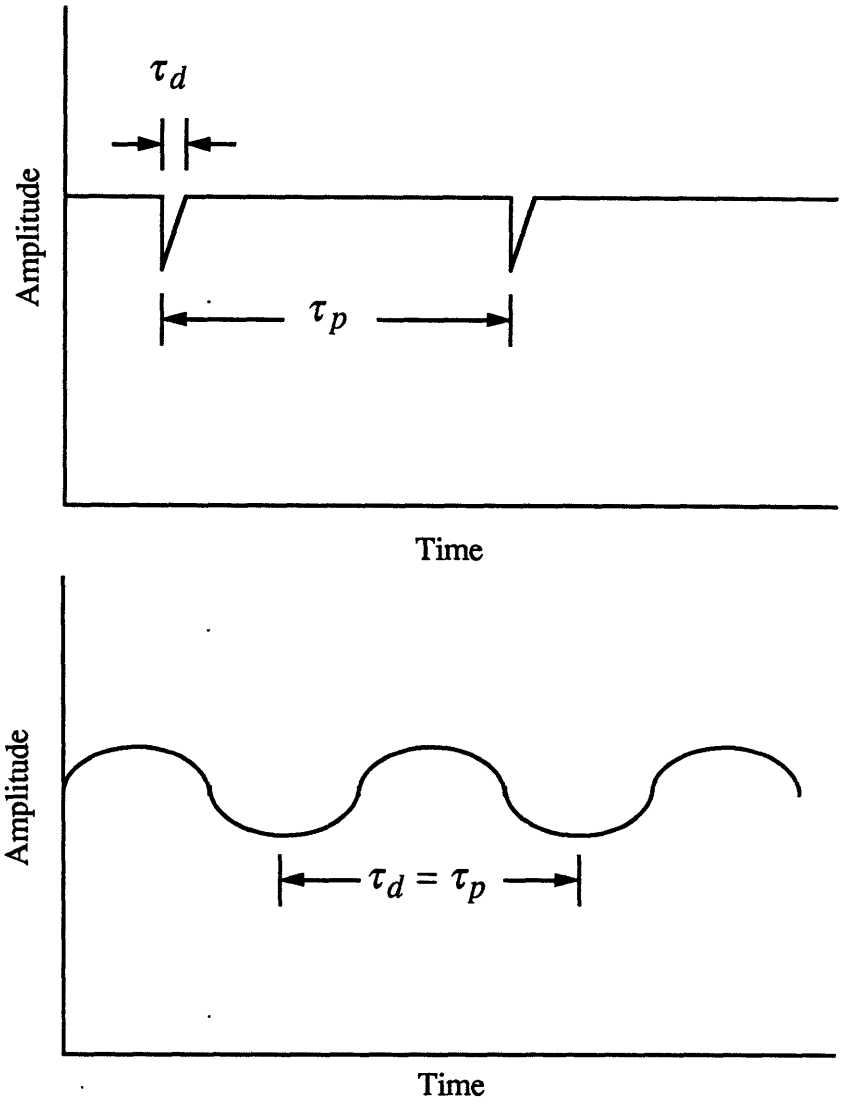

Figure 2.8 Two periods associated with a propagating disturbance for a stationary observer. A narrow pulse-like disturbance has two different periods for τd and τp (upper figure). A sinusoidal disturbance has equal periods for τd and τp.

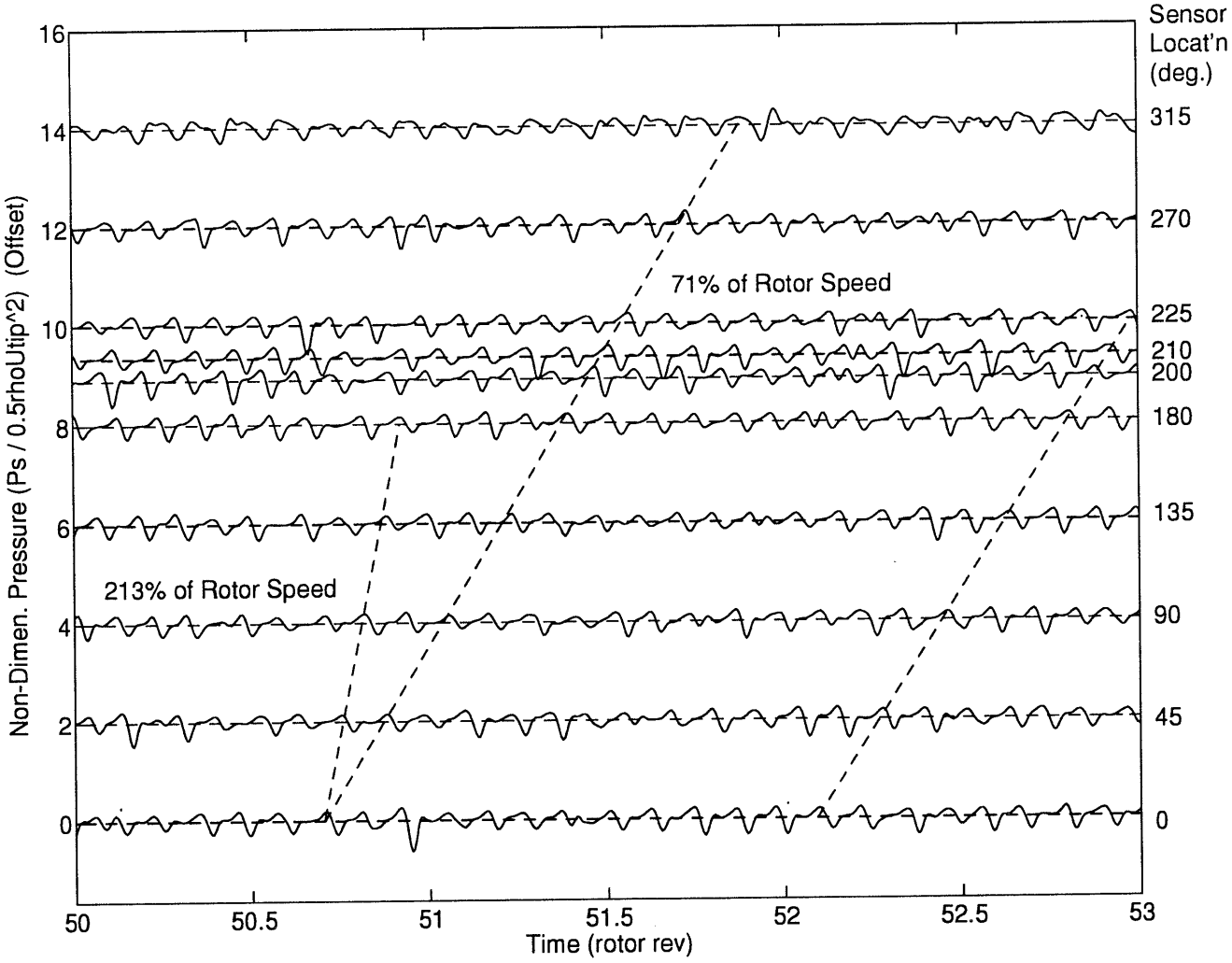

Figure 2.9 Casing static pressure traces at 1st stage rotor inlet of 12 equally spaced part-span stall cells propagating around the annulus. Guidelines show true speed (71% of rotor speed) of the disturbance and false speed due to aliasing (213% of rotor speed).

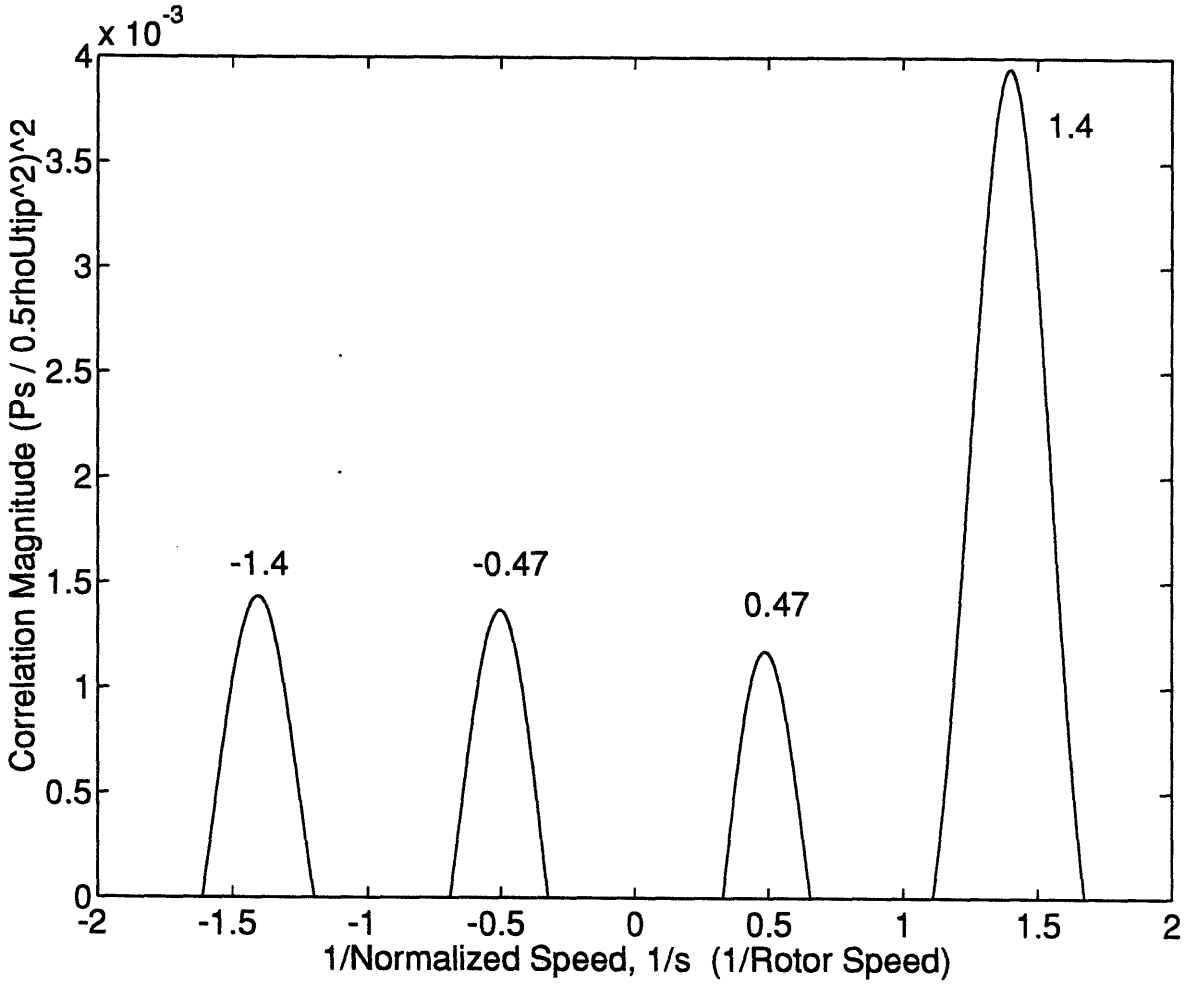

Figure 2.10 Cross-correlation of the pressure measurements in Figure 2.9. Note the large amplitude peak at 1/s = 1.4 and the smaller amplitude peaks caused by aliasing at 1/s = -1.4, -0.47, and 0.47.

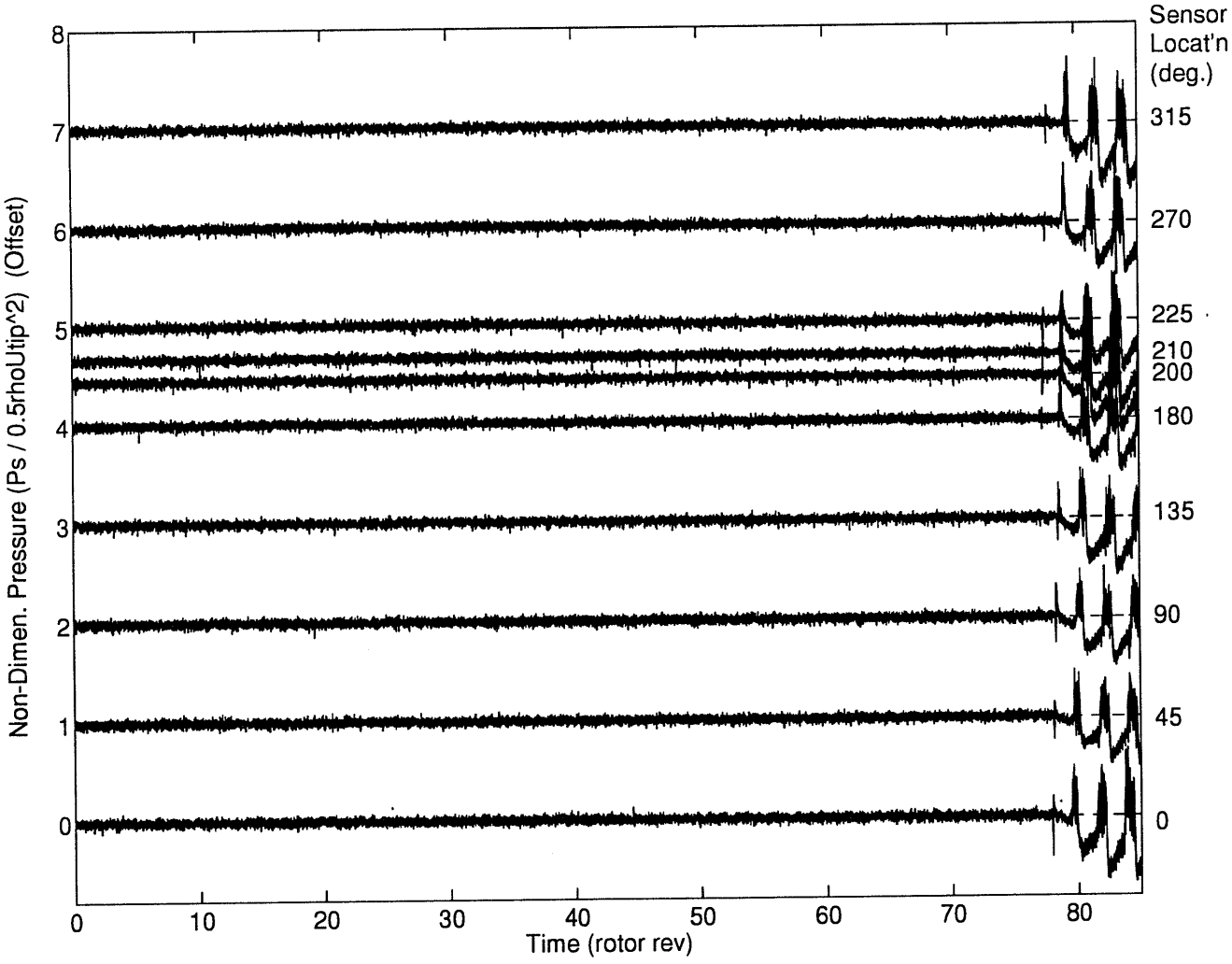

Figure 2.11 Casing static pressure traces at 1st stage rotor exit as compressor is throttled down into stall. The spike disturbane is first visible at approximately 77 rotor revolutions.

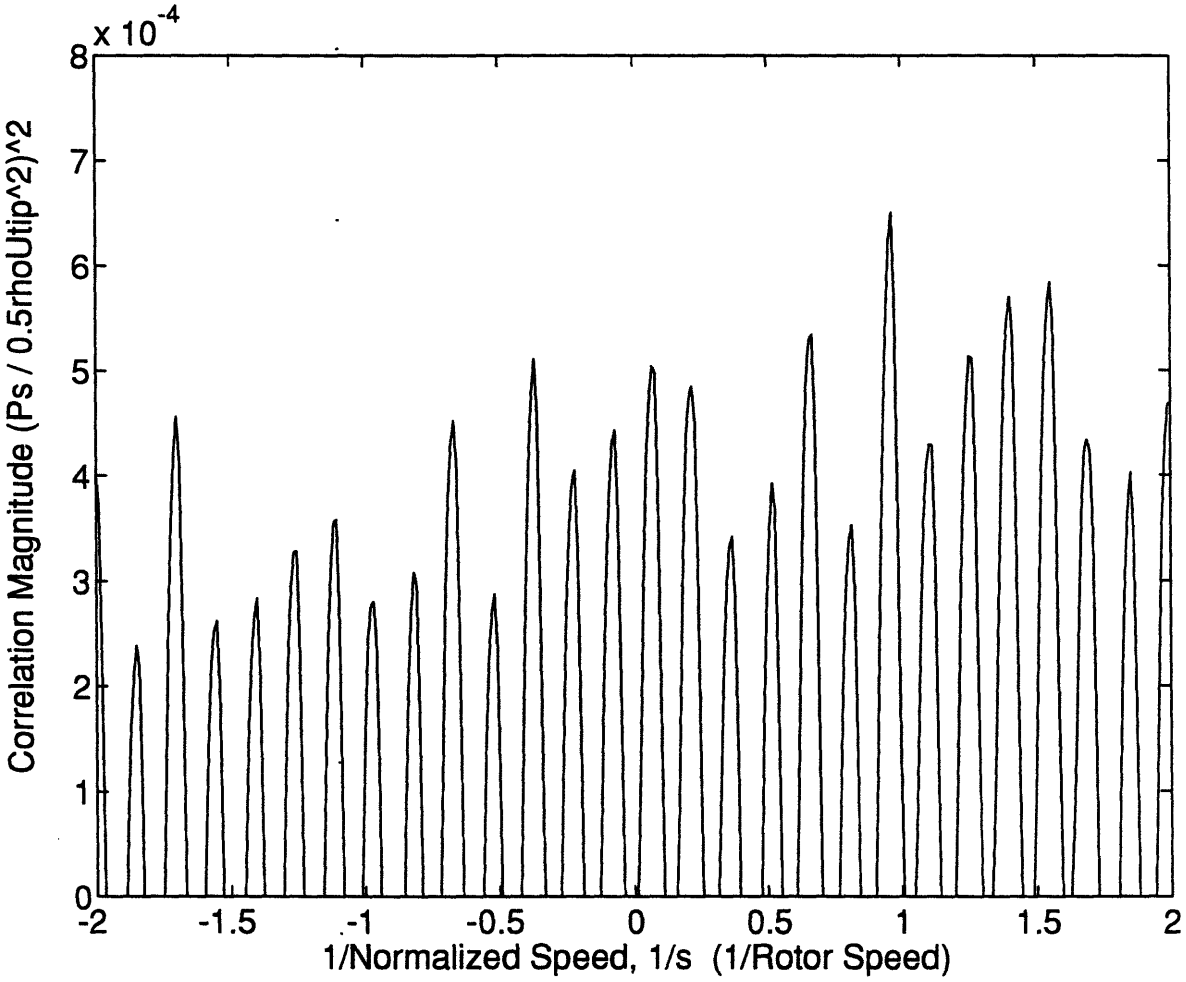

Figure 2.12 Cross-correlation of raw pressure measurements in Figure 2.11 for time interval of 5 to 70 rotor revolutions.

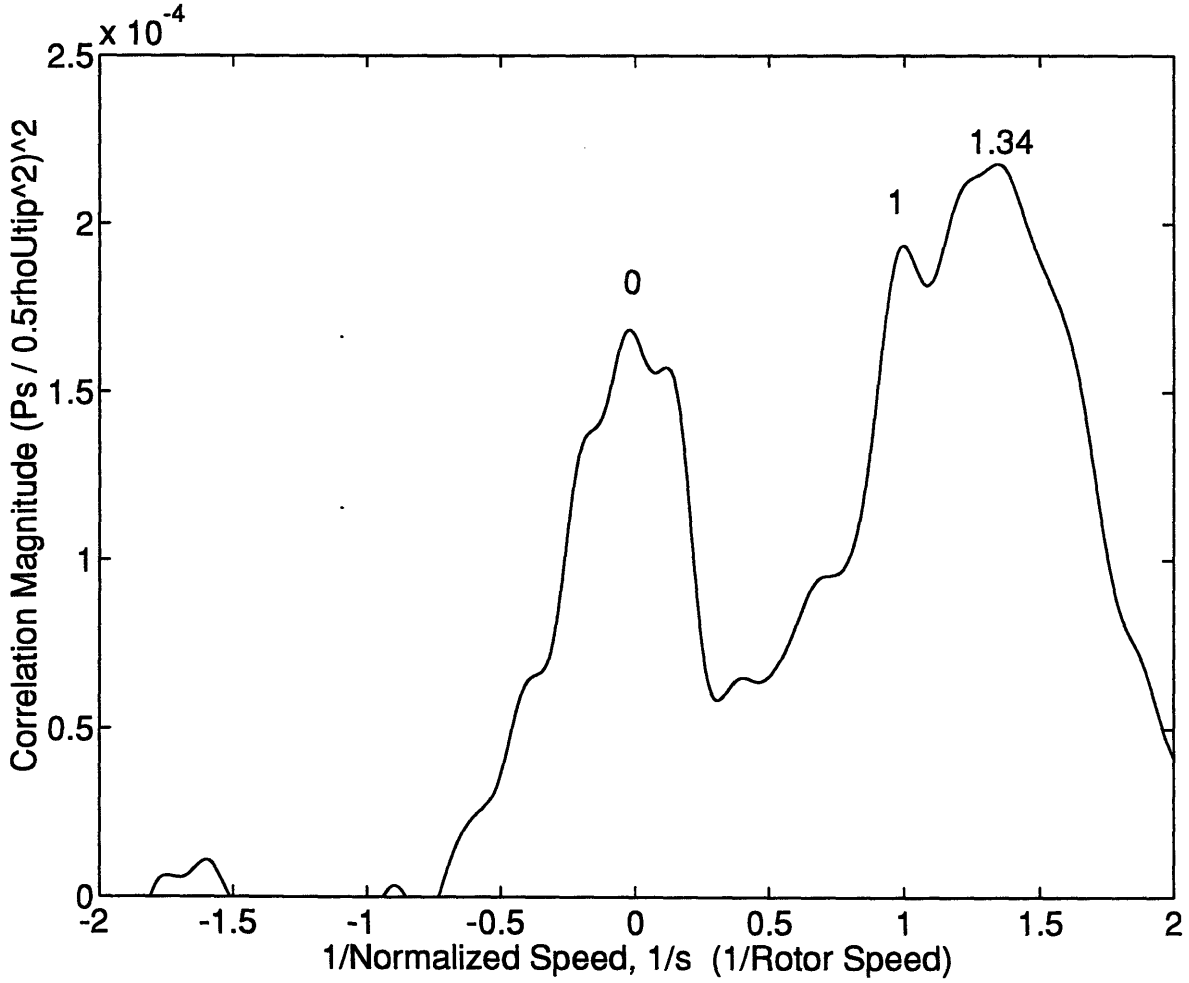

Figure 2.13 Cross-correlation of pressure measurements in Figure 2.11 for time interval of 5 to 70 rotor revolutions after blade passing has been filtered out. Note the three distinct peaks at 1/s = 0, 1, and 1.34.

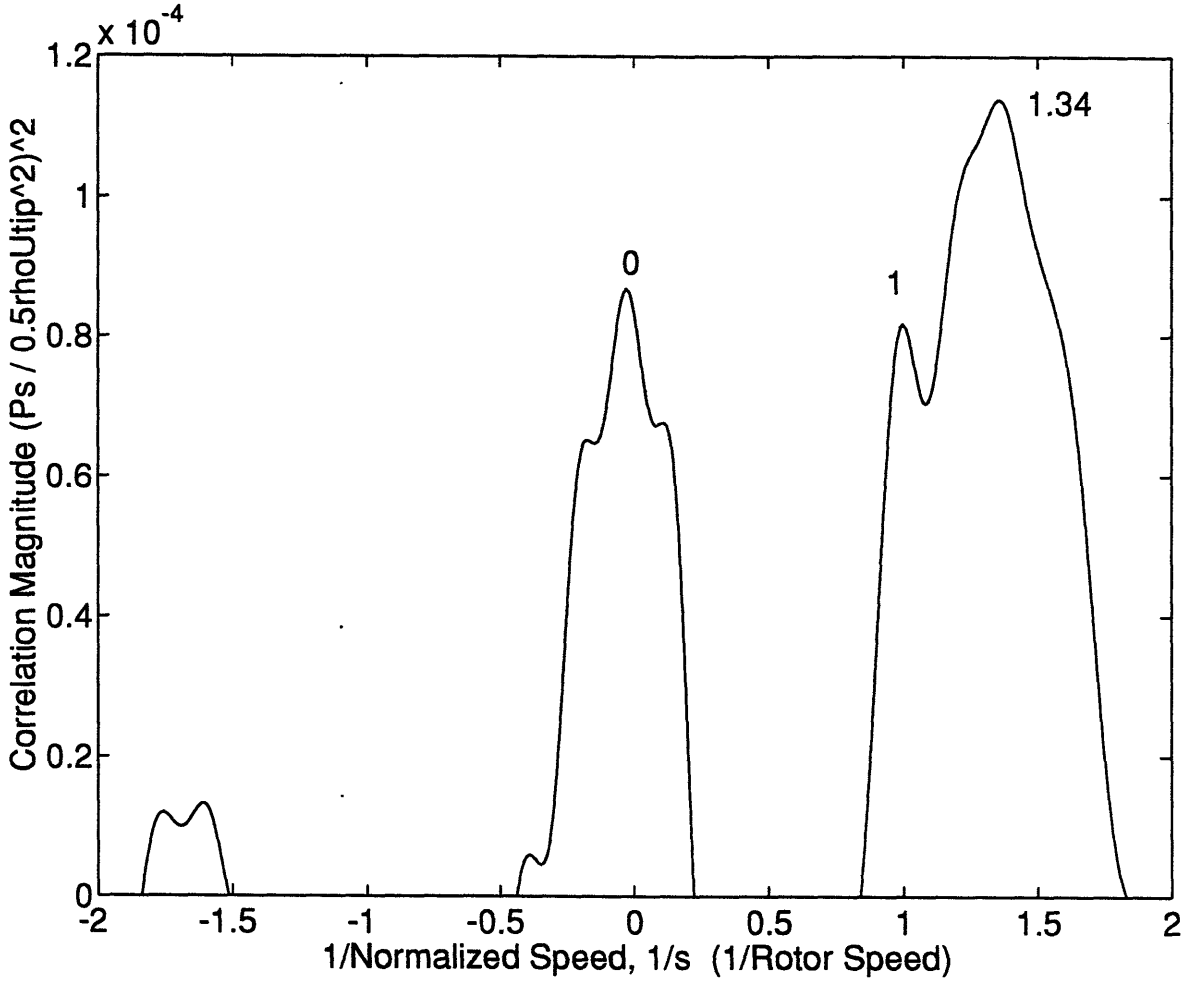

Figure 2.14 Cross-correlation of pressure measurements in Figure 2.11 for time interval of 5 to 70 rotor revolutions after the blade passing and low frequency noise components have been filtered out. Note the improved clarity of the three peaks at 1/s = 0, 1, and 1.34.

CHAPTER THREE

PRECURSOR FOR SHORT WAVELENGTH DISTURBANCE

3.1 Introduction

Long wavelength disturbances (modal waves) have been characterized by a precursor which grows slowly well before (up to several hundred rotor revolutions) compressor stall. In contrast, short wavelength disturbances have been previously characterized by the lack of a precursor. Day [2,4] has noted that when a spike becomes visually detectable in the time traces, the compressor stalls within 4-6 revolutions (Figure 1.4). This was a visual observation and there exists the possibility that spikes which are not easily detectable visually exist prior to stall. If these spikes exist and are somehow detected, they may serve as a "precursor" or a warning signal for stall onset.

In this chapter, the cross-correlation technique presented in Section 2.3 is used to re-examine the data of [4] and [12] to assess whether a precursor can be associated with a spike type disturbance. The results show, for the first time, that such a precursor does exist and is detectable if measurements are made with appropriate sensors and locations. If so, a spike precursor can be detected as far back as several hundred rotor revolutions prior to stall.

3.2 Compressors Studied

The two sets of compressor data examined are those from measurements taken by Silkowski [12] and Day [4] on the General Electric Low Speed Research Compressor (E^3 blading) and the Rolls-Royce Viper high speed compressor, respectively. Both compressors are known to exhibit spike

type disturbances prior to stall [4,12]. The E^3 compressor also exhibits a very weak modal wave type disturbance structure, but the modal wave is well damped and does not grow in amplitude prior to stall [19]. The Rolls-Royce Viper does not exhibit any modal wave type disturbance structure prior to stall [4]. A concise description of the compressor rigs and the associated instrumentation are given in the following sections.

3.2.1 GE LSRC E^3 Compressor

The GE Low Speed Research Compressor (LSRC), is a large-scale 4 stage low speed compressor (5 feet diameter). A schematic of the facility is shown in Figure 3.1. The compressor has a constant cross sectional area and a hub-to-tip ratio of 0.85. A more complete description of the compressor facility and the E^3 blading can be found in Wisler [20].

A detailed study of the stall inception characteristics of this compressor was made by Silkowski [12]. The data used for this study consist of measurements from a circumferential array of 10 high response casing pressure transducers which are located 0.2 chords upstream and downstream of the first stage rotor. Additional data are obtained from an array of 10 hot-wire anemometers with radial immersions of 20% and 80% of span from the casing. The circumferential locations of the probes are shown in Figure 3.2.

3.2.2 Rolls-Royce Viper

The Rolls-Royce Viper is a single spool compressor with a speed varying from 4000 to 13850 RPM. The hub to tip ratio varies from 0.5 at inlet to 0.85 at exit (Figure 3.3). A more complete description of the compressor

and the conducted experiments can be found in Day and Freeman [4]. The data used for this study consist of measurements from a circumferential array of 5 high response casing pressure transducers located at the first stage rotor inlet.

3.3 Method of Analysis

The method used to detect the presence of small amplitude short wavelength disturbances (spikes) is the cross-correlation technique outlined in Section 2.3. If spikes are present in the data, the cross-correlation will show a peak at the propagation rate of the spikes. This will serve as the precursor. To determine how far back in time the precursor can be detected, the data is first segmented from the stall point into uniformly sized sampling windows. A sampling window size of 50 rotor revolutions is chosen because it is found by trial and error to be a good compromise between signal-to-noise ratio and temporal resolution of the precursor.

The examined data have been taken at relatively low sampling rates, 1.2 and 0.5 times the blade passing frequency for the E^3 and the Viper compressors, respectively. No lowpass filtering is thus necessary to remove blade passing noise (see Section 2.3.2). The E^3 data, however, is highpass filtered at the rotor frequency to remove the effects of a modal wave (propagating at 10% of rotor speed) which added low frequency noise to the correlation. The filtering does not affect the locations and the relative heights of the cross-correlation peaks, and only serves to help isolate the individual peaks.

3.4 Results of Precursor Detection

The results of the cross-correlation show that a precursor can be associated with a spike type stall inception. For the E^3 compressor, there is a spike precursor at least 350 rotor revolutions prior to stall. The Viper compressor shows spike precursors at least 350 and 100 rotor revolutions prior to stall at 81% and 83% corrected speeds, respectively. At 98% corrected speed, the Viper compressor does not show any precursor, but it is unclear whether the stall inception process is via spikes.

3.4.1 GE LSRC E^3 Compressor

Static pressures behind the first stage rotor for the E^3 compressor are shown in Figure 3.4. The data are for a compressor speed of 800 RPM. The point of stall is set at t = 0 in Figure 3.4 and is defined as the time when a spike is seen growing into rotating stall or surge. The cross-correlation plots, which indicate level of correlation when sensor signals of sampling window size of 50 rotor revolutions are shifted relative to the adjacent sensor signals, are shown in Figure 3.5 for sequential time intervals. At t = -350 rotor revolutions, three significant peaks are visible. The highest peak, at 1/s = 1 or s = 100% of rotor speed, is caused by rotor asymmetry. The second highest peak, centered about 1/s = 0, is caused by an axisymmetric disturbance. The third peak at 1/s = -1.7 or s = -59% of rotor speed is unexplained and is likely an aliasing peak (Section 2.3.1). At the right of the rotor asymmetry peak, around 1/s = 1.4 or s = 71% of rotor speed, there appears to be some correlation, and a peak is observed by t = -250 rotor revolutions. By t = -50 rotor revolutions, the peak at 1/s = 1.4 becomes dominant, and it continues to

grow in amplitude right up to the stall point at t = 0. This peak at 1/s = 1.4 is the spike precursor. It is viewed as associated with a spike for two reasons:

1) The correlation peak is growing as the time approaches the stall point while the rest of the peaks are not.

2) The peak is at the speed corresponding to the initially observed propagation rate of a spike (71% of rotor speed) at stall of this compressor.

The growth of the peak at 1/s = 1.4 is illustrated by a surface plot as shown in Figure 3.6. The peaks due to rotor asymmetry and axisymmetric disturbance do not grow in amplitude as the compressor nears the stall point. However, the peak due to the spikes, which exists from t = -350, begins to show steady growth from t = -150. The E^3 compressor, therefore, shows a precursor associated with spikes from at least 350 rotor revolutions prior to stall.

3.4.2 Rolls-Royce Viper

The Rolls-Royce Viper compressor data are analyzed for three compressor speeds, 81%, 83%, and 98% of corrected speed, or 11,178 RPM, 11,454 RPM, and 13,524 RPM, respectively. The static pressures at the first stage rotor inlet for the Rolls-Royce Viper compressor at 81% of corrected speed are shown in Figure 3.7. The stall point is again at t = 0 (Figure 3.7), and the cross-correlation plots are shown in Figure 3.8 for sequential time intervals. At t = -450 rotor revolutions, there is one dominant peak at 1/s = 1 which is attributed to rotor asymmetry. The other small peaks are unexplained and are thought to be aliasing peaks. By t = -250, there is a definite peak growing at 1/s = 1.7 or s = 59% of rotor speed. The peak at 1/s = 1.7 becomes dominant by t = -50 and continues to grow right up to stall. This

peak is again viewed as a precursor associated with a spike because it satisfies the two reasons stated above (Note: the observed propagation rate of a spike at stall is 59% of rotor speed for this compressor, not 71%). At 81% of corrected speed, the Viper compressor thus shows a precursor associated with the spikes from at least 350 rotor revolutions prior to the stall point. In fact, if the peak at $1/s = 1.7$ is traced back, there is evidence to show that there is a precursor at least 450 rotor revolutions prior to stall. The growth of the correlation peak at $1/s = 1.7$ is illustrated in a surface plot as shown in Figure 3.9.

The static pressures for the Viper compressor at 83% corrected speed are shown in Figure 3.10, and the cross-correlation plots are shown in Figure 3.11. The correlation plots are similar to those at 81% corrected speed, except that the peak at $1/s = 1.7$ (i.e. at the observed speed of a spike) does not show growth until $t = -100$ rotor revolutions to the stall point. The peak at $1/s = 1.7$ then continues to grow to become dominant just prior to stall ($t = 0$). At 83% corrected speed, the Viper compressor shows a spike precursor from about 100 rotor revolutions prior to the stall point. The surface plot of the growth of the spike precursor peak is shown in Figure 3.12.

The static pressures for the Viper compressor at 98% corrected speed are shown in Figure 3.13, and the cross-correlation plots are shown in Figure 3.14. At this speed, there is a peak associated with rotor wake asymmetry but no precursor associated with a spike. There is no precursor because there is no correlation peak which is observed growing prior to stall. It is unclear if the type of disturbance structure seen just prior to surge is a spike since there is

little propagation. In summary, the Viper compressor at 98% corrected speed does not show a precursor associated with a spike.

3.5 Discussion

3.5.1 Amplitude Growth of Precursor

The level of correlation associated with the spikes becomes progressively greater as the compressors near stall. There are three possible reasons for this: 1) The spikes are growing in amplitude (i.e. the pressure or velocity perturbations are increasing). 2) The spikes are growing circumferentially. 3) Many more spikes are being formed. It is also possible for some combination of the three to occur.

To investigate why there is increased correlation as the compressors near stall, the static pressure measurements at the first rotor exit of the E^3 compressor are examined. The measurements show that the increased level of correlation is caused not by an increase in the pressure perturbation amplitude or the circumferential size of the spikes but by an increase in the level of activity in the formation and decay of spikes. This is a new discovery since (matched) compressors were thought to go into stall immediately after formation of a spike. The spikes, rarely traveling beyond 1/2 rotor revolution before decaying, are constantly forming when the compressor is throttled down to near stall. As the compressor approaches stall, the rate of formation and decay of the spikes increases.

The pressure traces close to stall ($t \approx -20$ rotor revs) and far from stall ($t \approx -370$ rotor revs) are shown in Figures 3.15 and 3.16, respectively. The

traces have been shifted such that any disturbances traveling at 70% rotor speed line up vertically. At close to stall, the spikes are seen forming and decaying more frequently as shown by the dashed guidelines. The circumferential size, however, remains consistent at about 2 blade pitches wide (Figure 3.17) regardless of how close the compressor is to stall. The maximum pressure perturbation amplitude also remains constant at about $\Delta P/0.5\rho U_{tip}^2 = 0.1$. At stall, however, one of the spike grows beyond this level and develops into a rotating stall cell (Figure 3.18).

3.5.2 Origin of Precursor

The development of these spikes prior to stall is likely result of a slight stage mismatching in the compressor. In a multi-stage compressor, spikes may develop in the first stage if the flow is locally unstable. However, if the mismatch of the stages is such that the flow of the downstream stages is still stable, the spike, which are local instabilities, will grow only until they feel the influence of the downstream stages. This effect has been demonstrated by Silkowski [12]. When the mass flow rate of an intentionally mismatched compressor was reduced to a certain level, spikes randomly developed in the first stage (Figure 3.19). However, the spikes were prevented from growing past a certain amplitude by the stabilized downstream stages. In each of the compressors that has been analyzed, there may be a slight mismatching of the stages, allowing the formation of a spike precursor.

3.6 Probe Location

The choice of type of sensor and location is critical to the detection of a

spike precursor. Sensor types and locations are listed in Table 3.1 in order of clarity of the cross-correlation peak associated with a spike precursor. Based on the results to date at low speed (E^3 compressor), the best choice for detecting a spike precursor is an array of casing static pressure transducers at the first stage rotor exit (Figure 3.20). The spike precursor at s = 1.4 is clearly visible and dominant. Hot-wire anemometers at the first stage rotor exit may also give information (Figure 3.21), but the peak associated with rotor asymmetry is more dominant.

Sensors placed upstream of the first stage rotor are less successful in detecting spike precursors at the low speeds. The detection of a spike precursor in the E^3 compressor is marginal using a pressure transducer array at first stage rotor inlet (Figure 3.22) and is not possible using a hot-wire anemometer array at the same location (Figure 3.23). However, at high speeds (Viper compressor), an array of pressure transducers at first stage rotor inlet appears to be adequate for detection of spike precursors.

3.7 Summary

For the first time, it is demonstrated that a precursor can be associated with a spike type stall inception. A spike precursor, detectable using cross-correlations, can extend as far back as 450 rotor revolutions prior to stall. The precursor is created by small amplitude spikes which randomly appear and then decay away, usually after propagating less than 1/2 revolutions around the annulus, when the compressor is throttled down to near stall. The maximum perturbation amplitude and circumferential size remain relatively constant regardless of how close the compressor is to stall, but the formation

and decay of spikes become more frequent. At stall, a single spike grows beyond a certain limiting perturbation amplitude and forms into a rotating stall cell, usually in less than 5 rotor revolutions.

Table 3.1 Best Sensors and Sensor Locations for Detecting Spikes

Sensor	Axial Location	Radial Immersion	Clarity of Correlation Peak
Pressure transducer	first stage rotor exit	casing	best
Hot-wire anemometer	first stage rotor exit	tip region	fair
Pressure transducer	first stage rotor inlet	casing	marginal
Hot-wire anemometer	first stage rotor inlet	tip region	no peak

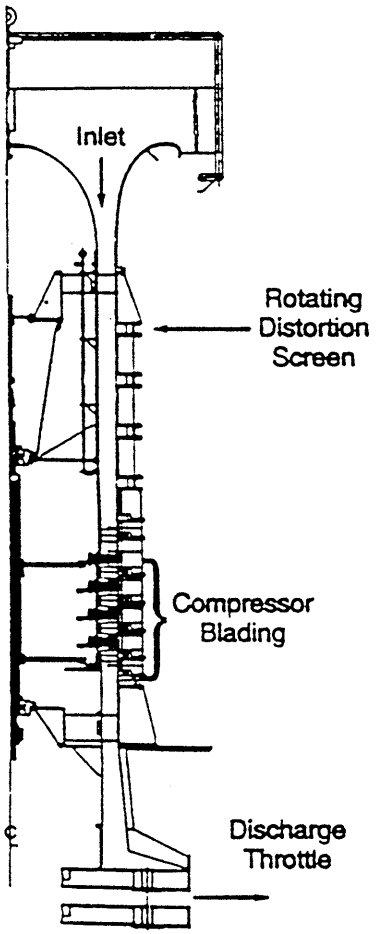

Figure 3.1 Schematic of GE Low Speed Research Compressor

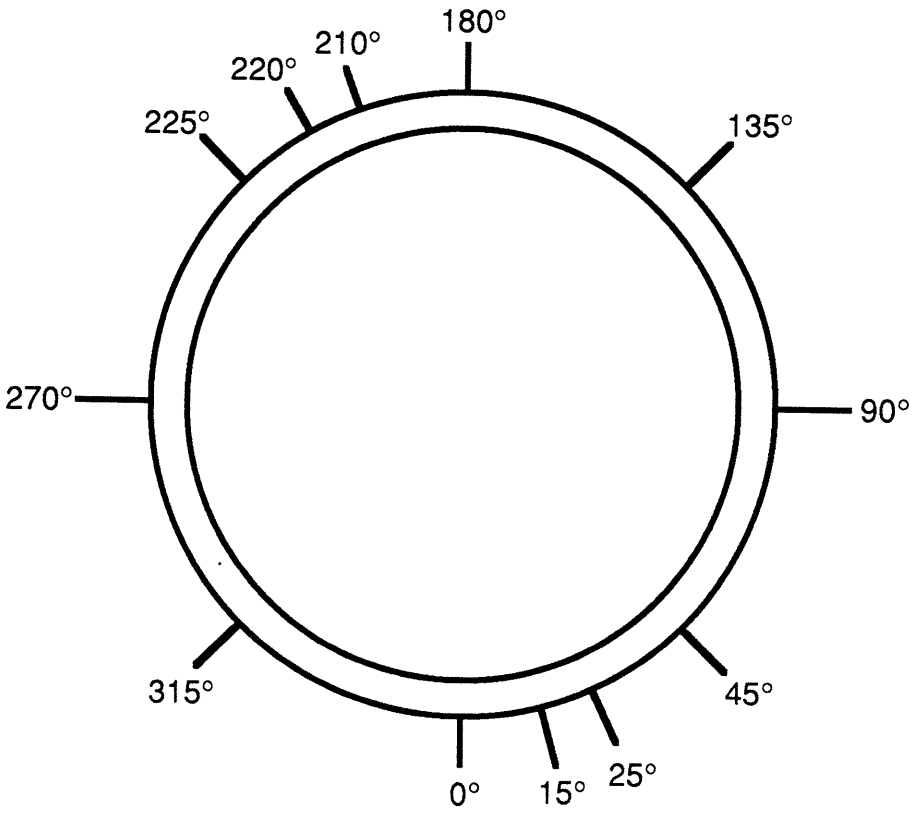

Figure 3.2 Circumferential locations of the sensors

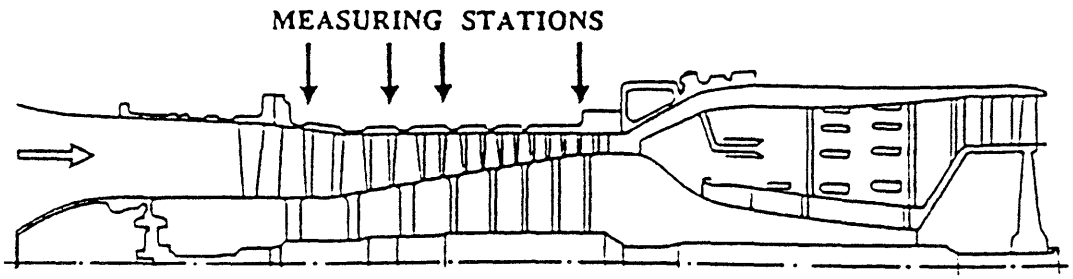

ROLLS-ROYCE VIPER ENGINE Mk 522

NUMBER OF STAGES:	8
SLS THRUST:	3330 lbf
COMPRESSOR PRESSURE RATIO:	5:1
SHAFT SPEED:	13850 rpm

Figure 3.3 Schematic of Rolls-Royce Viper engine

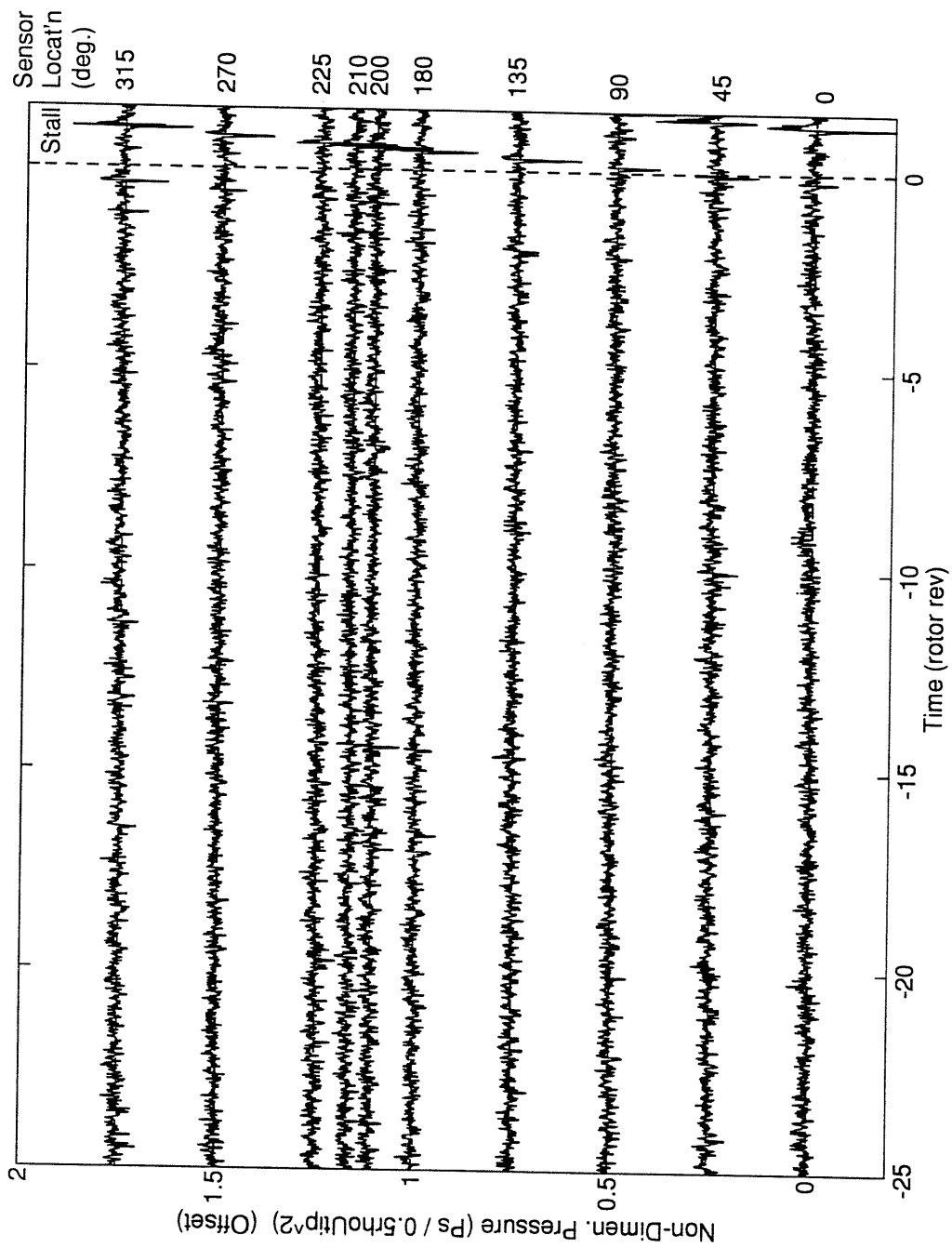

Figure 3.4 Casing static pressure traces at 1st stage rotor exit of the E^3 compressor. Stall point is marked by a dashed line.

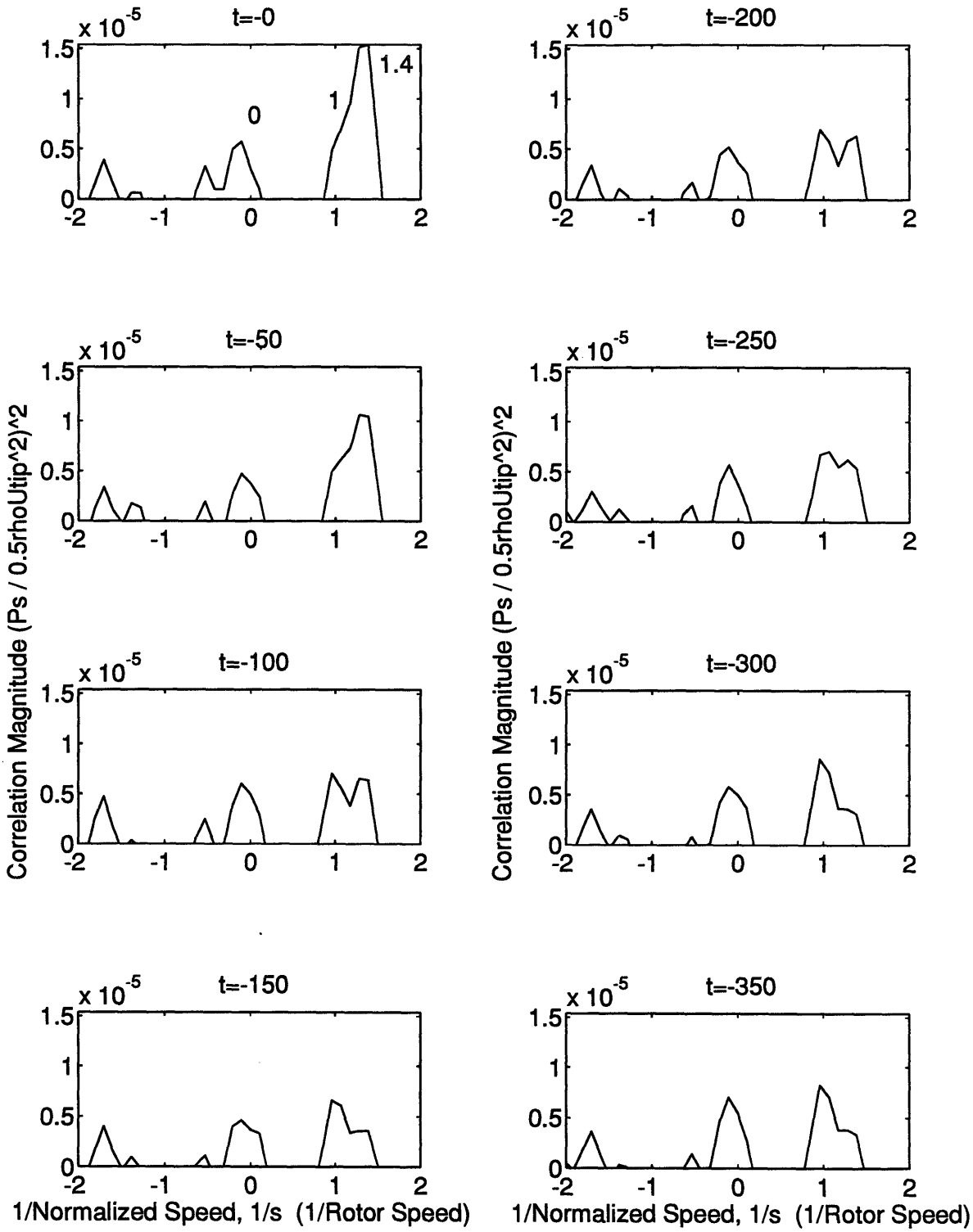

Figure 3.5 Cross-correlations of measurements in Figure 3.4 for sequential time intervals up to stall point (t = -0). Note the growth in height of the peak at 1/s = 1.4.

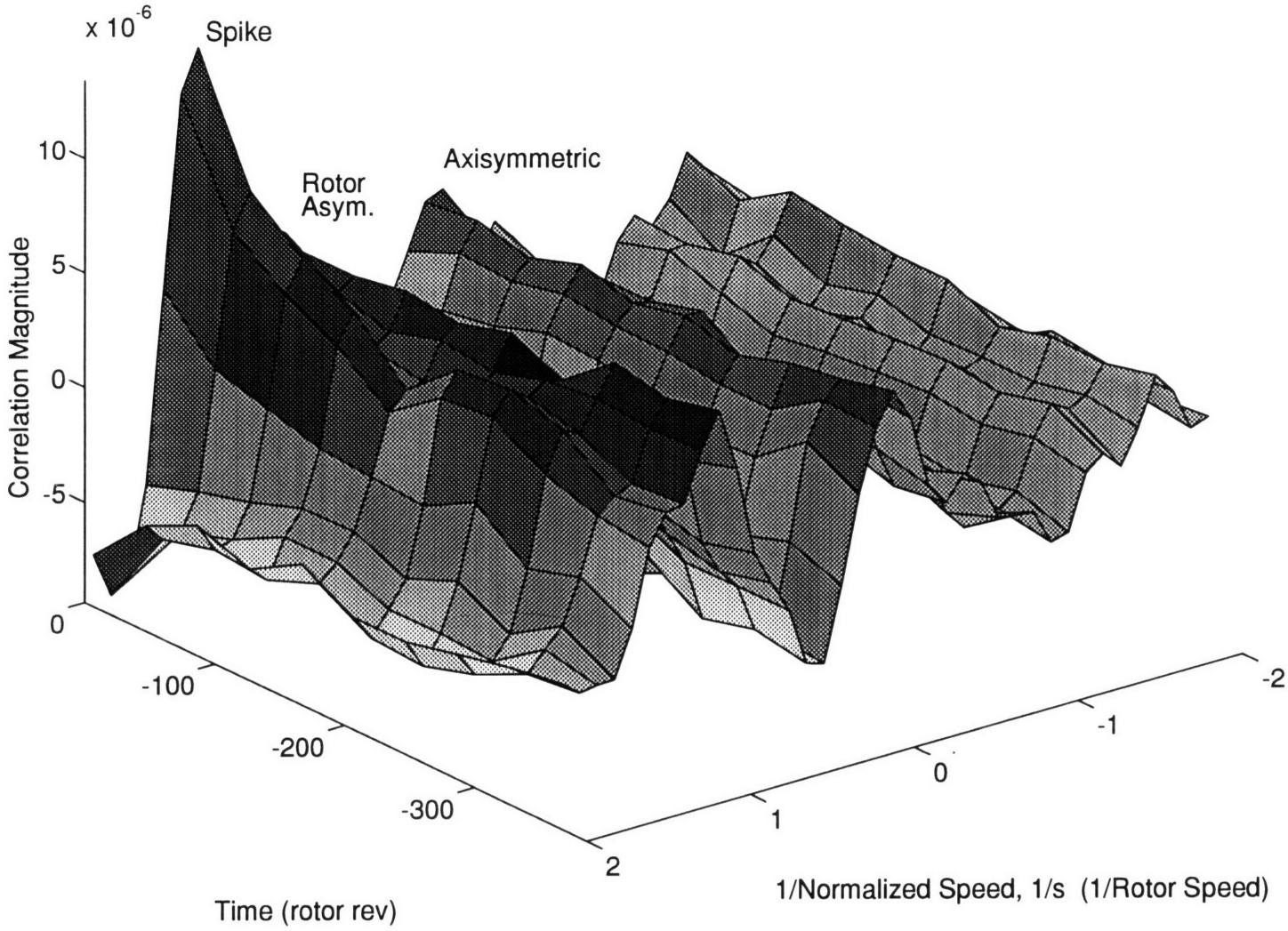

Figure 3.6 Surface plot of the cross-correlations in Figure 3.5. Note that only the peak at the propagation rate of a spike is growing in amplitude.

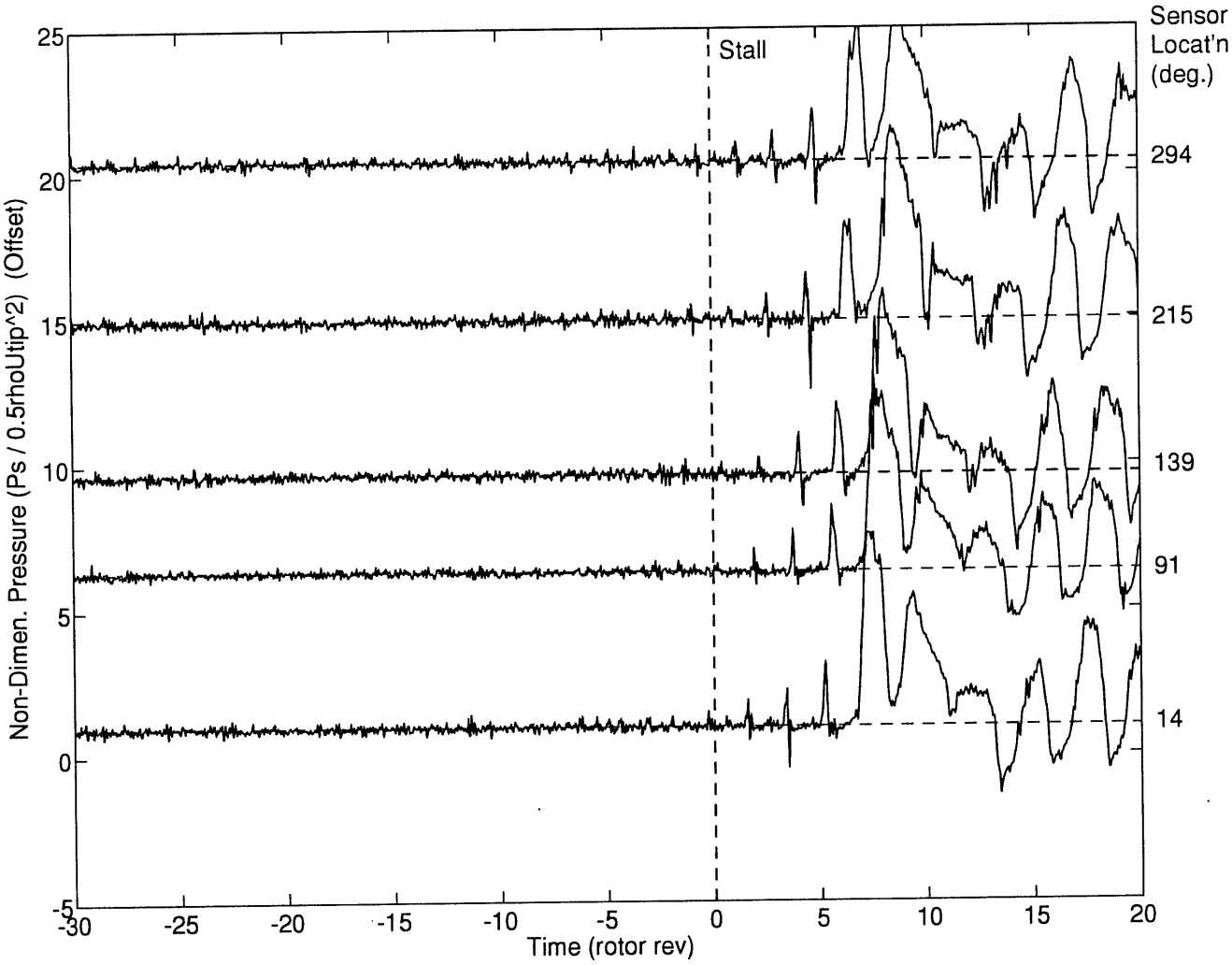

Figure 3.7 Casing static pressure traces at 1st stage rotor inlet of the Viper compressor at 81% of corrected speed. Stall point is marked by a dashed line.

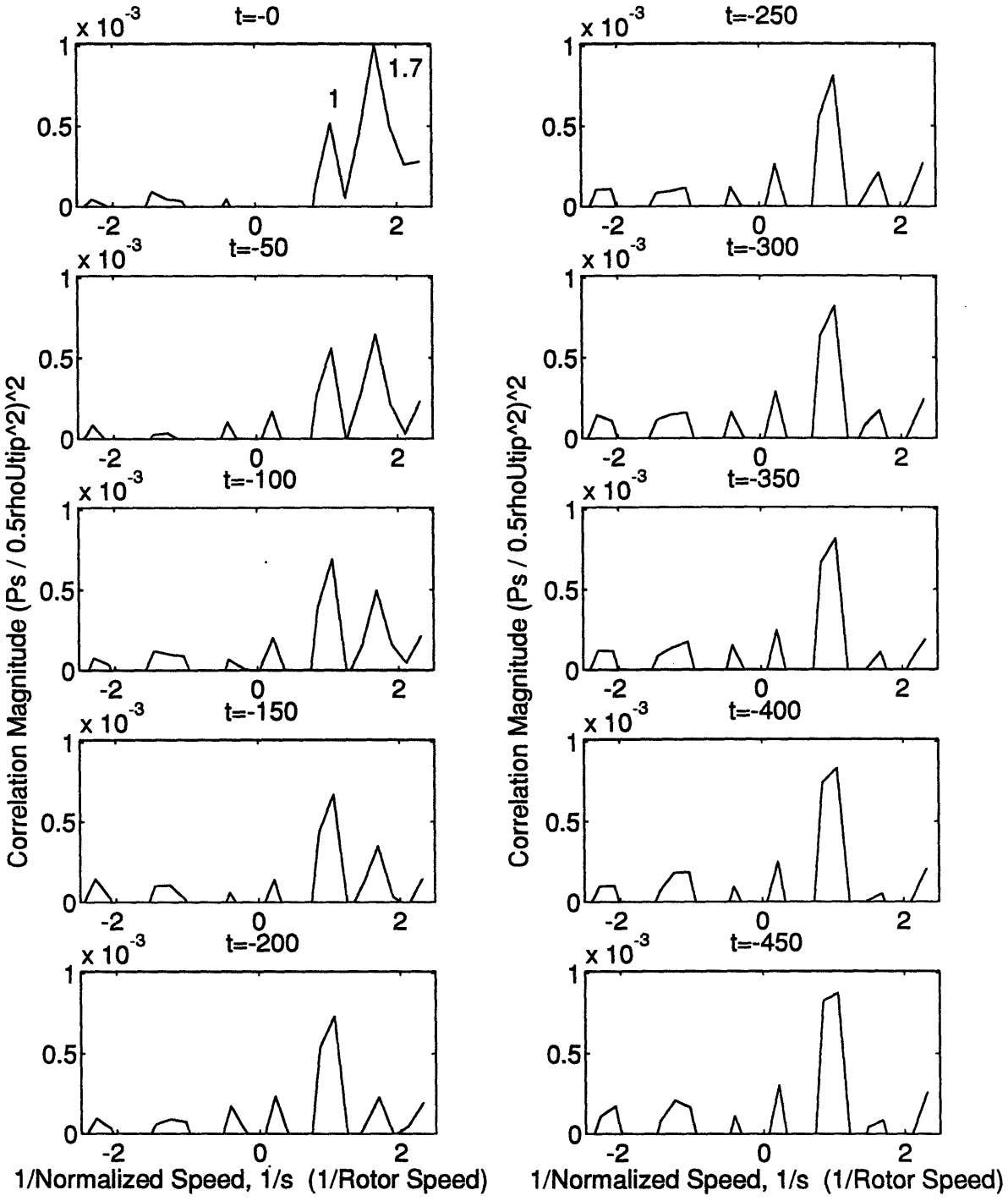

Figure 3.8 Cross-correlations of measurements in Figure 3.7 for sequential time intervals up to stall point (t = -0). Note the growth in height of the peak at 1/s = 1.7.

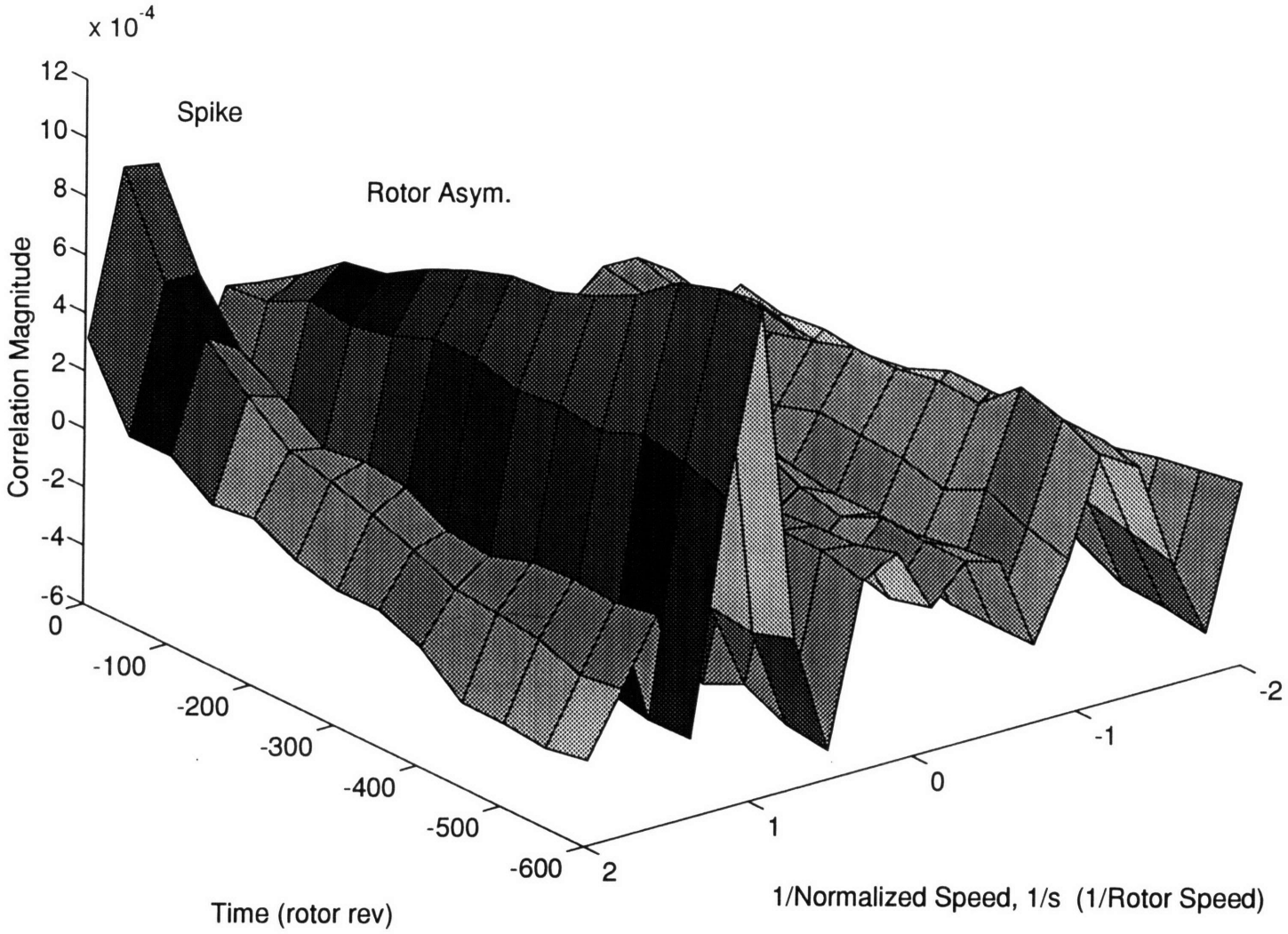

Figure 3.9 Surface plot of the cross-correlations in Figure 3.8. Note that only the peak at the propagation rate of a spike is growing in amplitude.

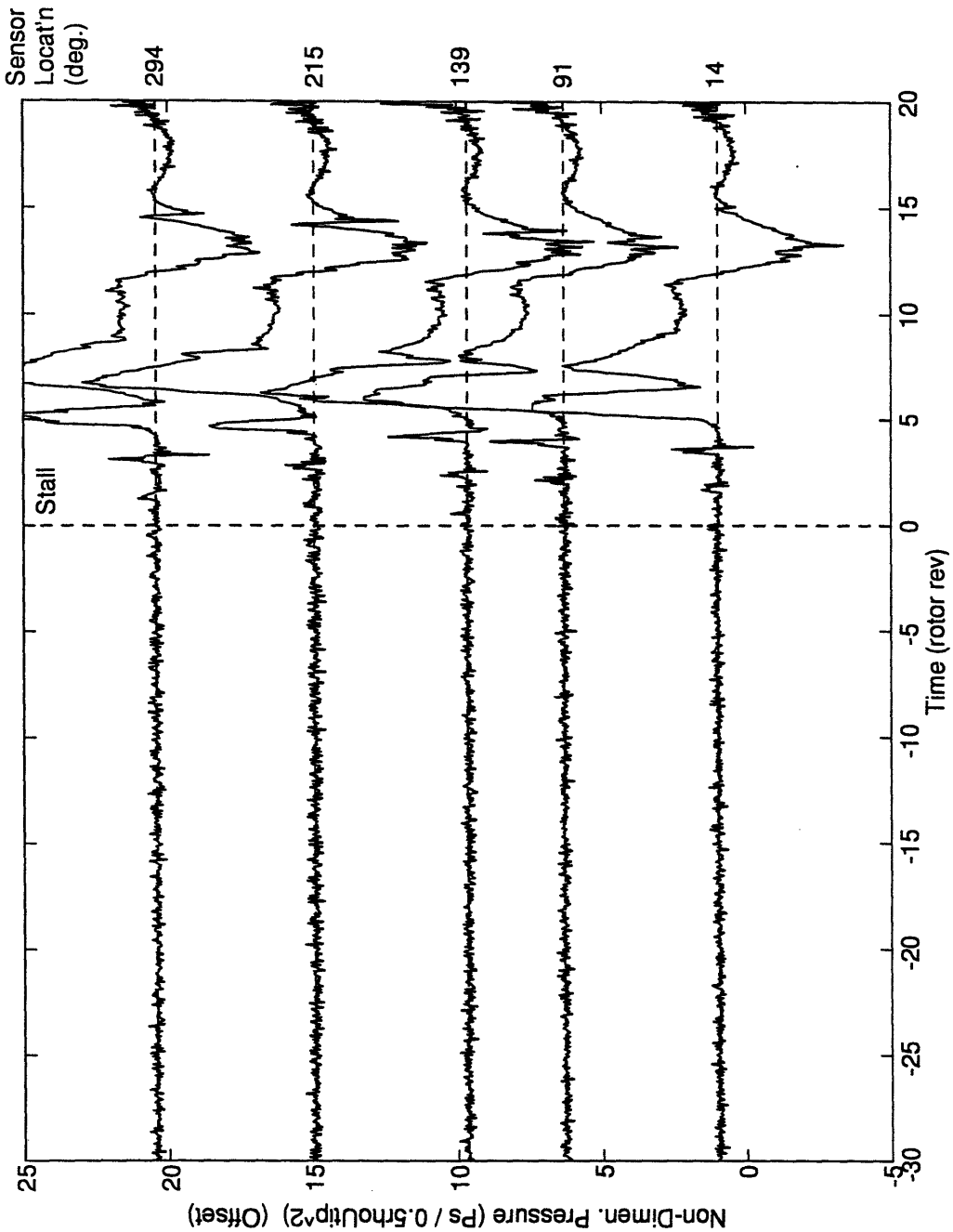

Figure 3.10 Casing static pressure traces at 1st stage rotor inlet of the Viper compressor at 83% of corrected speed. Stall point is marked by a dashed line.

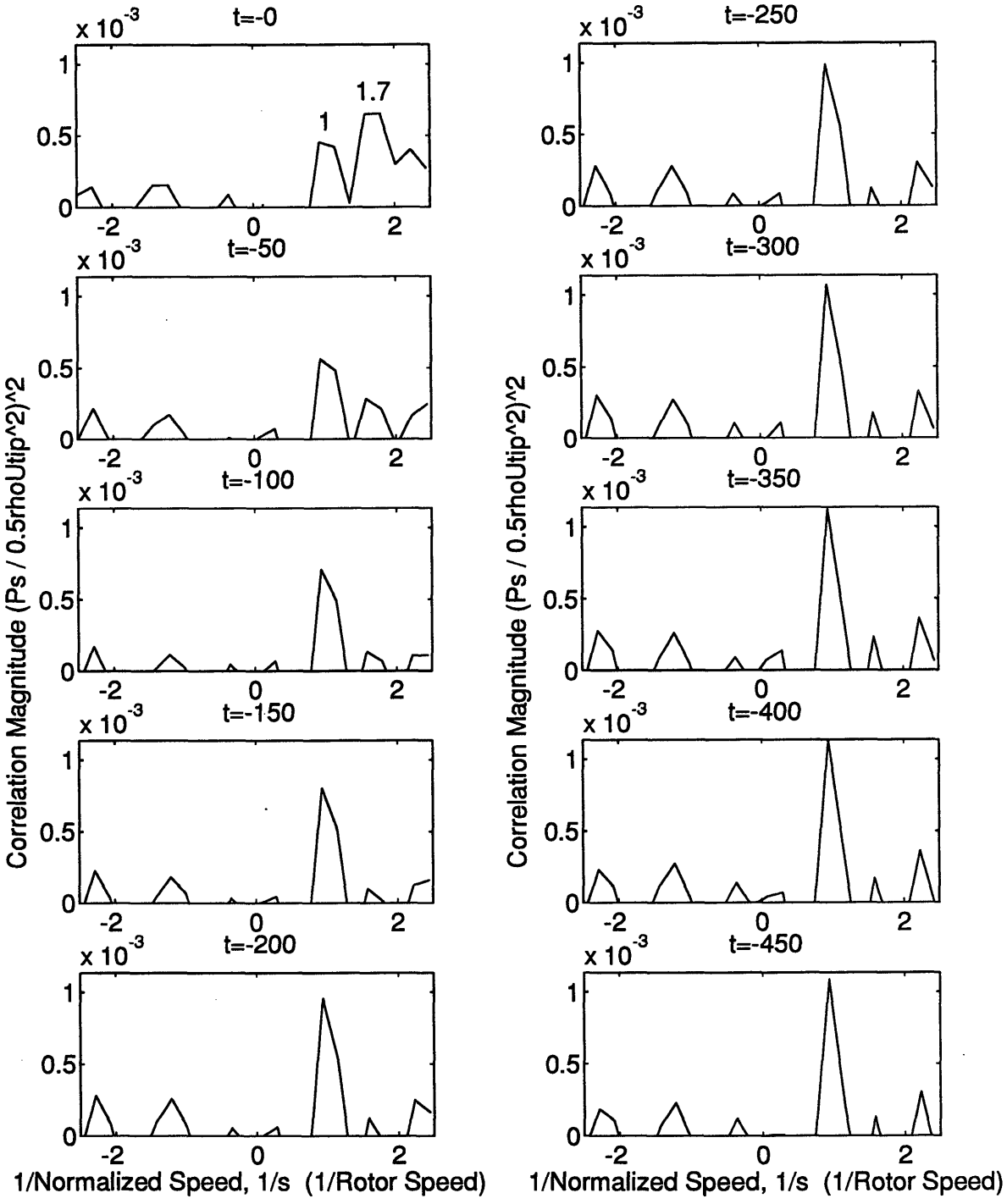

Figure 3.11 Cross-correlations of measurements in Figure 3.10 for sequential time intervals up to stall point (t = -0). Note the growth in height of the peak at 1/s = 1.7.

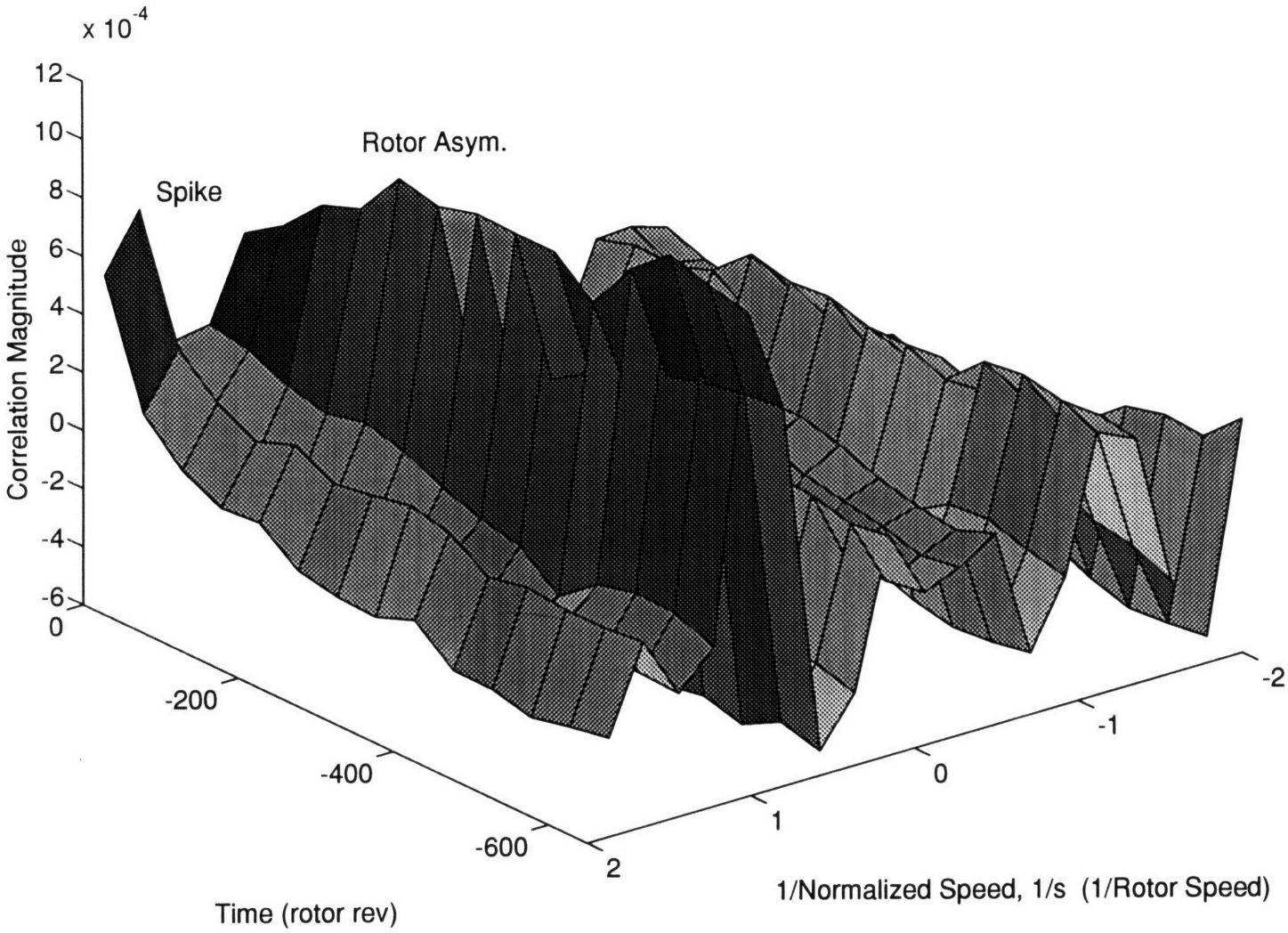

Figure 3.12 Surface plot of the cross-correlations in Figure 3.11. Note that only the peak at the propagation rate of a spike is growing in amplitude.

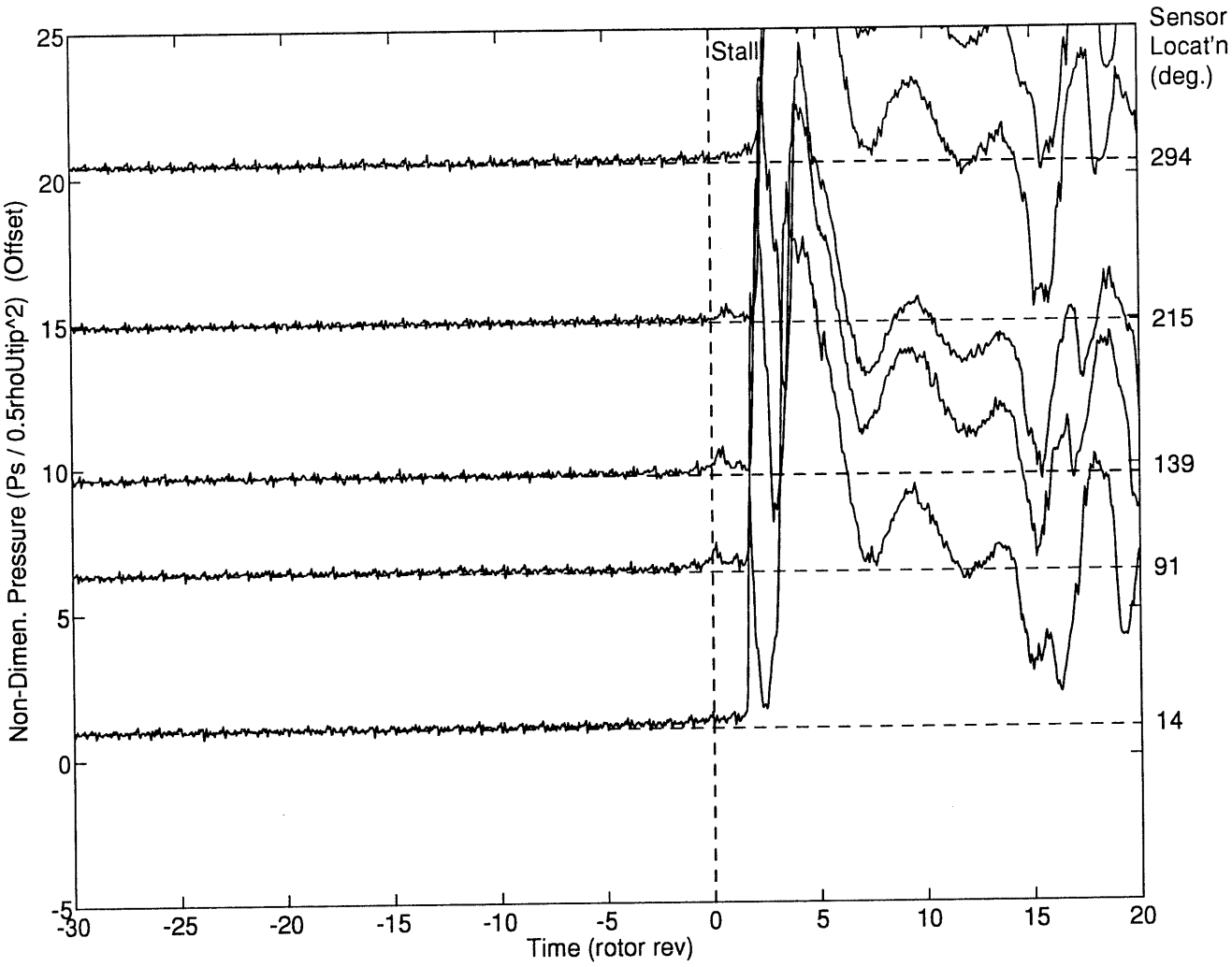

Figure 3.13 Casing static pressure traces at 1st stage rotor inlet of the Viper compressor at 98% of corrected speed. Stall point is marked by a dashed line.

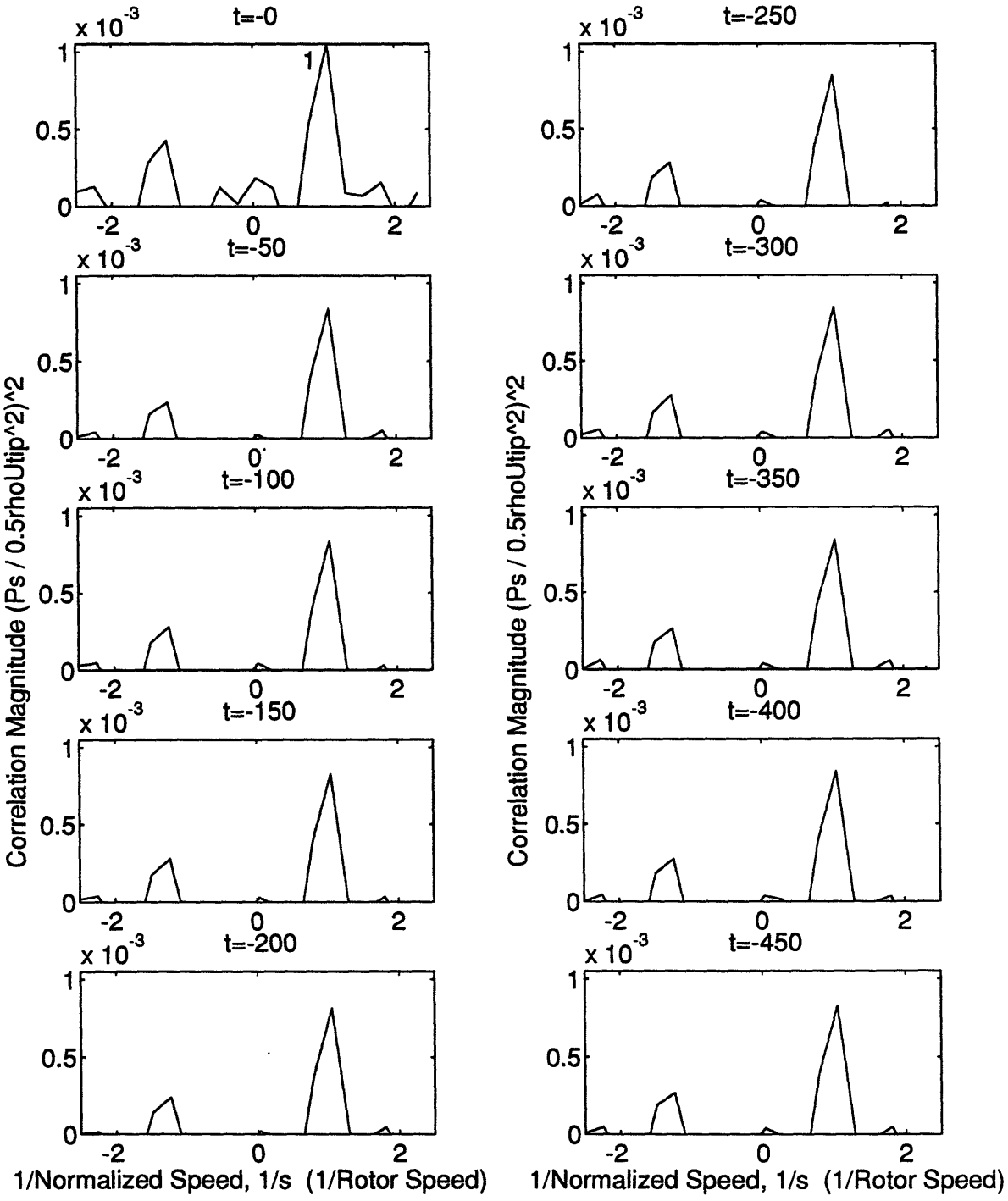

Figure 3.14 Cross-correlations of measurements in Figure 3.13 for sequential time intervals up to stall point (t = -0). No peak is seen growing in amplitude as the compressor approaches stall.

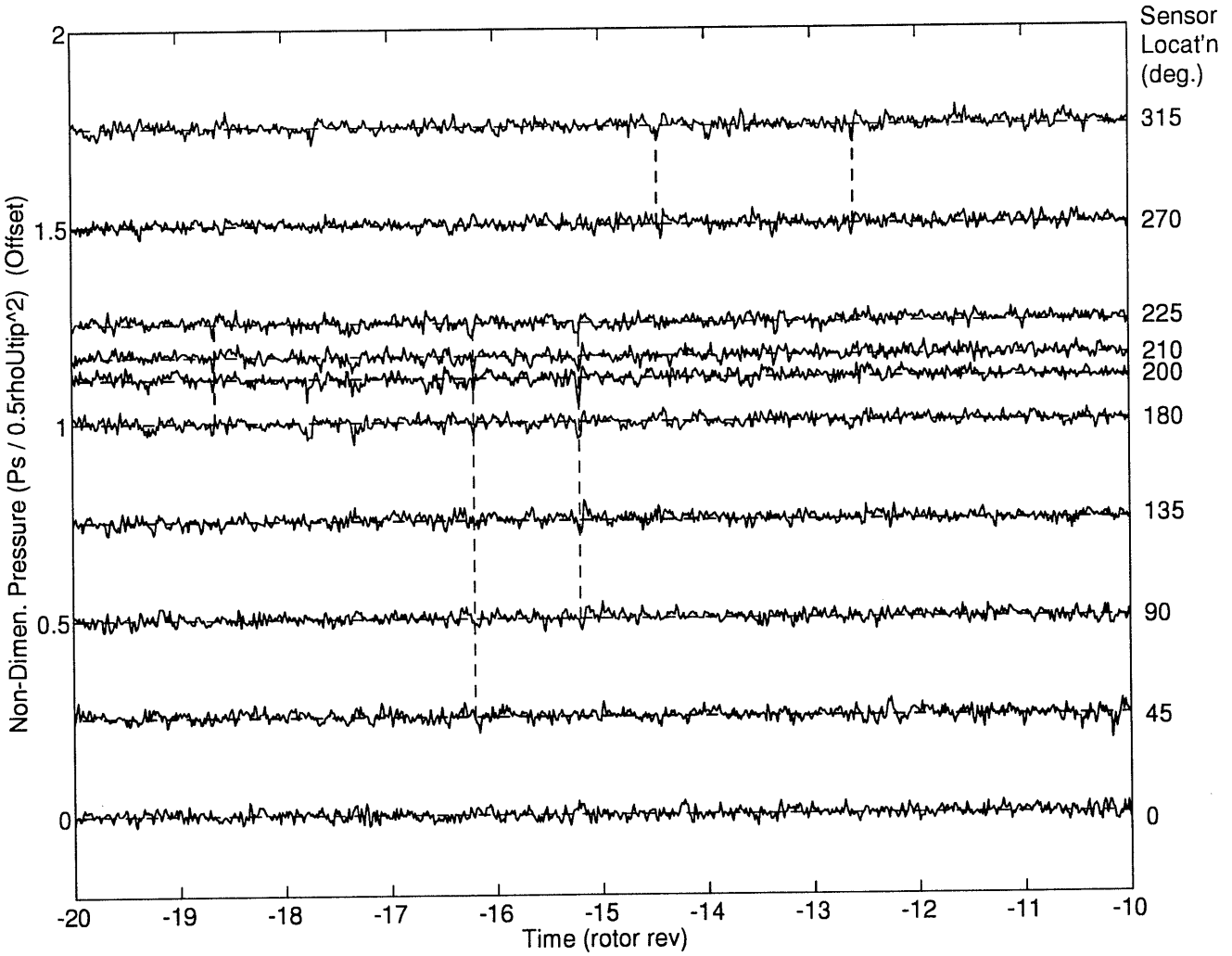

Figure 3.15 Illustration of frequent formation and decay of spikes close to stall. The pressure traces are shifted relative to the first pressure trace such that any disturbance traveling at 71% of rotor speed line up in a vertical line. Guide lines are drawn to identify propagating spikes.

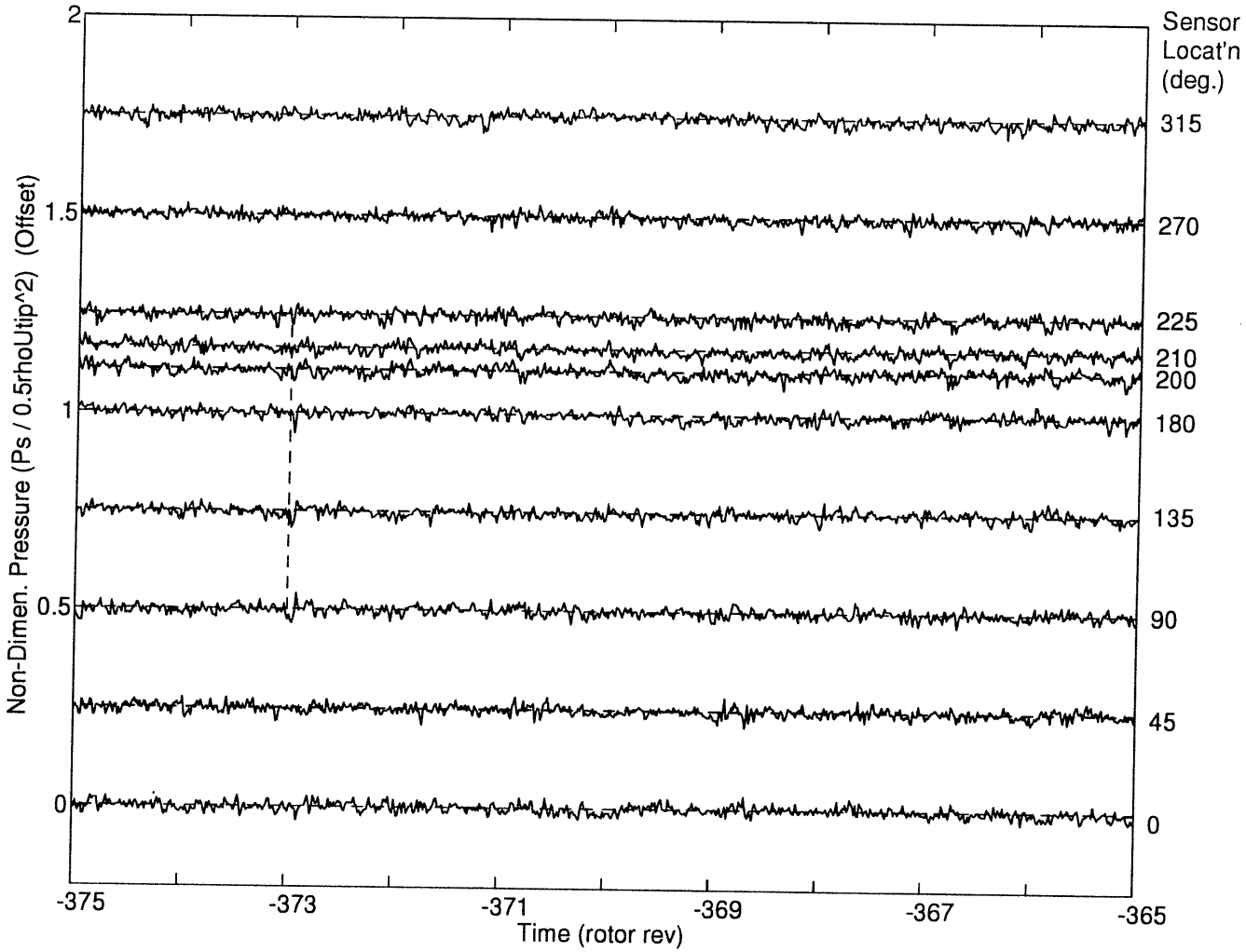

Figure 3.16 Illustration of formation and decay of spikes far from stall. The pressure traces are shifted relative to the first pressure trace such that any disturbance traveling at 71% of rotor speed line up in a vertical line. Guide line is drawn to identify a propagating spike.

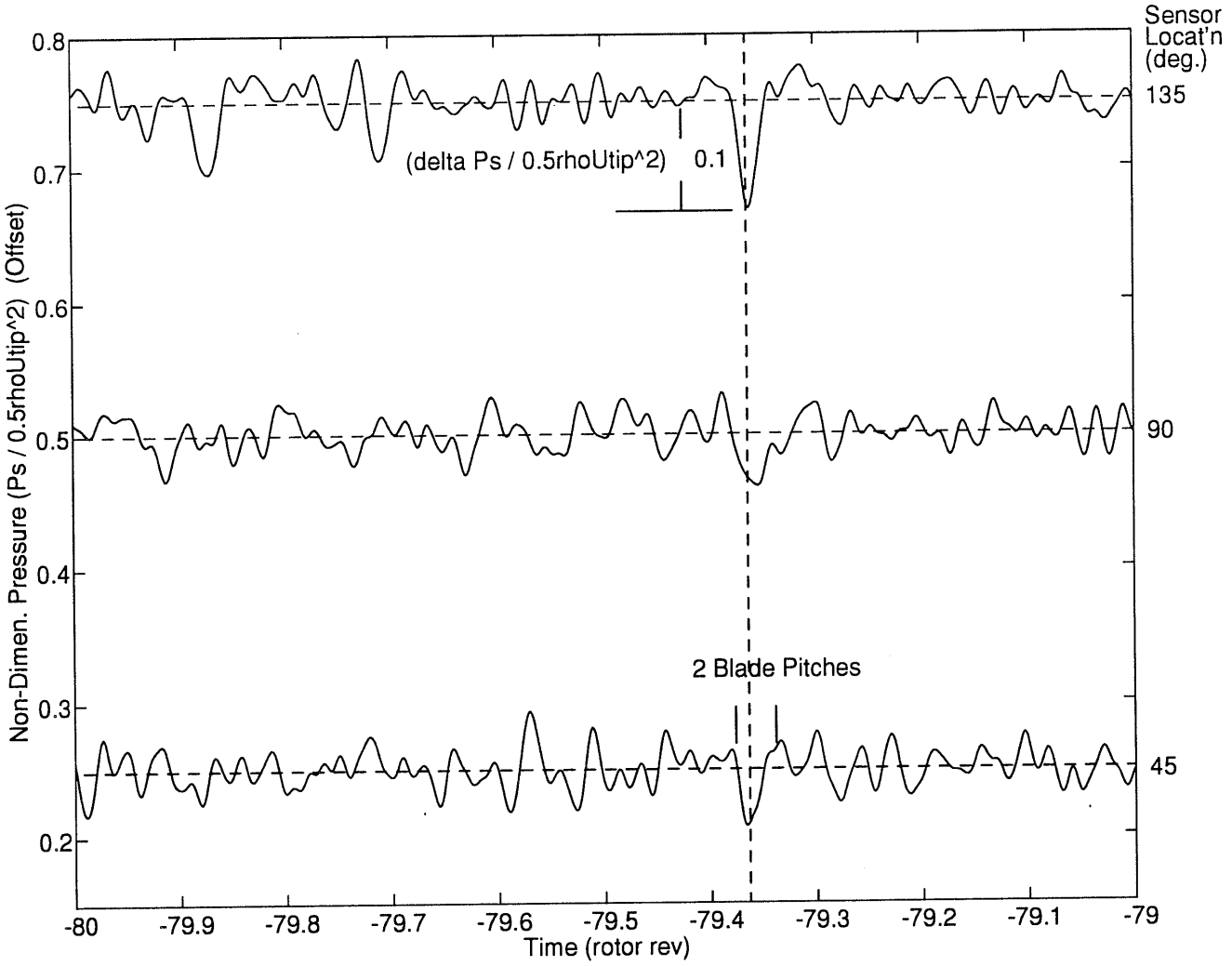

Figure 3.17 Illustration of circumferential size and pressure perturbation amplitude of a spike. The pressure traces are shifted relative to the first pressure trace such that any disturbance traveling at 71% of rotor speed line up in a vertical line. The spike is about 2 blades pitches wide and has pressure perturbation amplitude of about (delta P / 0.5rhoUtip^2) ≈ 0.1.

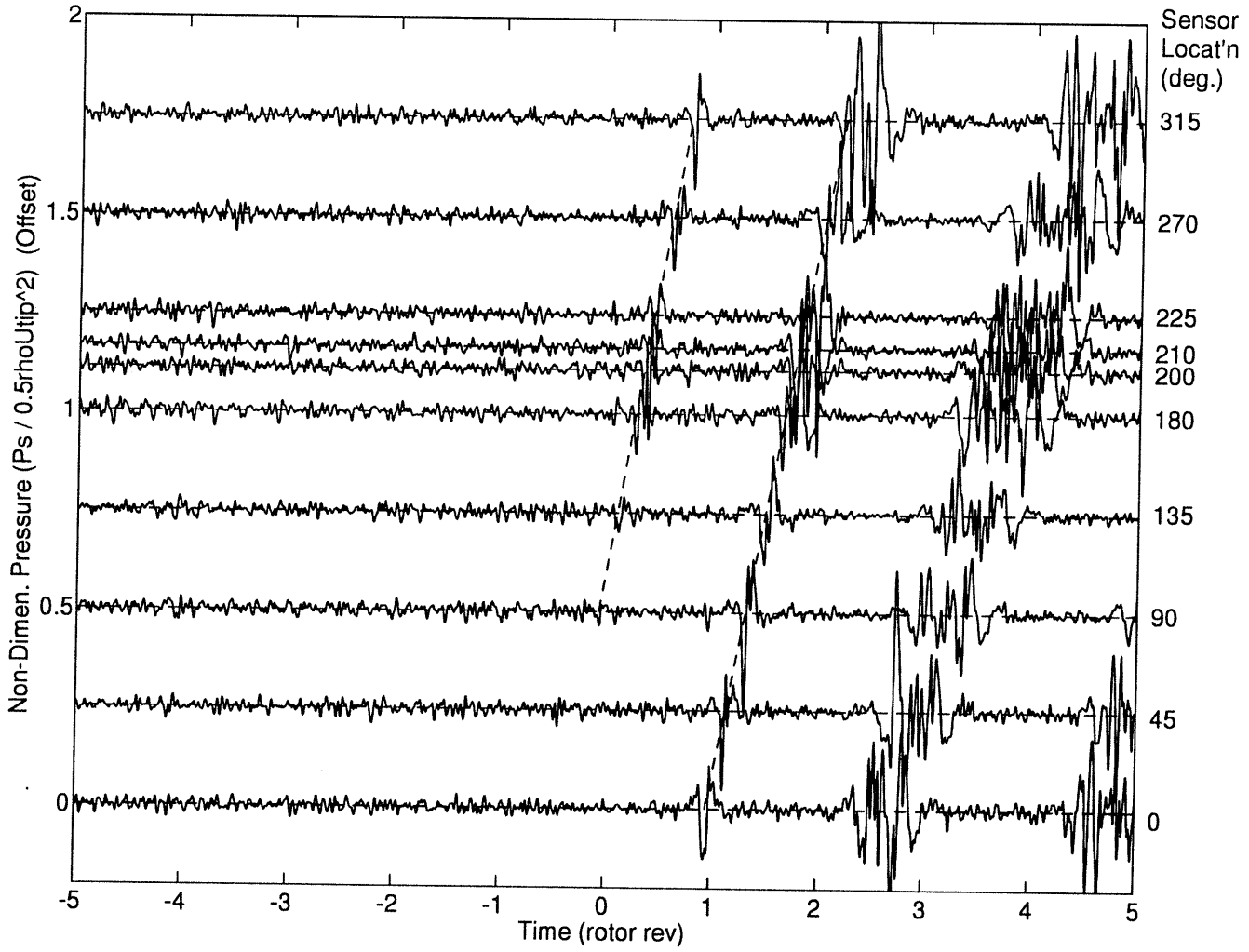

Figure 3.18 A spike growing larger in amplitude than allowable for compressor stability and growing into a stall cell.

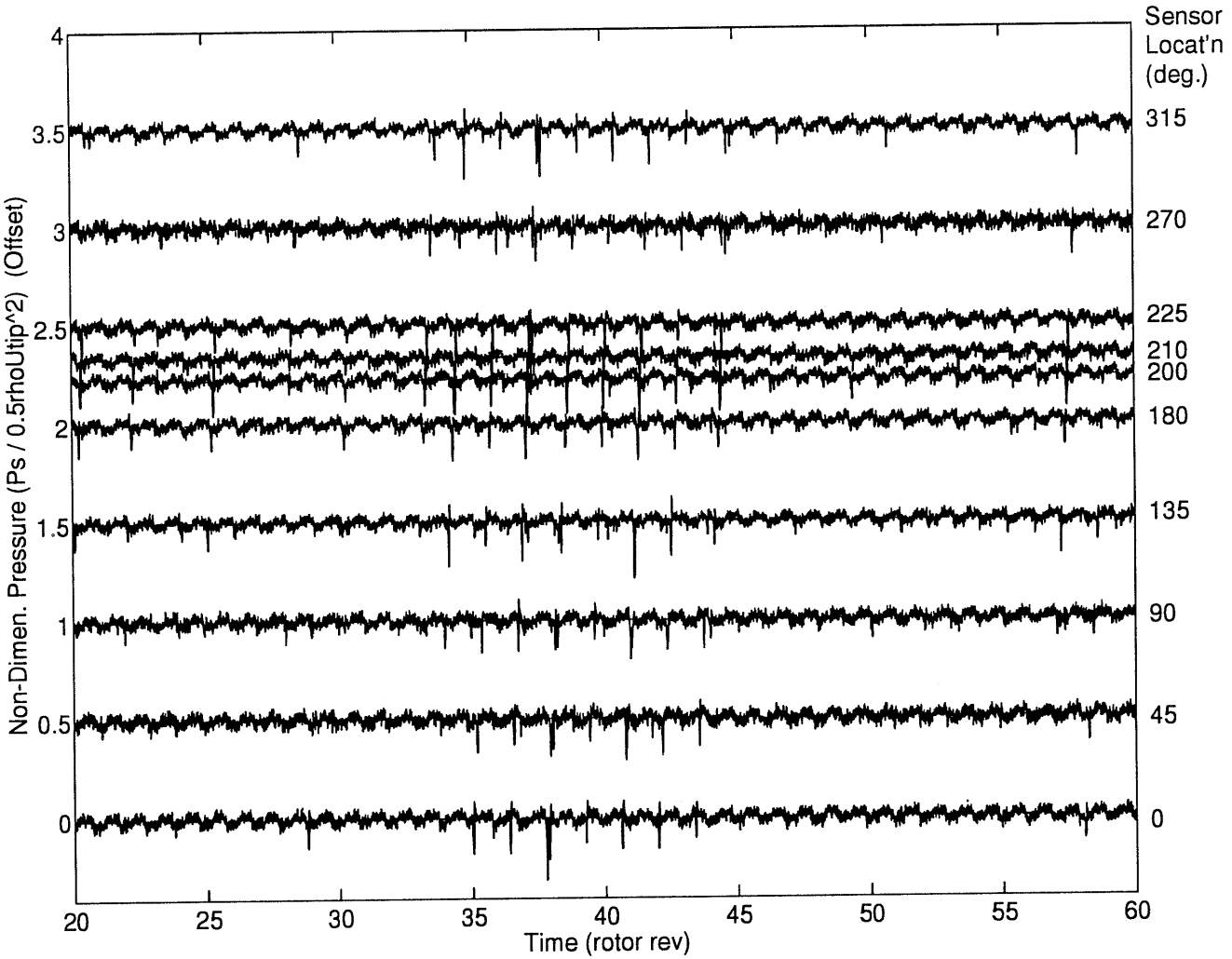

Figure 3.19 Casing static pressure traces showing large amplitude spikes propagating around the annulus of a mismatched compressor.

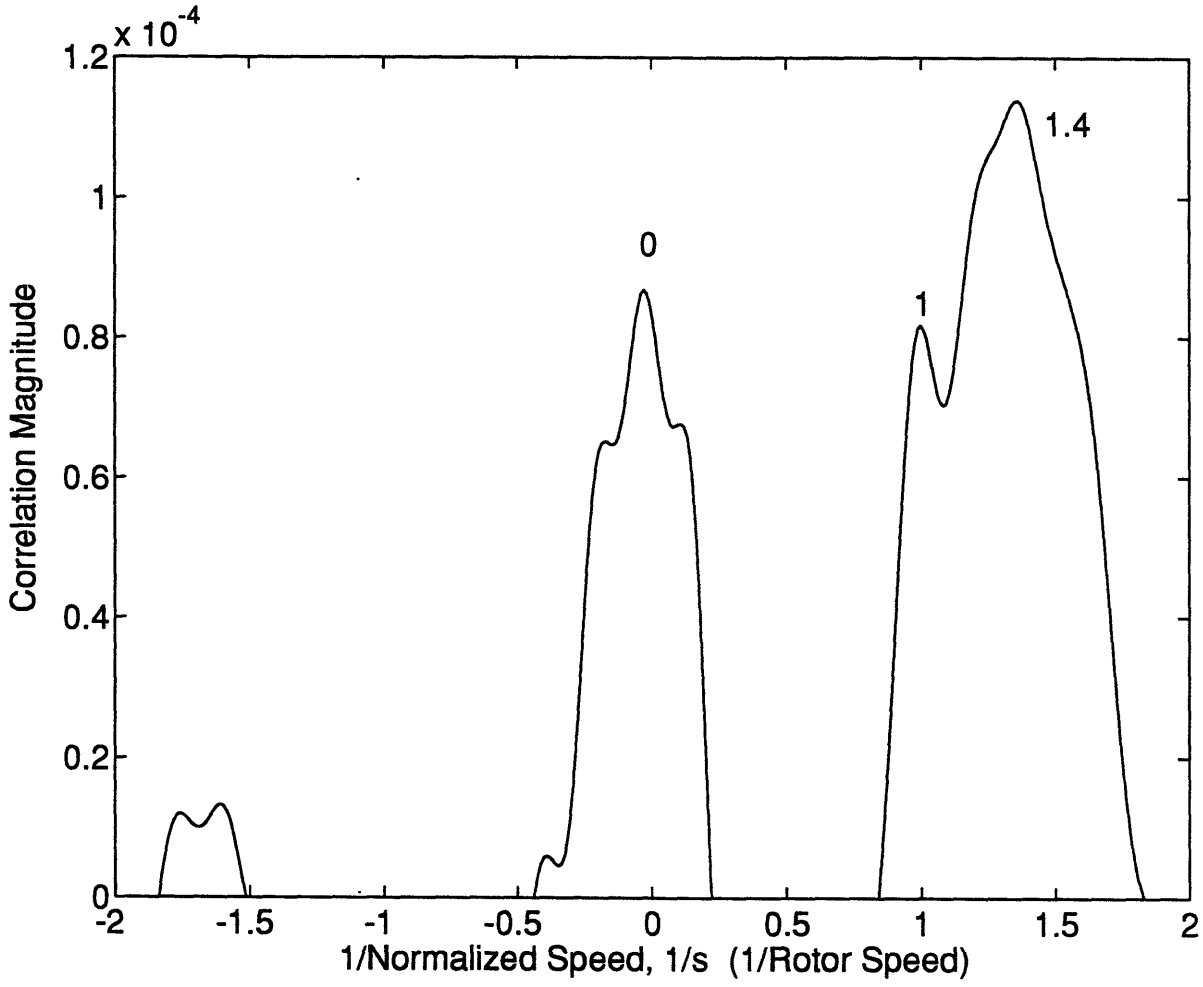

Figure 3.20 Example of clarity of the cross-correlation peak associated with a spike precursor for an array of casing static pressure transducers at 1st stage rotor exit.

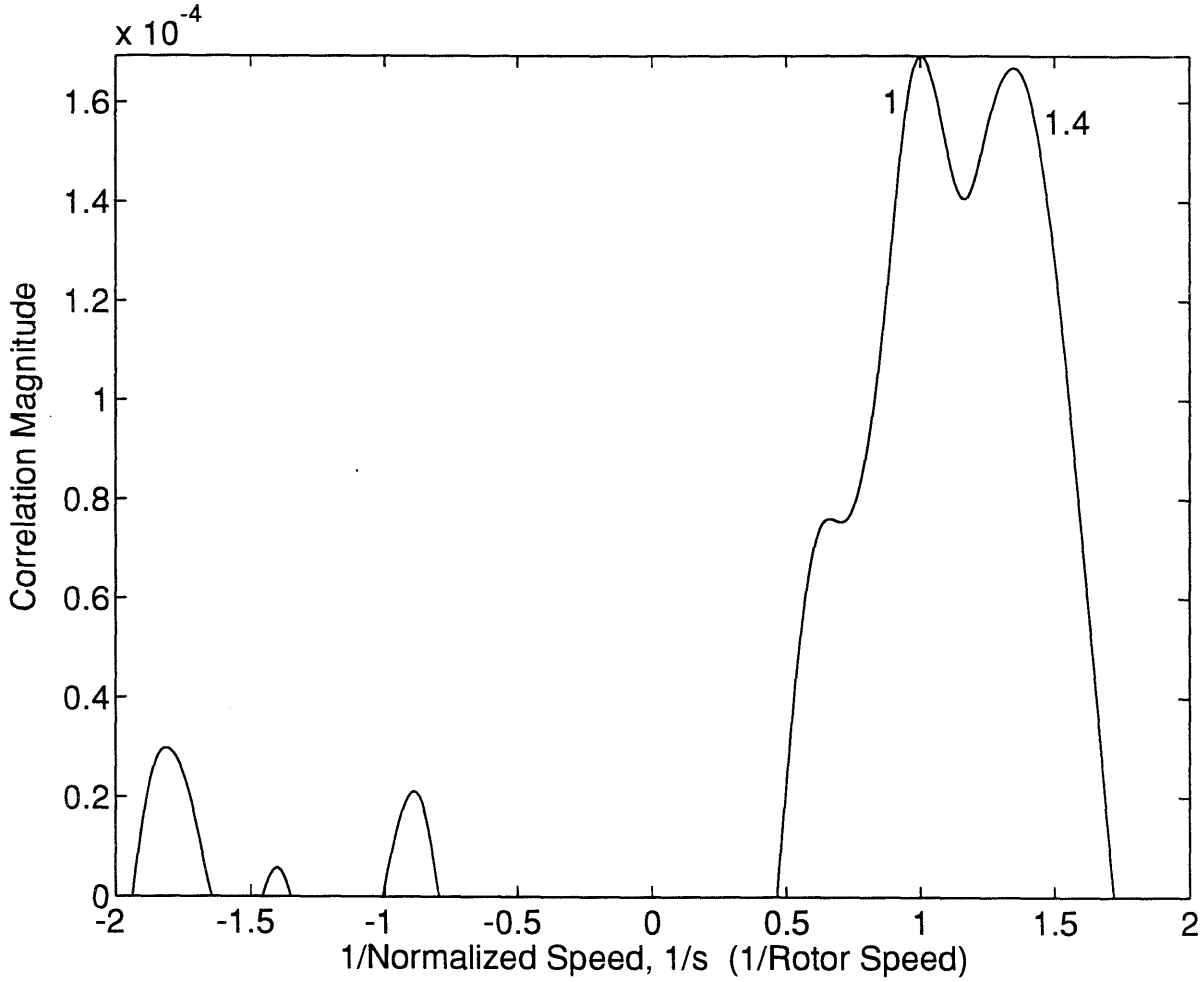

Figure 3.21 Example of clarity of the cross-correlation peak associated with a spike precursor for an array of hot-wire anemometers placed near the blade tip at 1st stage rotor exit.

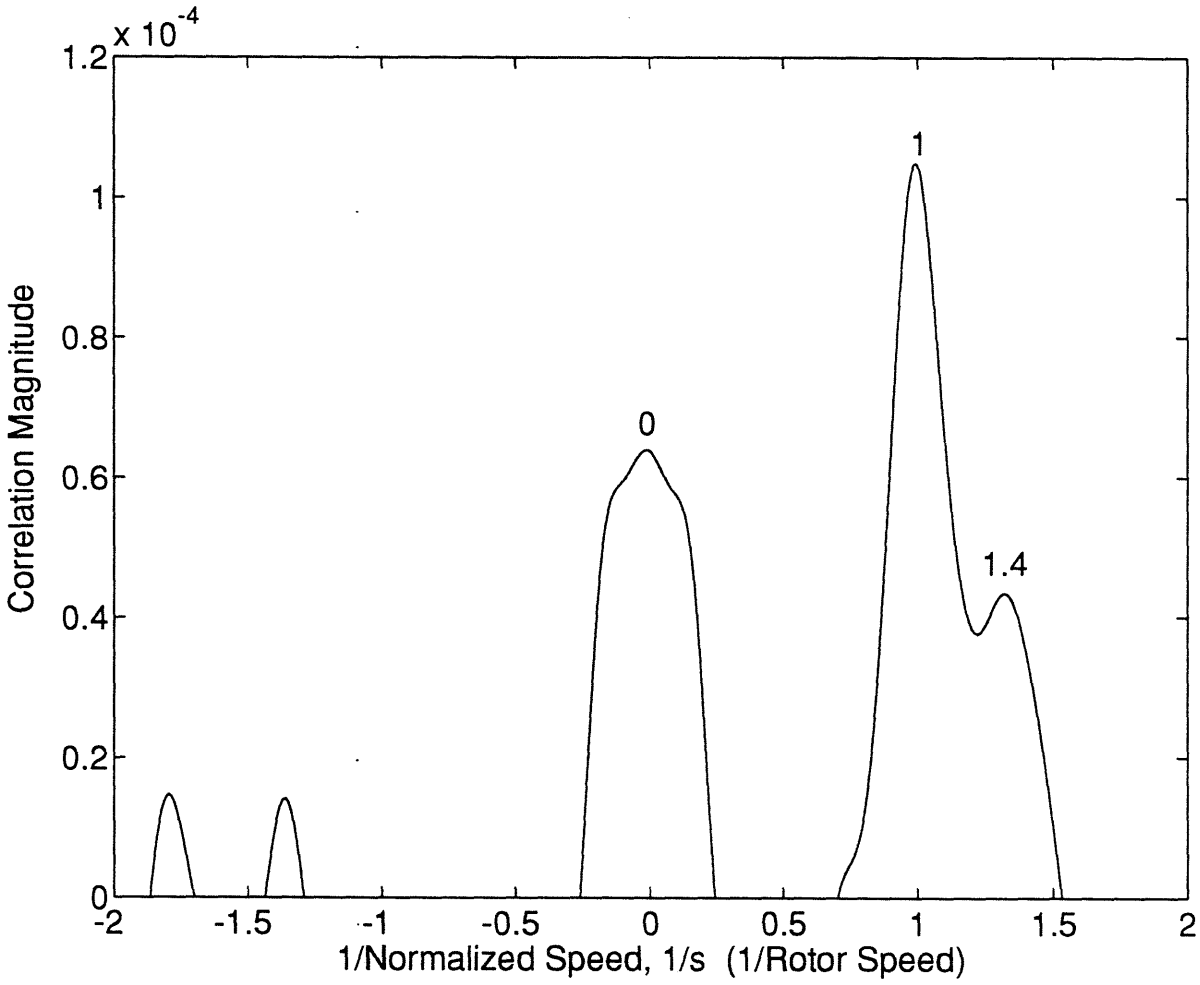

Figure 3.22 Example of clarity of the cross-correlation peak associated with a spike precursor for an array of casing static pressure transducers at 1st stage rotor inlet.

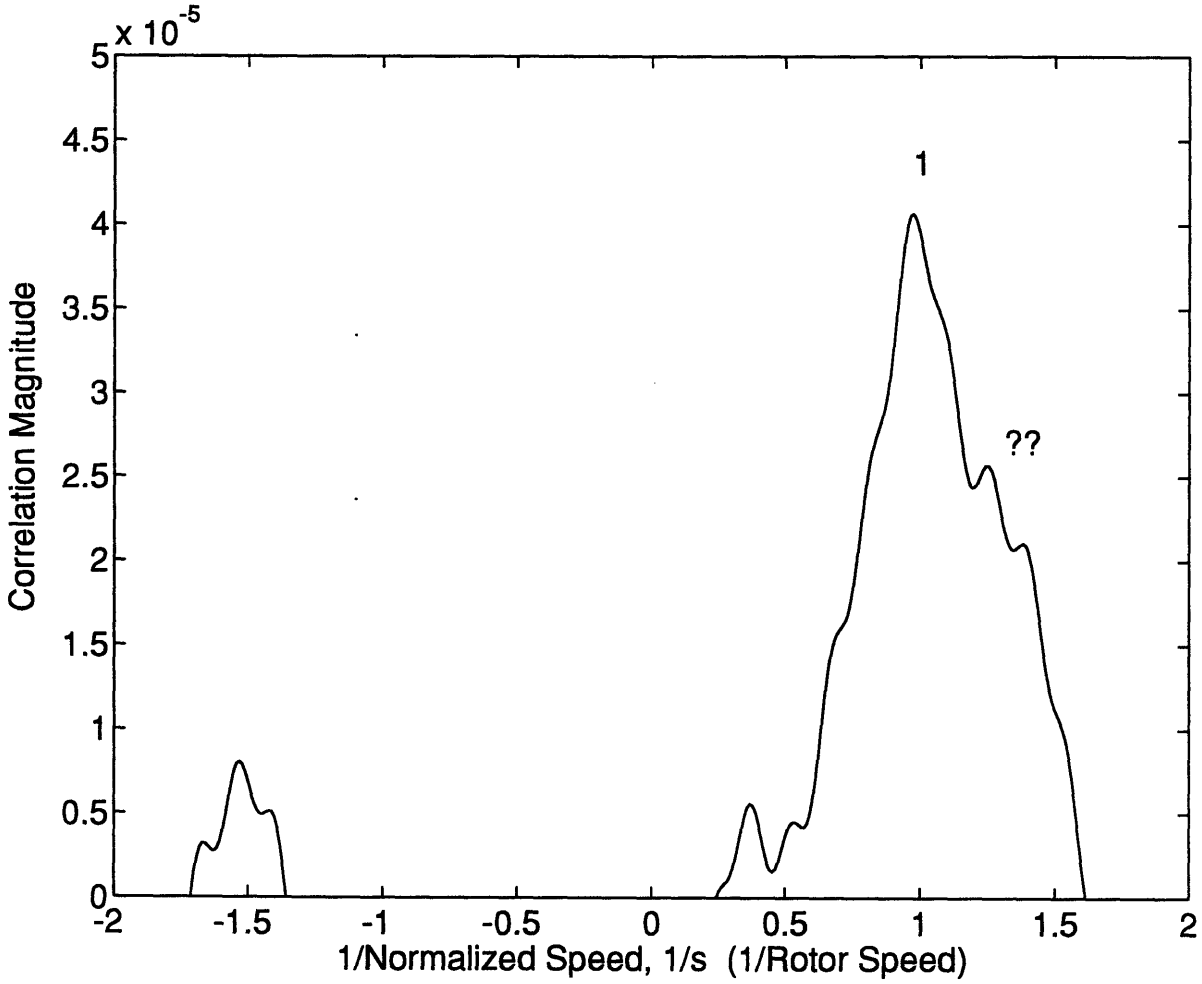

Figure 3.23 Example of clarity of the cross-correlation peak associated with a spike precursor for an array of hot-wire anemometers placed near the blade tip at 1st stage rotor inlet. Note the lack of discernible peak associated with a spike.

CHAPTER FOUR

MIT THREE STAGE COMPRESSOR EXPERIMENTS

4.1 Introduction

This chapter describes two sets of experiments conducted on the MIT Three Stage compressor to examine the conditions under which spikes may develop. As suggested by Day [16], a set of experiments was carried out to investigate the influence of the first stage pressure rise characteristic or whether increasing the pressure rise of the first stage relative to the other stages would yield conditions favorable to the formation of spikes.

A second set of experiments addresses whether spike disturbances develop in the MIT Three Stage compressor, and more importantly whether it is the cause of instability when the compressor is operated below the natural stalling flow rate under active control.

4.2 Experimental Facility

The two experiments presented in this chapter were conducted at the MIT Three Stage compressor facility [14]. The configuration is a research compressor originally designed (and tested) at Pratt & Whitney with a constant cross-sectional area and a hub-to-tip ratio of 0.88. The stalling characteristics of the compressor have been investigated by Gamache [15], Lavrich [9], and Garnier [3], and the use of active control for increasing the stable flow range has been demonstrated by Haynes [7]. The layout of the compressor is shown in Figure 4.1. The compressor has a short bell mouth

inlet duct and a long exit duct with an exhaust fan at the end. The exhaust fan was allowed to free-wheel during the present experiments.

The compressor is equipped with 12 movable servo-controlled guide vanes, or SGV's (Figure 4.2). These SGV's, which can swing ± 70°, are just downstream of the original IGV's which have a fixed stagger angle of 8.1° (Figure 4.3). The SGV's are used for active feedback control of rotating stall as well as for changing the mean inlet swirl into the first stage rotor.

4.2.1 Instrumentation

An array of hot-wire anemometers was the primary tool used to examine the time dependent process of stall inception. The hot-wire anemometers could be placed at various axial and circumferential locations in the compressor (Figure 4.4). The typical arrangement for detecting unsteady disturbance structures was to have an array of 8 hot-wire anemometers ahead of the IGV's and another array downstream of the first stage rotor. The hot-wire anemometers were radially located near the tip region to detect possible formation of spike type disturbances.

The hot-wire anemometer signals are digitized using a PC-controlled 16-bit analog-to-digital converter. The sampling rate for the experiments concerning the pressure rise of the first stage (Section 4.3) was 2.5 kHz with lowpass filtering at 1kHz. The compressor was set to run at 1800 RPM which produces rotor blade passing frequency of 1620 Hz. The sampling rate is sufficient to resolve a short wavelength disturbance having a length scale of order of several blade pitches.

The sampling rate used during active control experiments was limited to 500 Hz with lowpass filtering at 200 Hz. This is because the computer can complete the tasks of controlling the compressor and acquiring the hot-wire anemometer data at a maximum rate of 500 Hz. The compressor was ran at 2400 RPM during the active control experiments, corresponding to a blade passing frequency of 2160 Hz. The sampling rate is thus too low to resolve a short wavelength disturbance of the scale of few blade pitches; a spike traveling at 70% of rotor speed will not be detectable until it grows to a circumferential size of about 10 blade pitches or 20% of the annulus. The presence of spikes cannot be firmly established from the data acquired during the active control experiments.

4.3 First Stage Pressure Rise Experiments

The first set of experiments has been conducted to examine if increasing the first stage pressure rise relative to the other stages would create a condition favorable to the formation of spikes. This idea was set forth by Day [16] from his observations in experiments conducted at the Whittle Laboratory. Because spikes are localized disturbances developing in the first stage, the operating point of the first stage is likely to be important for their formation. If the stability of the first stage is decreased relative to the other stages, it may be that disturbances local to the first stage will develop.

To assess Day's hypothesis, the stagger angle of the SGV's on the MIT Three Stage compressor was decreased to reduce the flow swirl into the first stage rotor. This results in an increase in the pressure rise of the first stage

which can reduce the stability of the stage. The compressor was not set to be under active control so the stagger angle of the SGV's was held constant.

The experiments did not show the formation of spikes. One possible reason for this result is that enough relative destabilization of the first stage cannot be achieved on the MIT Three Stage compressor because the first stage was much more stable than that of the other stages initially. The operating point of the first stage may thus not have been altered enough to a level to result in adequate destabilization of the stage.

4.3.1 Pressure Rise Characteristics

The pressure rise characteristics of the first stage are presented in Figure 4.5. The nominal first stage pressure rise is achieved when the stagger angle is at 8.2° and the maximum achievable pressure rise at -15.0°. The plots of individual static pressure rises (Figures 4.6 - 4.8) show that the first stage has relatively lower static pressure rise than the other two stages at nominal SGV stagger angle. When the SGV's are turned to maximum stagger angle of -15.0, the static pressure rise of the first stage is increased to a level higher than that of the last two stages.

4.3.2 Disturbance Structures

For all levels of first stage pressure rise, the MIT Three Stage compressor exhibits modal wave type stall inception. The instantaneous axial velocities behind the first stage rotor obtained by an array of 8 equally spaced hot-wire anemometers are shown in Figures 4.9 - 4.11 for SGV stagger angles of 8.2°, -5.0°, and -15.0°, respectively. Modal wave disturbances are clearly

visible for all SGV stagger angles in the raw velocity traces. The PSD's of the spatial Fourier harmonic coefficients (SFHC) are shown in Figures 4.12 - 4.14 for each stagger angle. The PSD's show that the first mode of the modal wave, propagating at 30% of rotor speed, is present even when the pressure rise of the first stage is increased above the pressure rise of the latter two stages (i.e. -15.0 ° SGV stagger angle).

There is a possibility that short wavelength disturbances (spikes) do exists but are too small to be observed. After filtering of the modal waves, cross-correlations were tried to detect the presence of spikes. The cross-correlation results, which are shown in Figures 4.15 - 4.17, show no evidence of any disturbance traveling near 70% of rotor speed (the expected propagation rate of a spike) for any SGV stagger angle.

4.3.3 Discussion

Failure to produce spikes may be due to lack of sufficient change in the first stage operating point to destabilize the stage prematurely. The pressure rise is determined by the flow swirl into the first stage generated by the SGV's, but the amount of swirl is limited by flow separation on the SGV's. A better compressor to test is one which already has a relatively high first stage loading. An even better compressor to test is one which can be mismatched by closing the rotors of the latter stages. It has already been demonstrated that a mismatched compressor will operate with an unstable first stage in [12]. With mismatching, the relative loading of the first stage can be increased without being limited by IGV flow separation. Under such operating

conditions, a compressor which exhibits modal wave may begin exhibiting spikes.

4.4 Acoustic Disturbances in An Actively Controlled Compressor

Even under active control where the modal waves are suppressed, the MIT Three Stage compressor becomes unstable after certain level of flow reduction. Haynes [7] attributed this instability to the inadequacy of the controller (constant gain) in continued suppression of the modal waves as the mass flow is reduced. However, recent attempts by Weigl [17] failed to extend the operating range of the compressor any further even with a more advanced H_∞ controller. The H_∞ controller was able to suppress better the modal waves until the identical mass flow rate achieved by the constant gain controller at which point the compressor would suddenly develop an instability. Thus a set of experiments was conducted on the MIT Three Stage compressor to determine: 1) why the compressor becomes unstable while operating under active control, and 2) whether the instability is caused by a localized disturbance in the first stage.

4.4.1 Experimental Results

As the compressor is throttled down into stall while operating under active control, an acoustic type disturbance, not a localized disturbance, is observed growing in amplitude. While the sampling rate is too low to absolutely determine whether there were any localized disturbance structures (Section 4.2.1), there was no evidence of the latter in the velocity traces downstream of the first stage rotor (Figure 4.18) or in the cross-correlation

plot (Figure 4.19). The single lobe disturbance in Figure 4.18 is not a spike because it is too slow, only 39% of rotor speed, and too large circumferentially, covering about half of the annulus.

The likely cause of stall can be found from examining the PSD's of SFHC computed from the axial velocity measurements from an array of 8 equally spaced hot-wire anemometers upstream of the IGV's (Figure 4.20 - 4.21). The PSD's show that an acoustic disturbance oscillating at 39% of rotor frequency (16 Hz) exists prior to compressor stall. As evidence of the amplitude growth of this acoustic disturbance as the compressor nears stall, the PSD's of signals from an array of 4 Kulite static pressure transducer at the compressor exit for sequential time intervals prior to stall are presented in Figure 4.22.

4.4.2 Discussion

Acoustic disturbance has been observed by Gysling [8] on the MIT single stage compressor during his active control experiments. Gysling noted that acoustic disturbances associated with a quarter wavelength standing wave developing between the inlet duct and the throttle of the compressor, although not observed during natural stall inception, may be observed when an actively controlled compressor operates in the unstable region of the map with large positive overall pressure rise slope. The set of experiments shows that an acoustic type disturbance structure, not a spike type disturbance structure, is most likely responsible for the cause of instability in the MIT Three Stage compressor operating under active control.

4.5 Summary

Two sets of experiments were conducted on the MIT Three Stage compressor to examine whether spike type disturbances develop under compressor operating conditions of higher relative first stage pressure rise and/or active control. However, the compressor, which exhibits modal wave type disturbance during stall inception, did not exhibit spikes when the pressure rise of the first stage was increased to the maximum/minimum available with the existing configuration. A possible reason for this is that destabilization of the first stage relative to the other stages cannot be achieved because the normal pressure rise of the first stage is too low. With active control, an acoustic type disturbance was observed growing prior to compressor instability. No evidence of short wavelength disturbances was found.

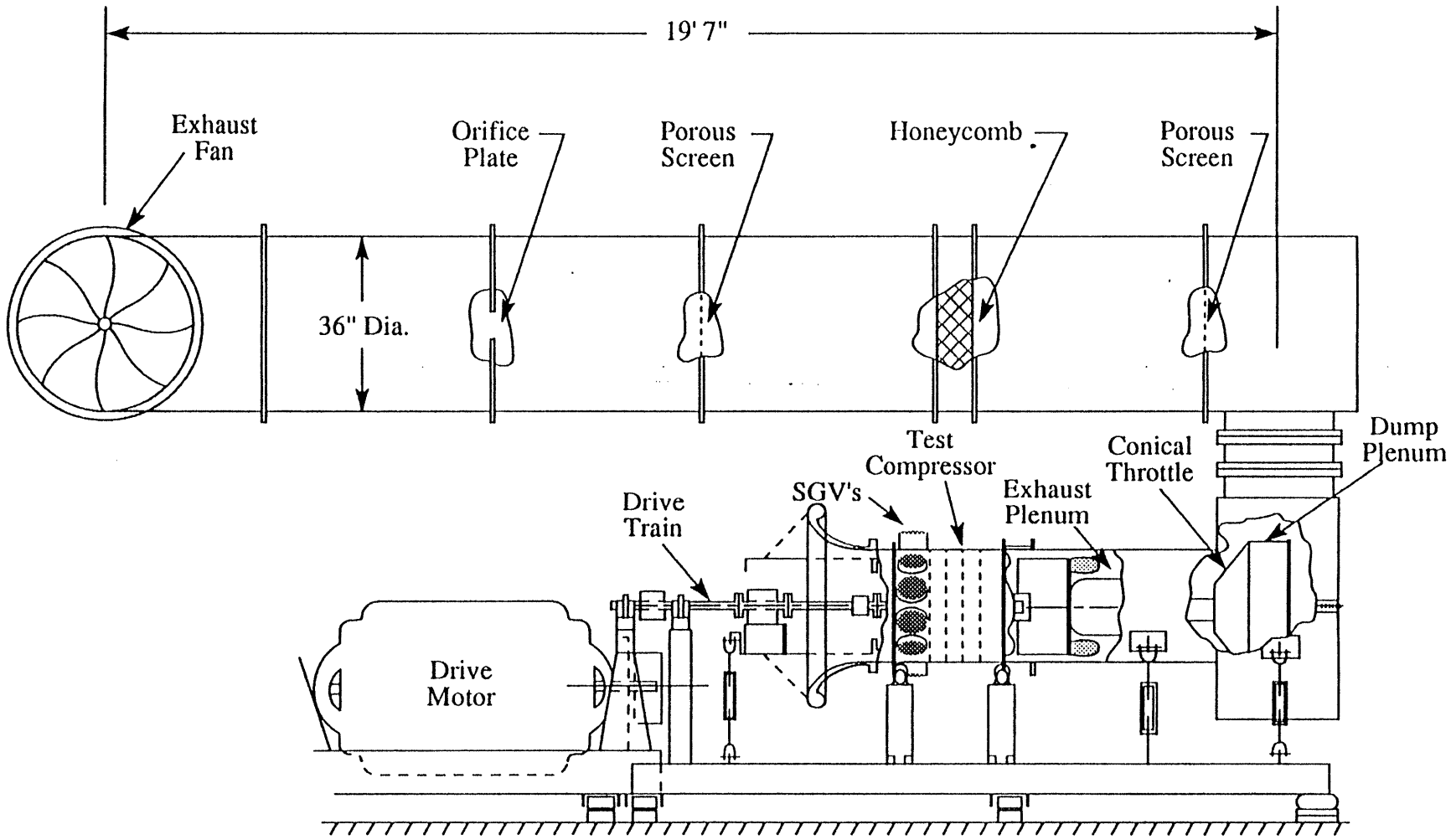

Figure 4.1 Side view schematic of the MIT Three Stage compressor facility

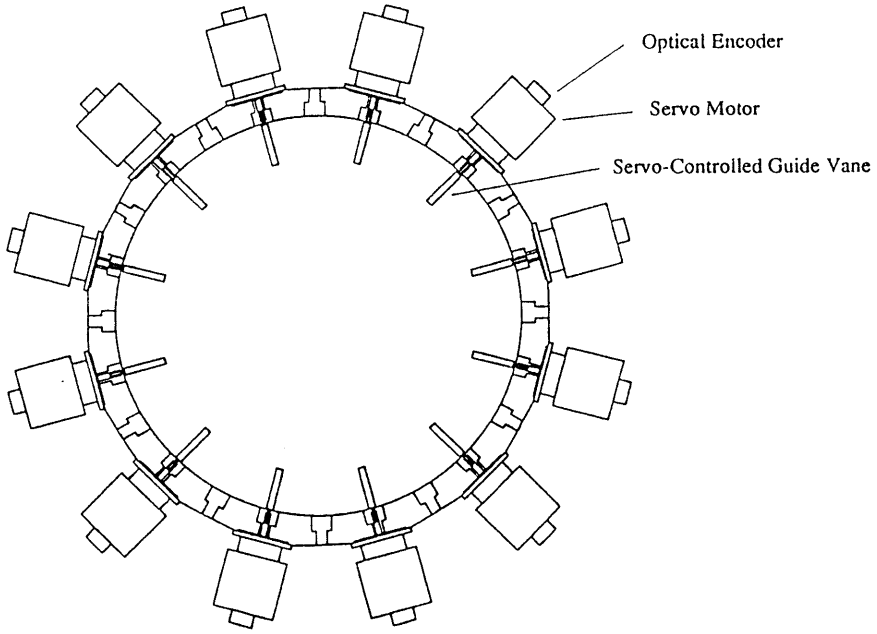

Figure 4.2 View of the Servo-Controlled Guide Vanes (SGV's)

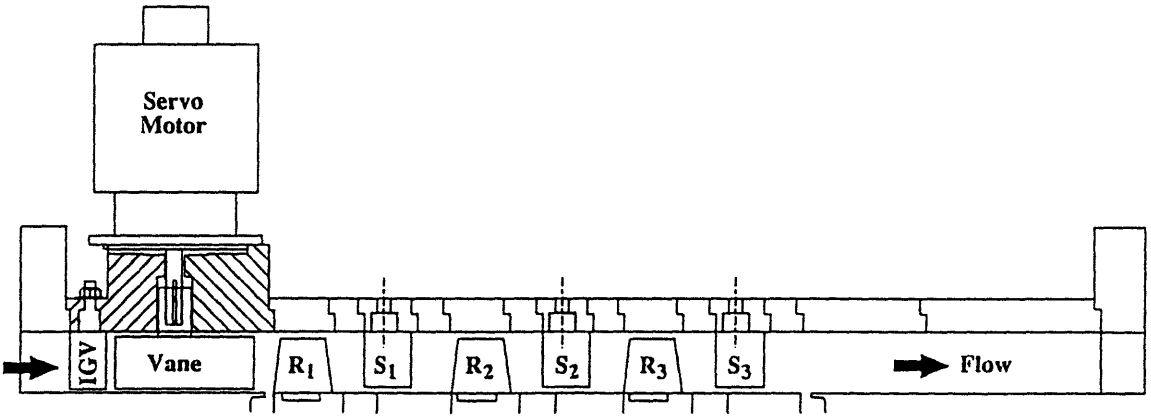

Figure 4.3 Side view of the MIT Three Stage compressor

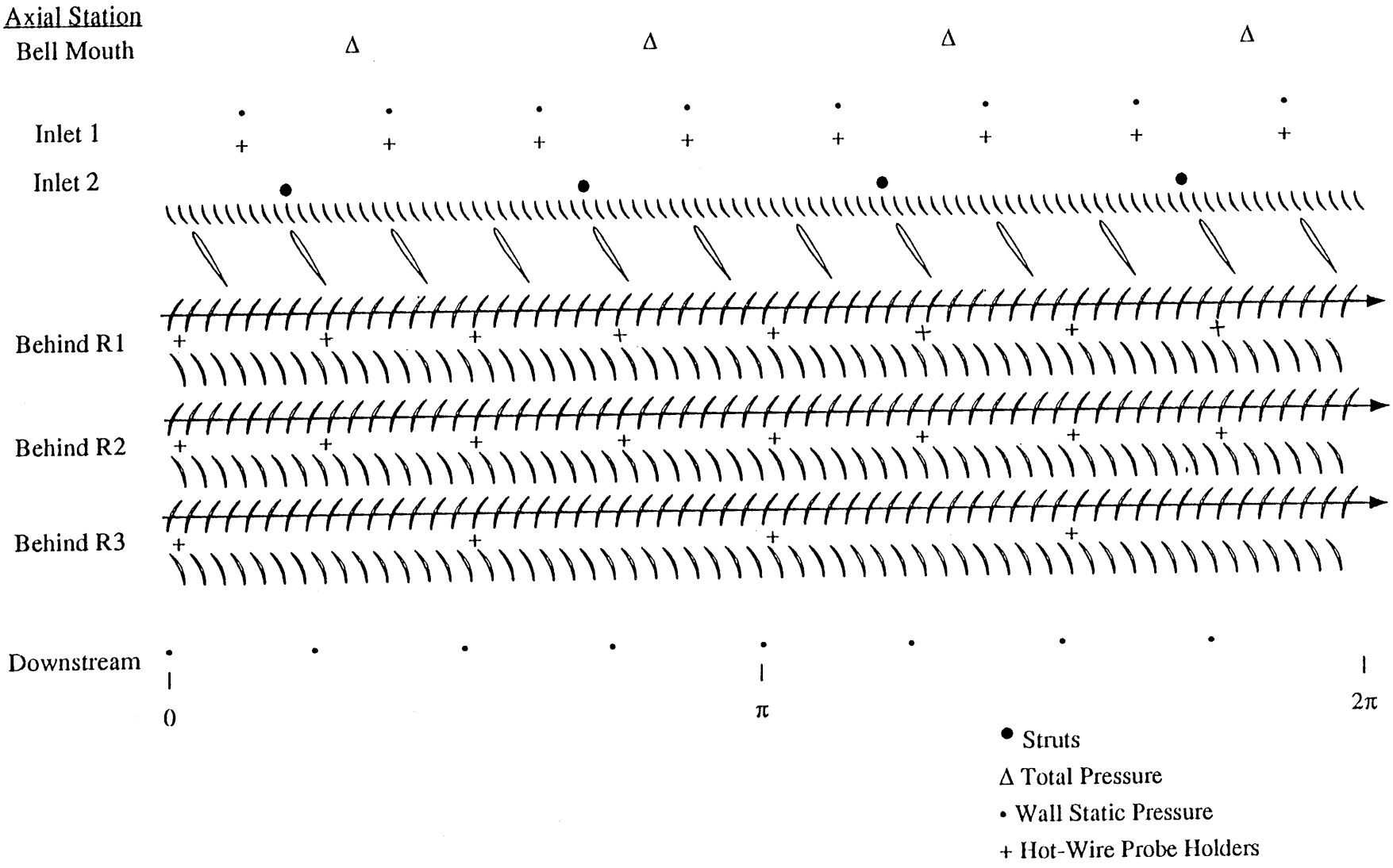

Figure 4.4 Layout of the instrumentation on the MIT Three Stage compressor

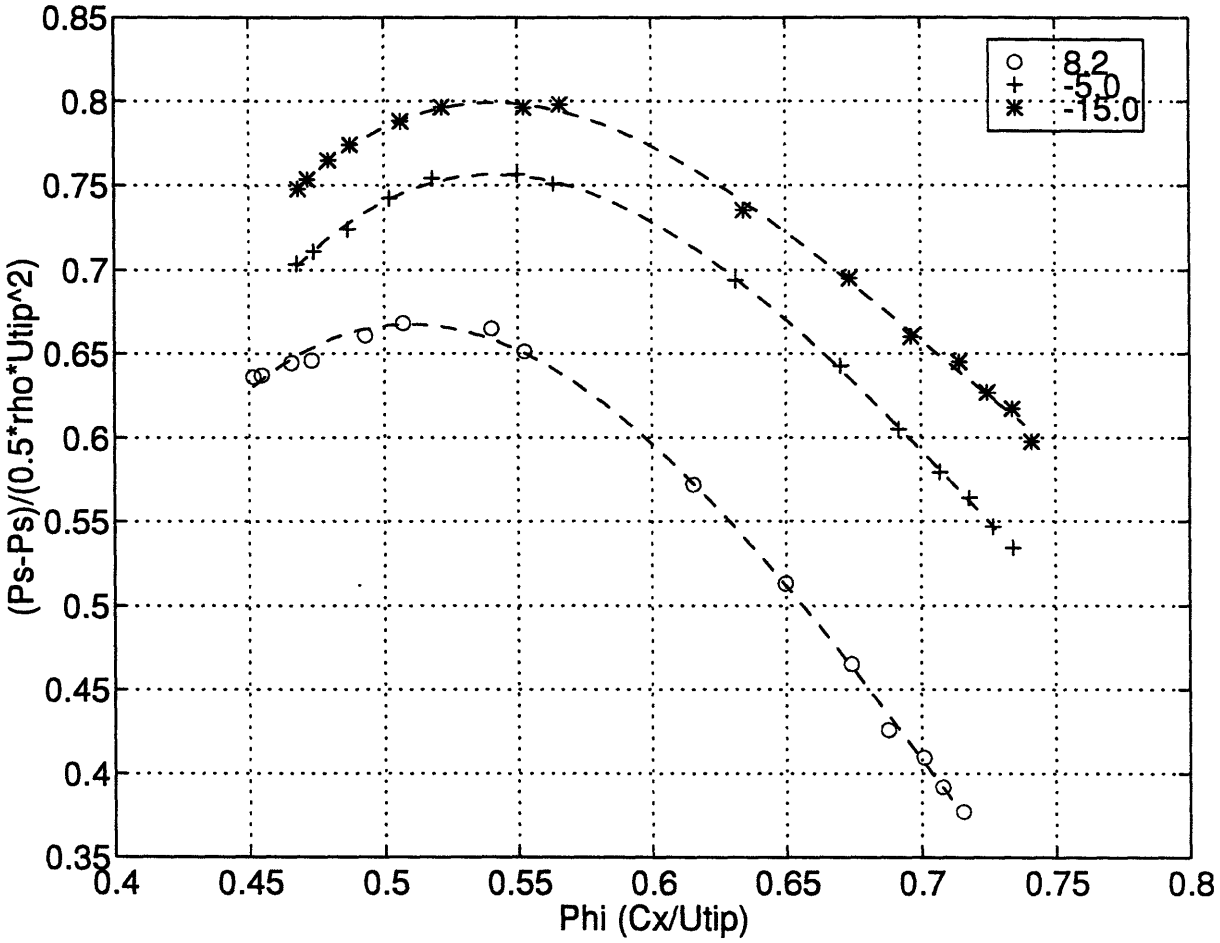

Figure 4.5 Static-to-static pressure rise characteristics of the 1st stage for various SGV stagger angles.

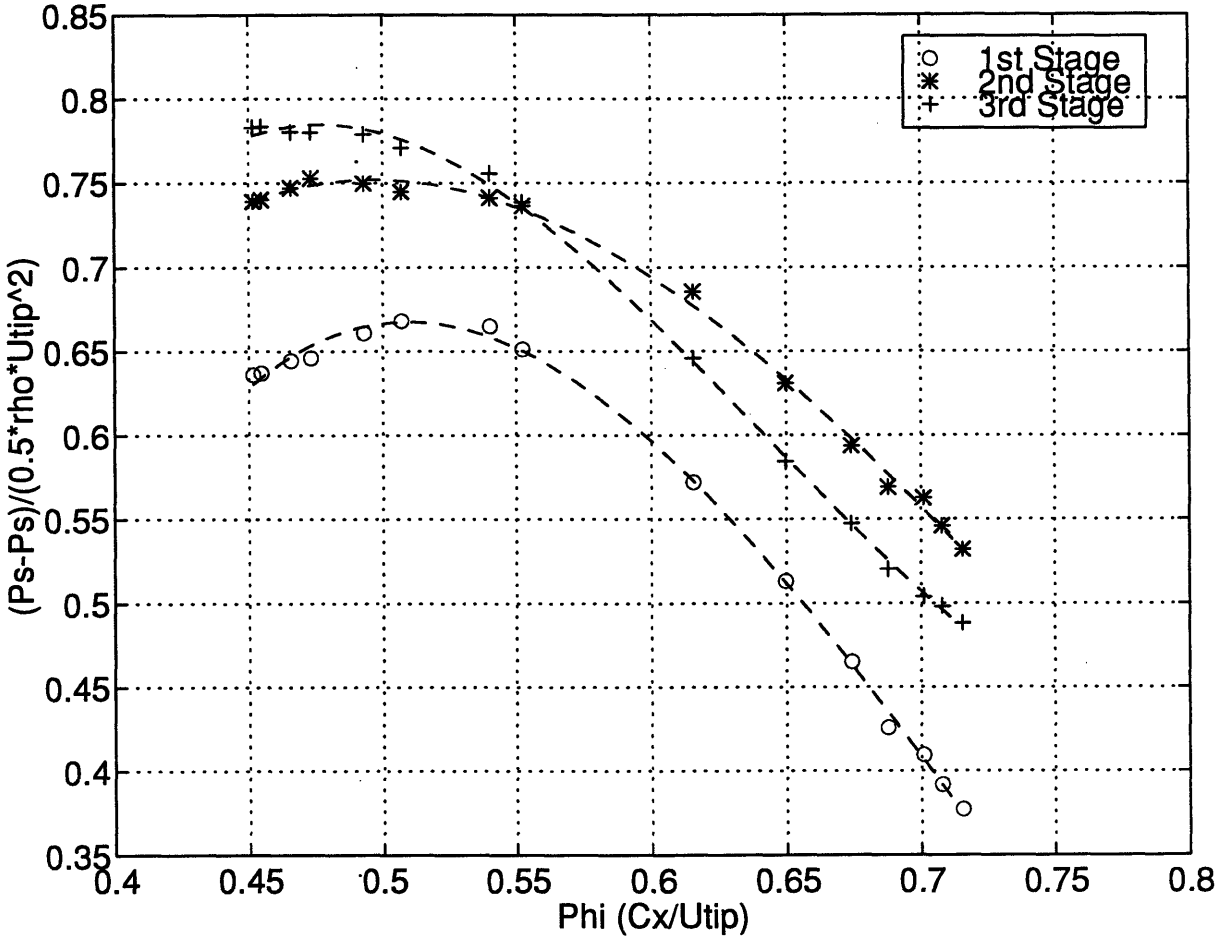

Figure 4.6 Static-to-static pressure rise characteristics of individual stages for SGV stagger angle of 8.2°. Note the relatively low pressure rise of the 1st stage in comparison with the other stages.

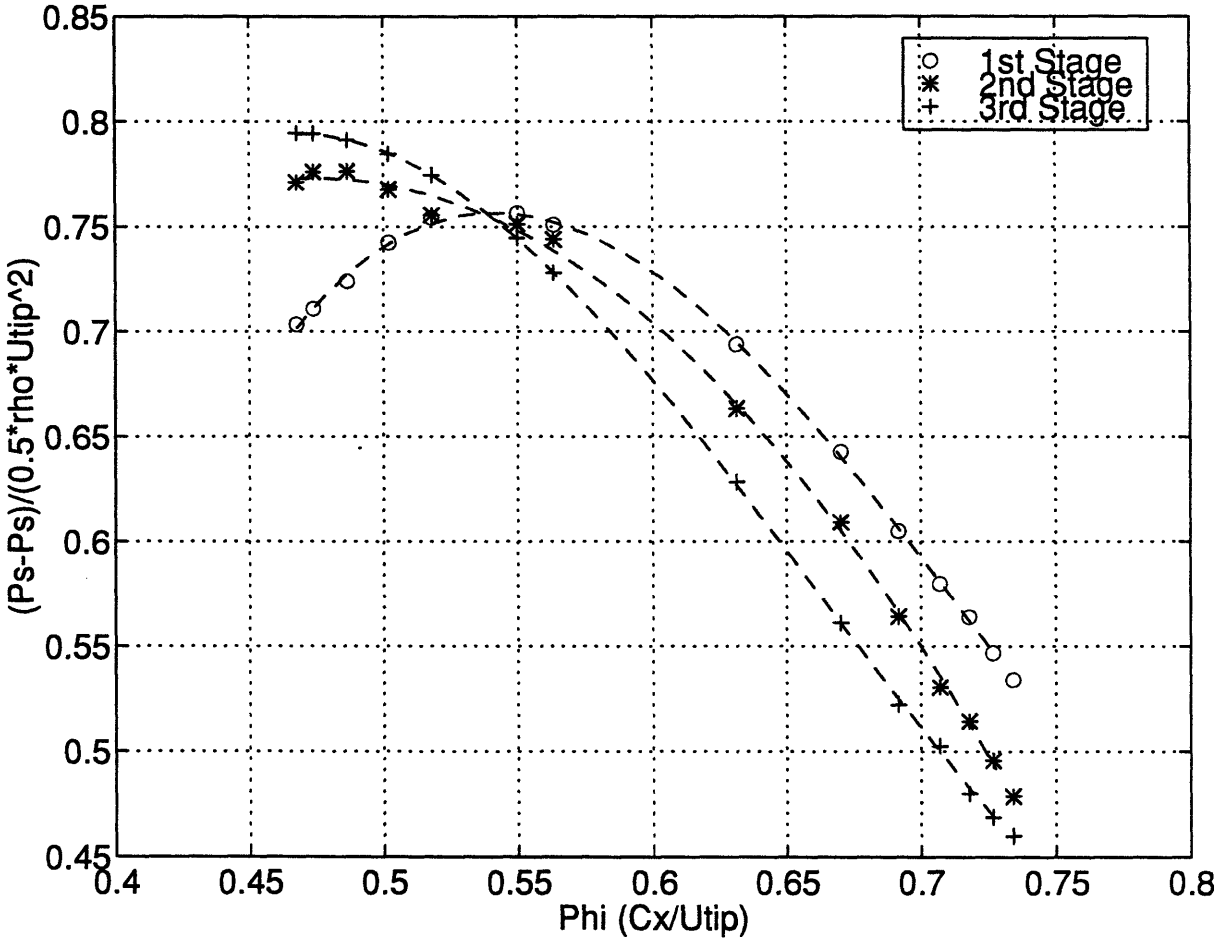

Figure 4.7 Static-to static pressure rise characteristics of individual stages for SGV stagger angle of -5.0°.

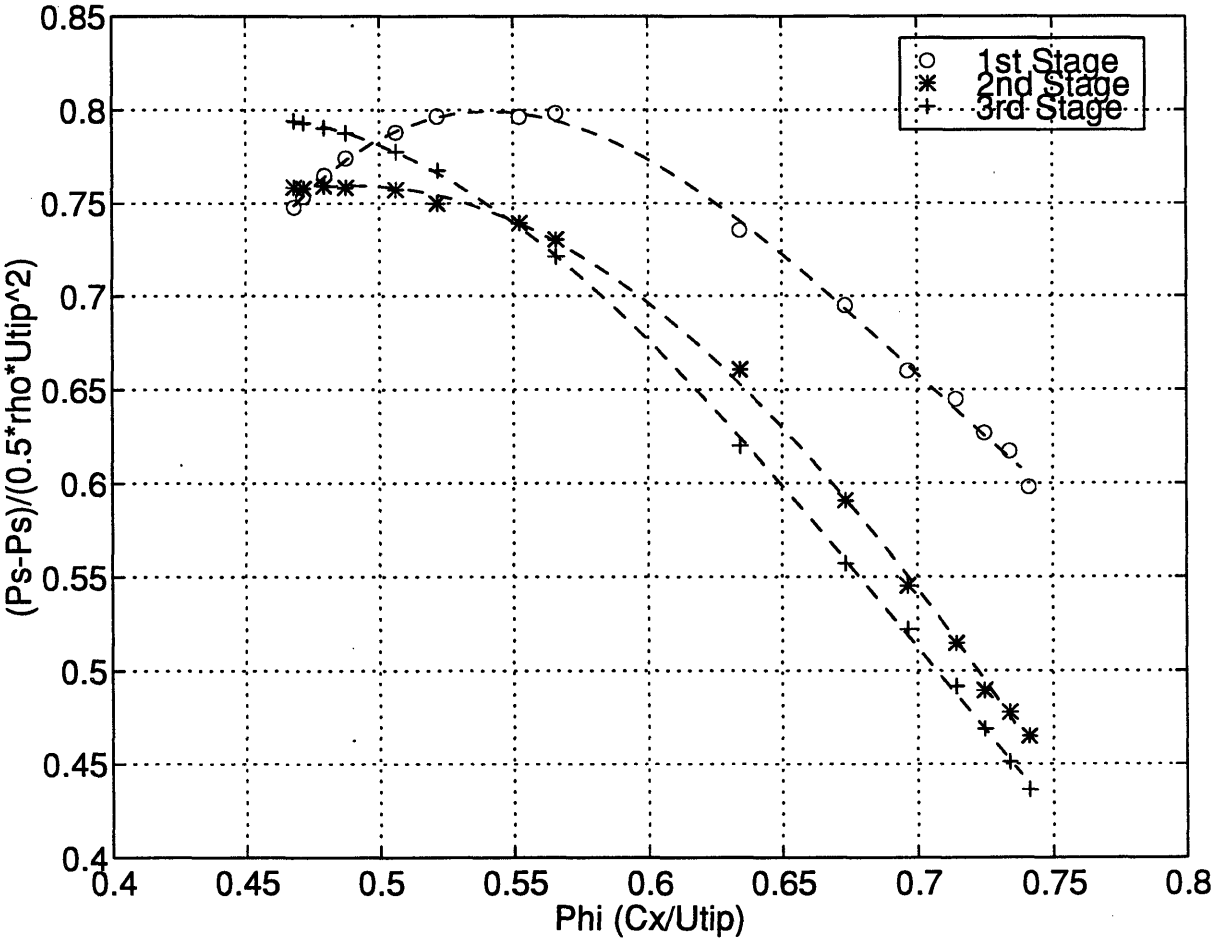

Figure 4.8 Static-to-static pressure rise characteristics of individual stages for SGV stagger angle of -15.0°.

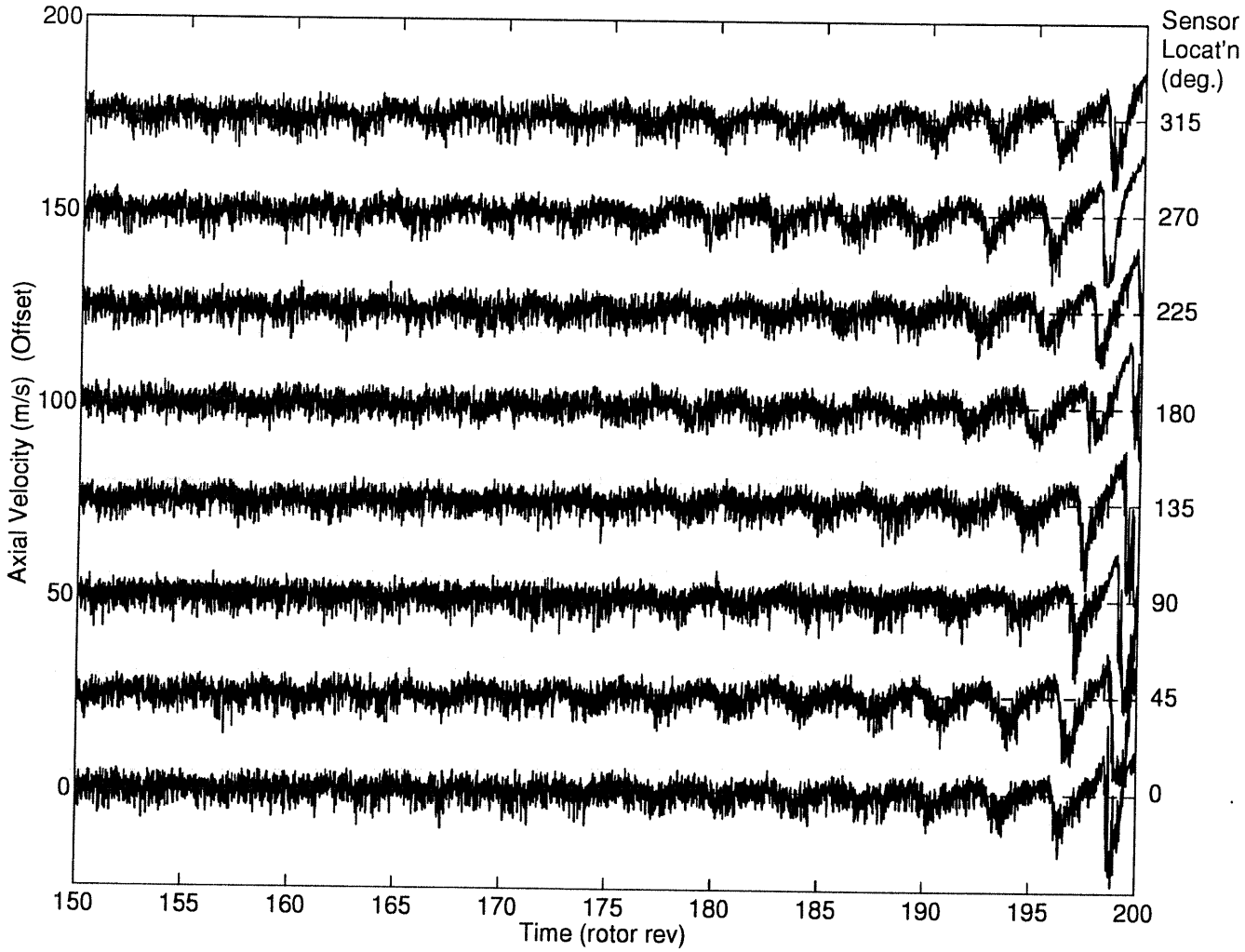

Figure 4.9 Hot-wire velocity traces near the tip at 1st stage rotor exit during stall inception with SGV stagger angle at 8.2°.

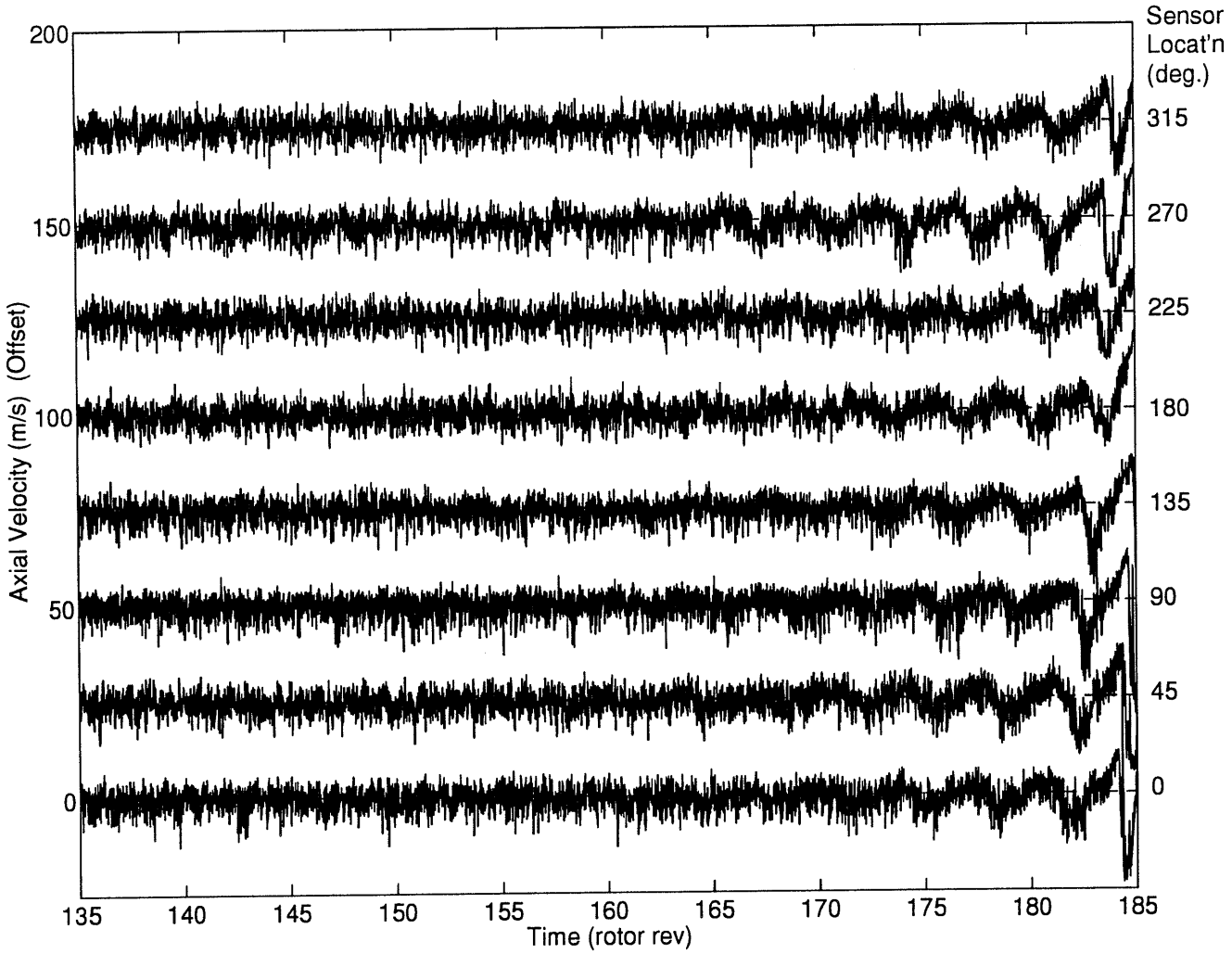

Figure 4.10 Hot-wire velocity traces near the tip at 1st stage rotor exit during stall inception with SGV stagger angle at -5.0°.

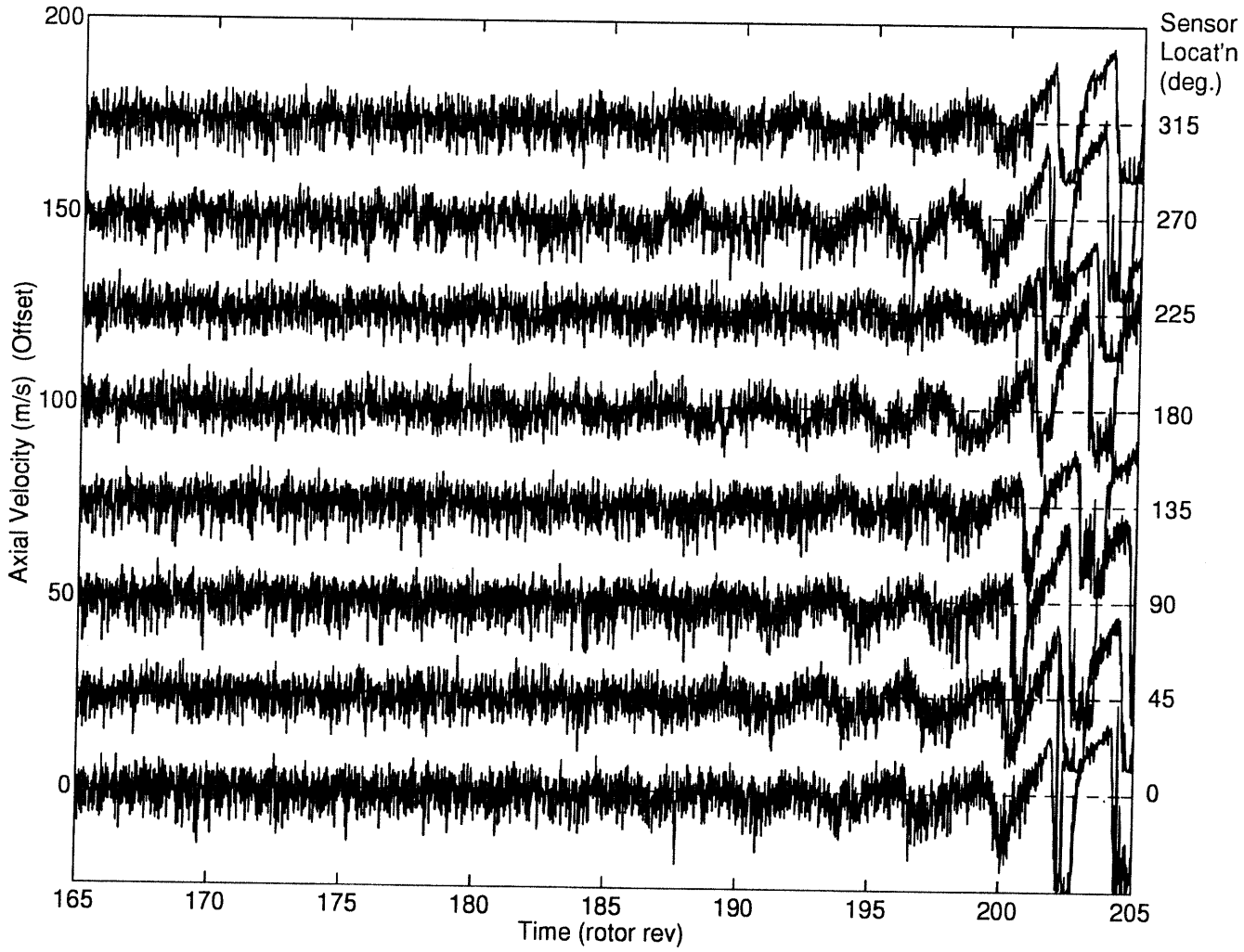

Figure 4.11 Hot-wire velocity traces near the tip at 1st stage rotor exit during stall inception with SGV stagger angle at -15.0°.

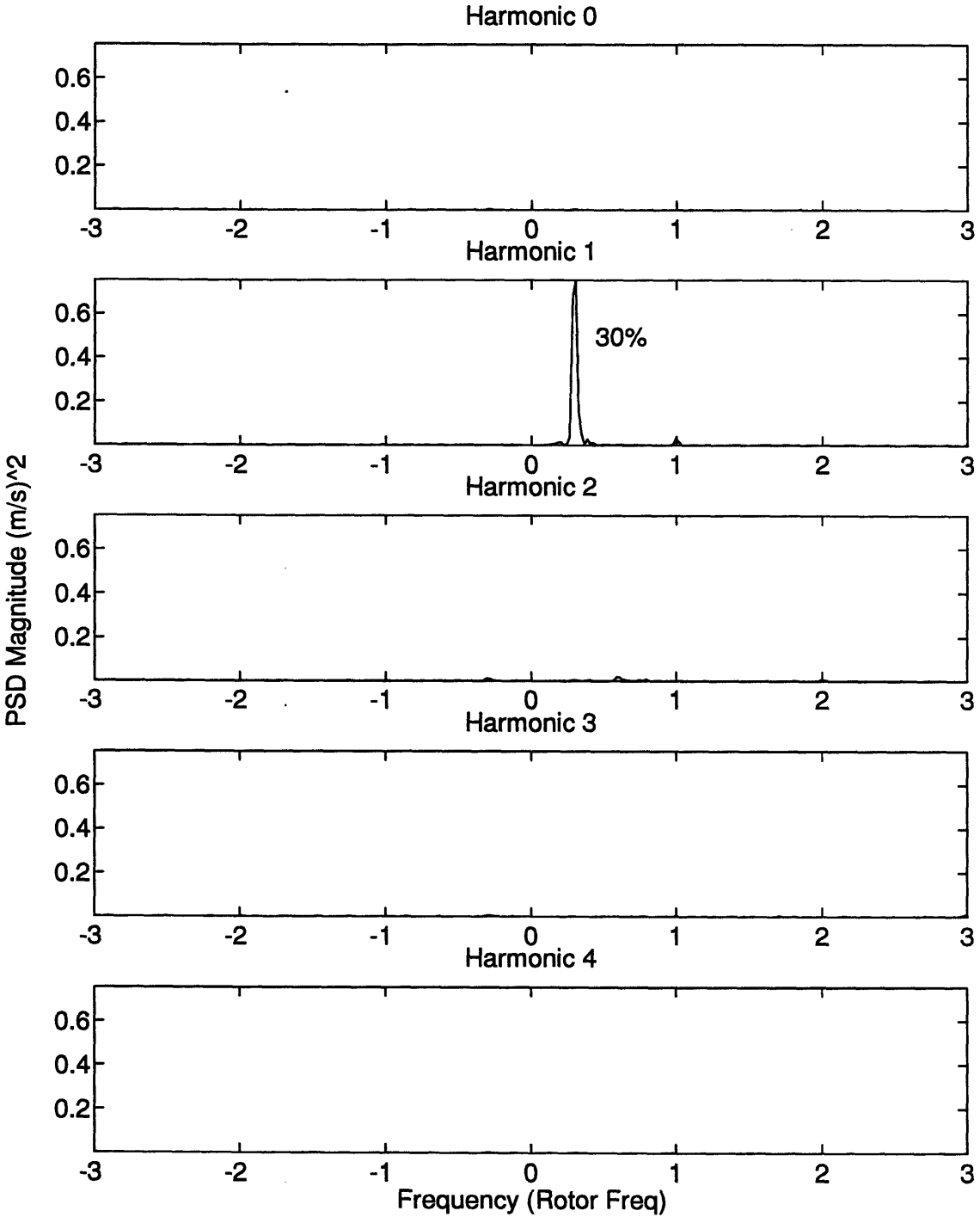

Figure 4.12 PSD's of SFHC prior to stall of measurements in Figure 4.9. Note the dominate peak at 30% of rotor frequency in the PSD of 1st spatial harmonic.

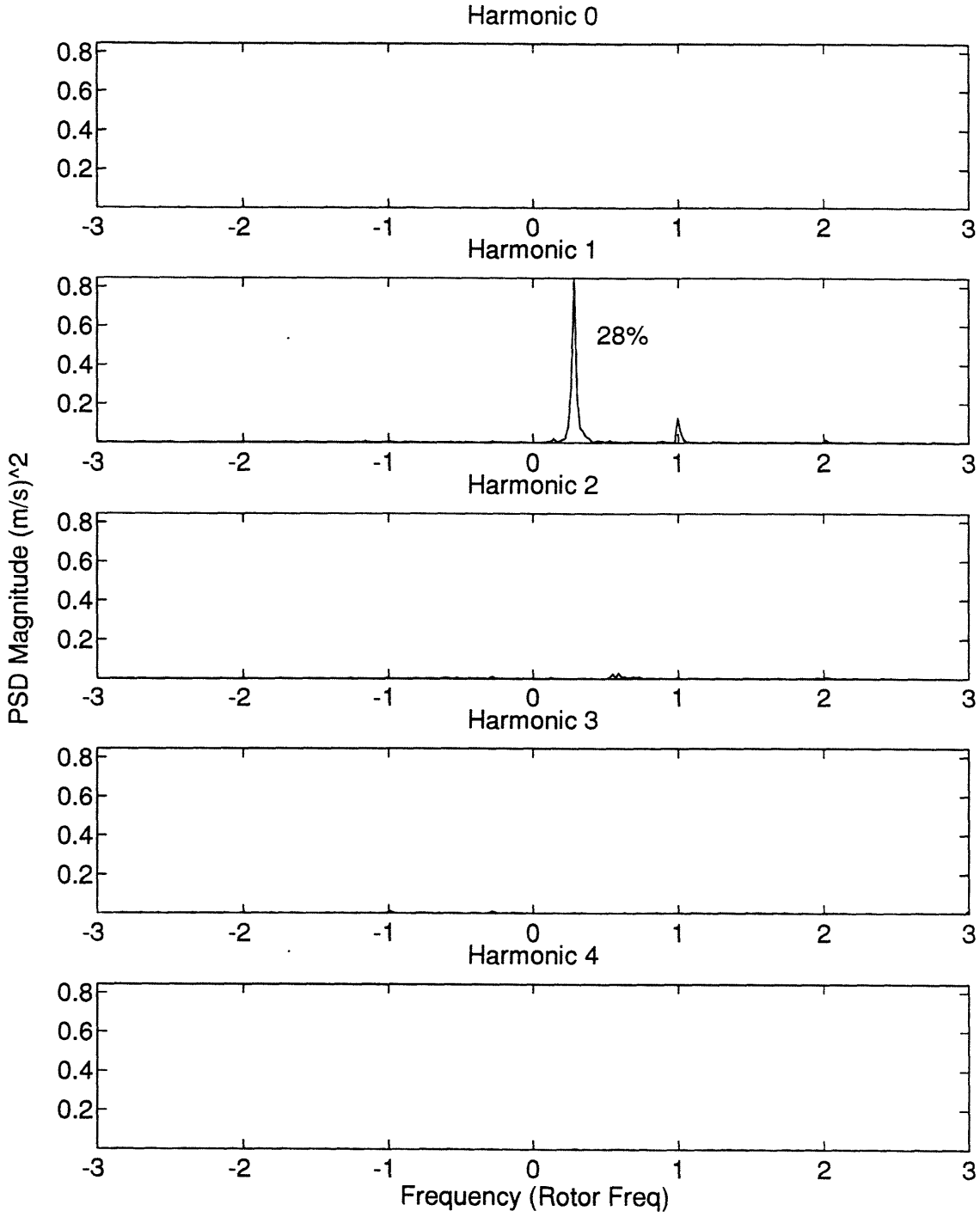

Figure 4.13 PSD's of SFHC prior to stall of measurements in Figure 4.10. Note the dominate peak at 28% of rotor frequency in the PSD of 1st spatial harmonic. A smaller peak at 100% of rotor frequency in the PSD of 1st spatial harmonic is due to rotor asymmetry.

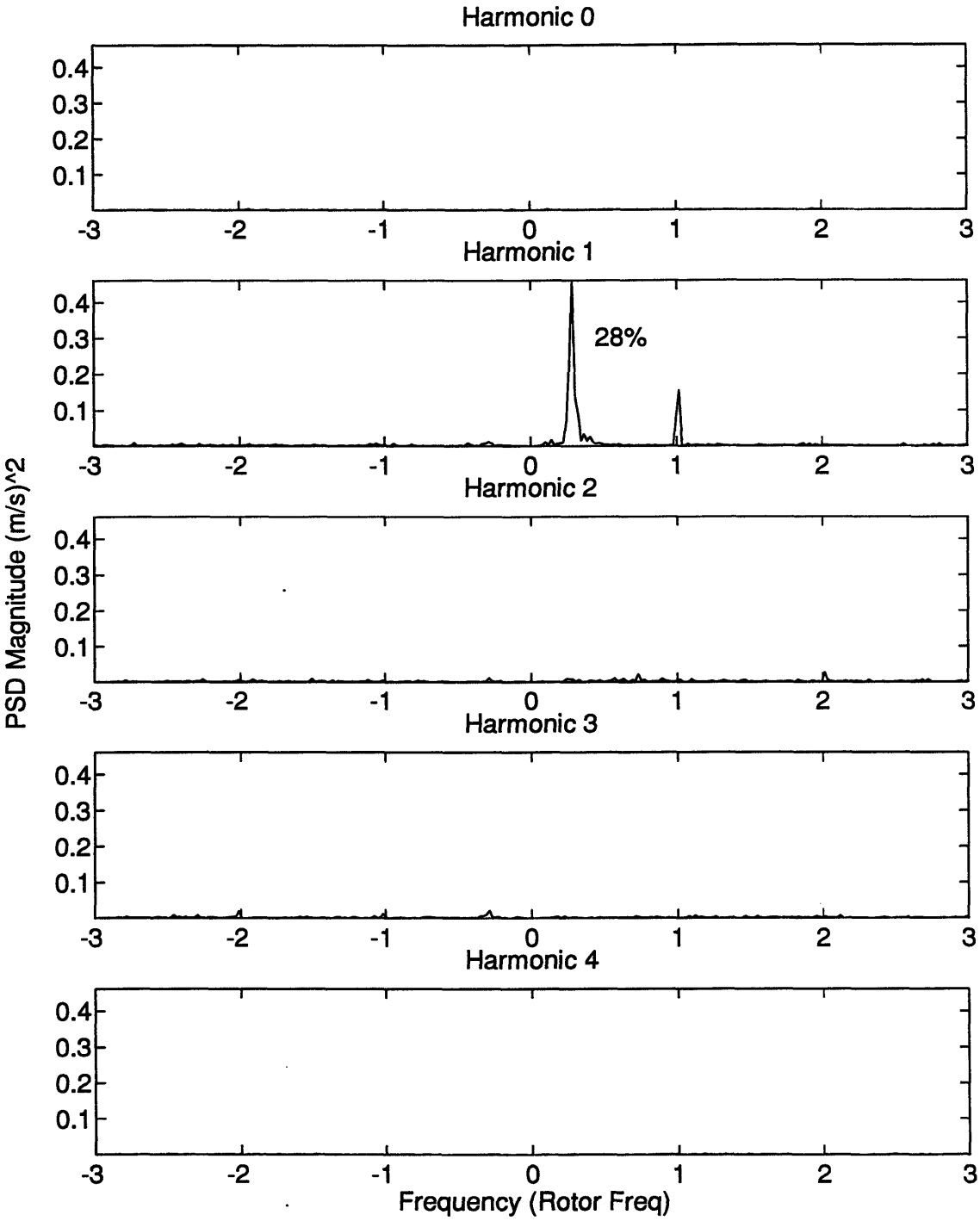

Figure 4.14 PSD's of SFHC prior to stall of measurements in Figure 4.11. Note the dominate peak at 28% of rotor frequency in the PSD of 1st spatial harmonic. A smaller peak at 100% of rotor frequency in the PSD of 1st spatial harmonic is due to rotor asymmetry.

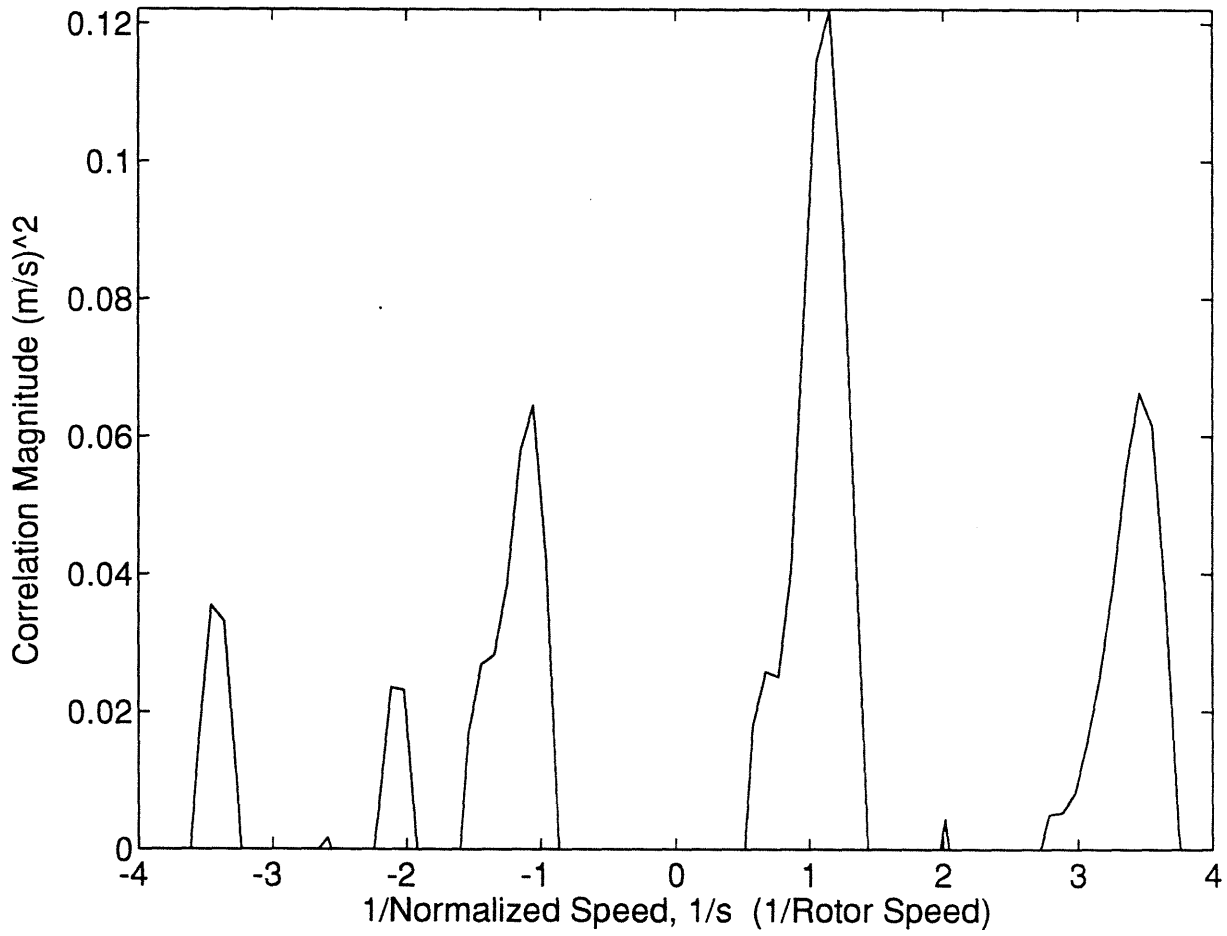

Figure 4.15 Cross-correlation of measurements in Figure 4.9 prior to stall. No peak is observed near 1/s = 1.4 (near 70% of rotor speed).

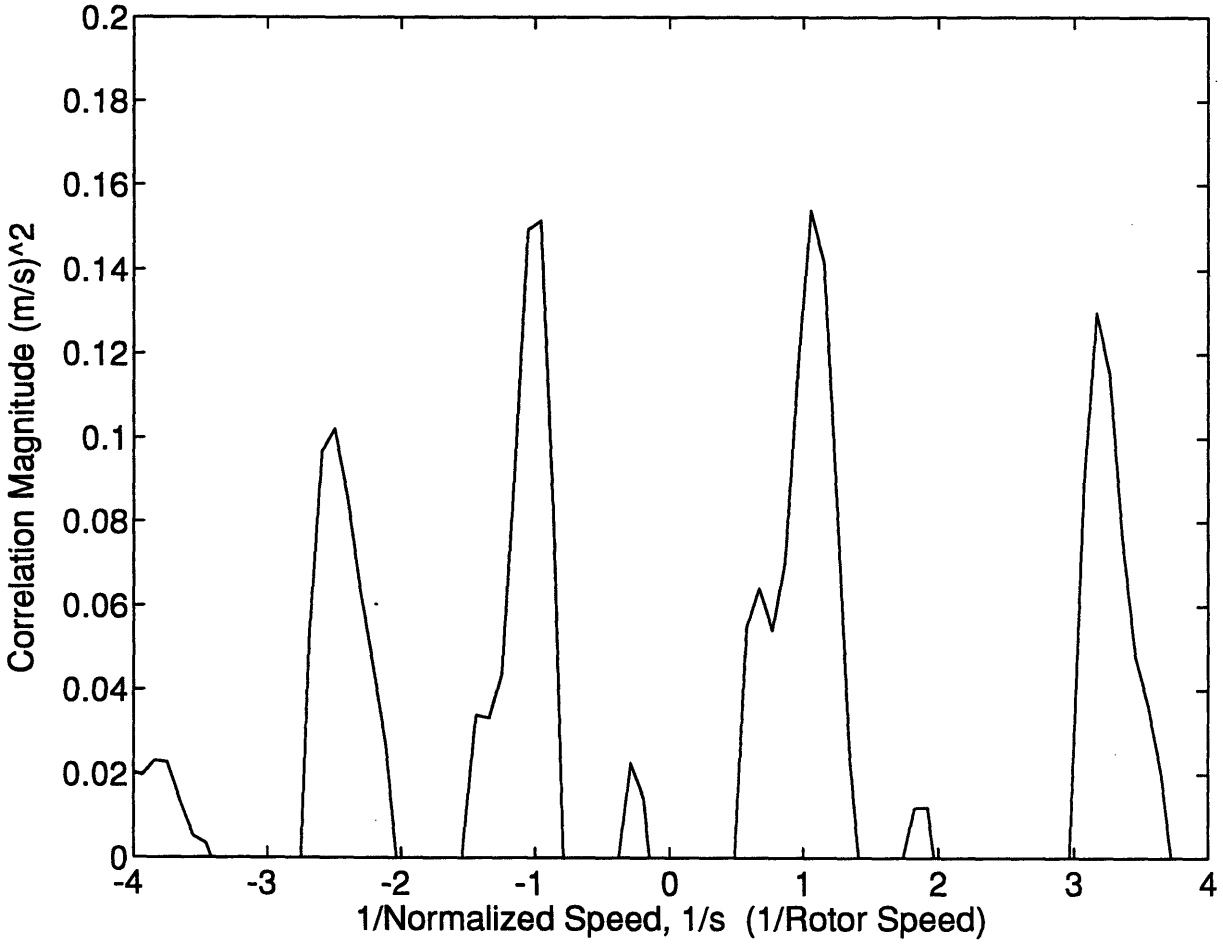

Figure 4.16 Cross-correlation of measurements in Figure 4.10 prior to stall. No peak is observed near 1/s = 1.4 (near 70% of rotor speed).

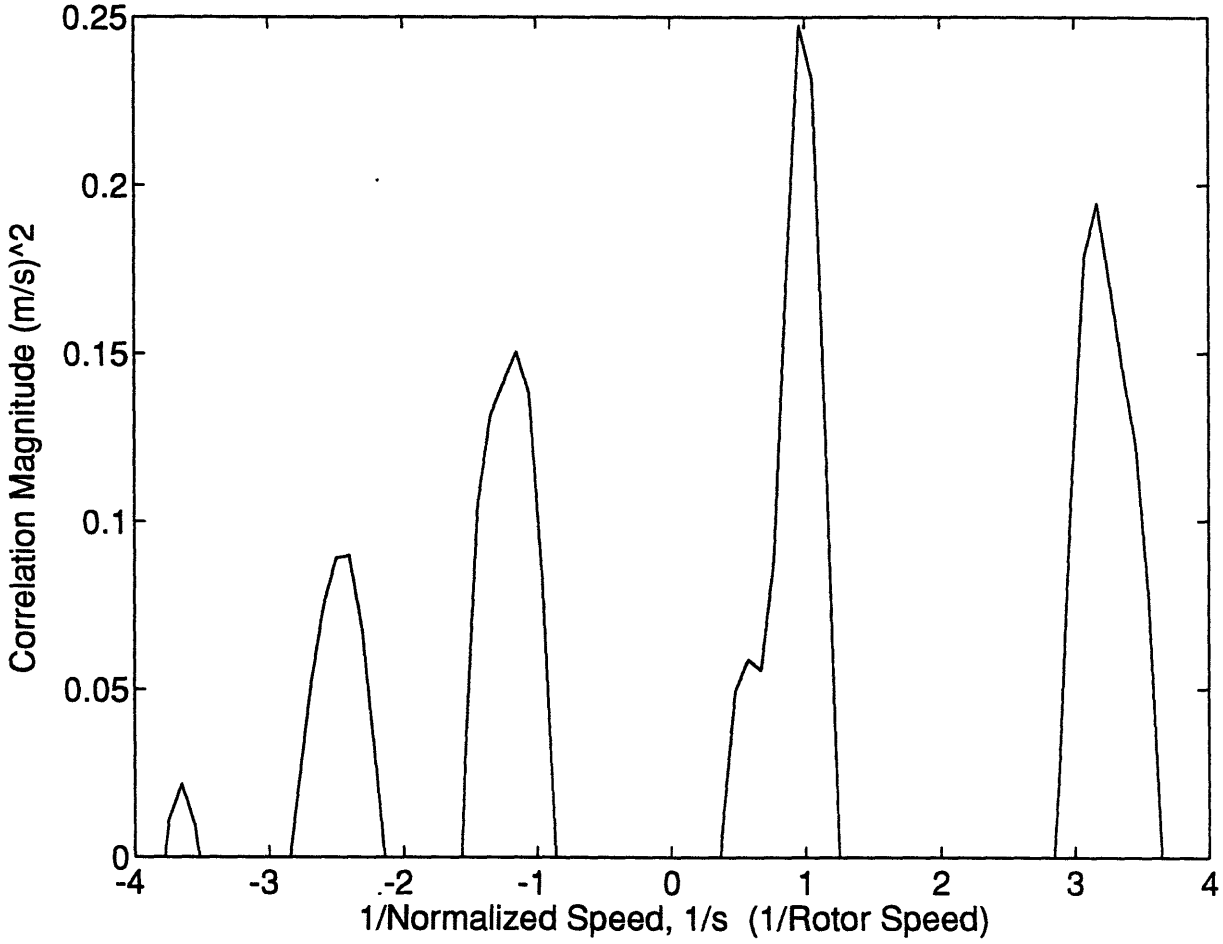

Figure 4.17 Cross-correlation of measurements in Figure 4.11 prior to stall. No peak is observed near 1/s = 1.4 (near 70% of rotor speed).

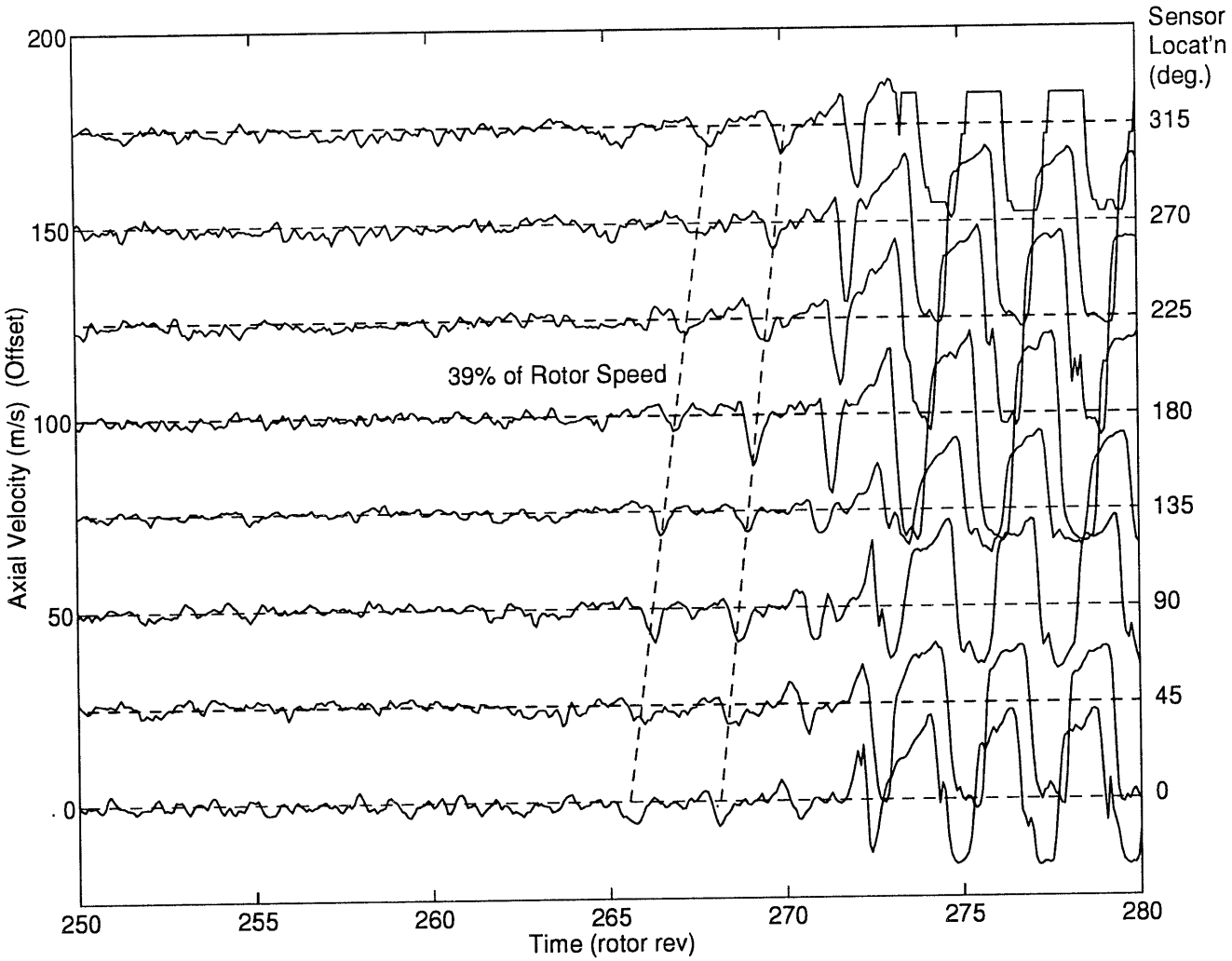

Figure 4.18 Hot-wire velocity traces near the tip at 1st stage rotor exit during stall inception of actively controlled compressor. The dashed lines illustrate the growth of a single lobed disturbance at 39% of rotor speed growing into a rotating stall cell.

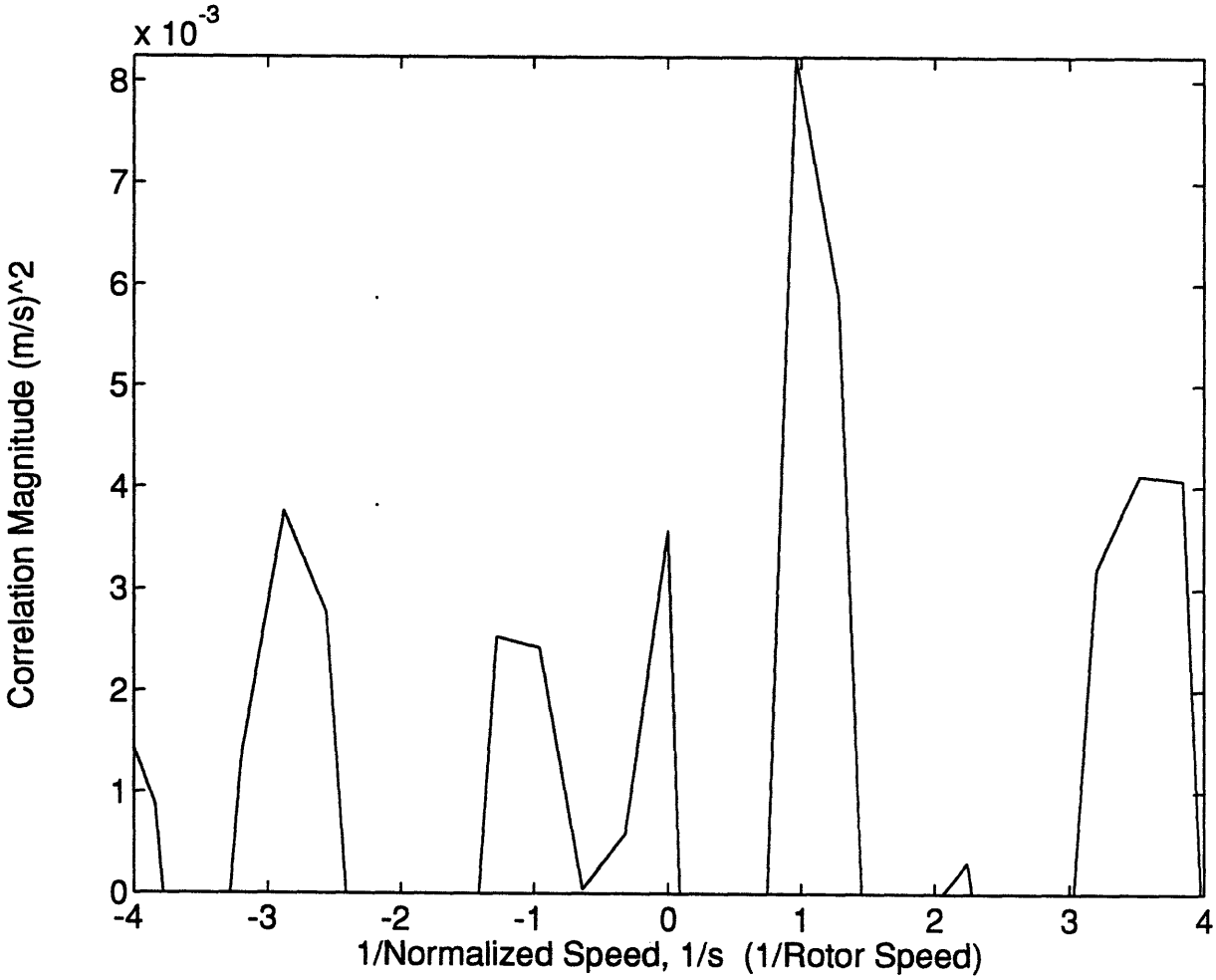

Figure 4.19 Cross-correlation of measurements in Figure 4.21 prior to stall. There is no evidence of any disturbance traveling near 70% of rotor speed or 1/s = 1.4. Note the peak at 1/s = 1 or at 100% of rotor speed due to rotor wake asymmetry.

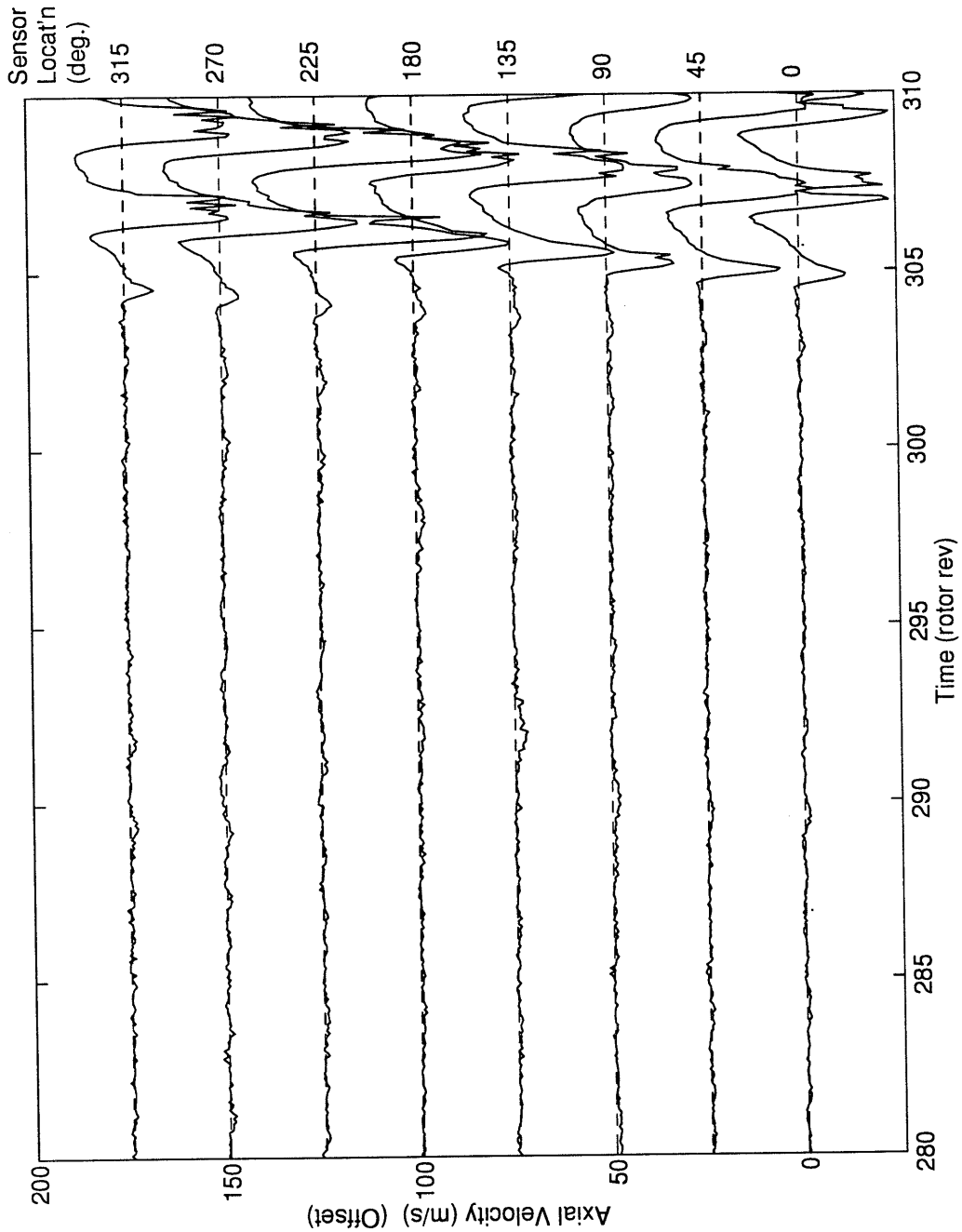

Figure 4.20 Hot-wire velocity traces near the tip at IGV inlet during stall inception of actively controlled compressor.

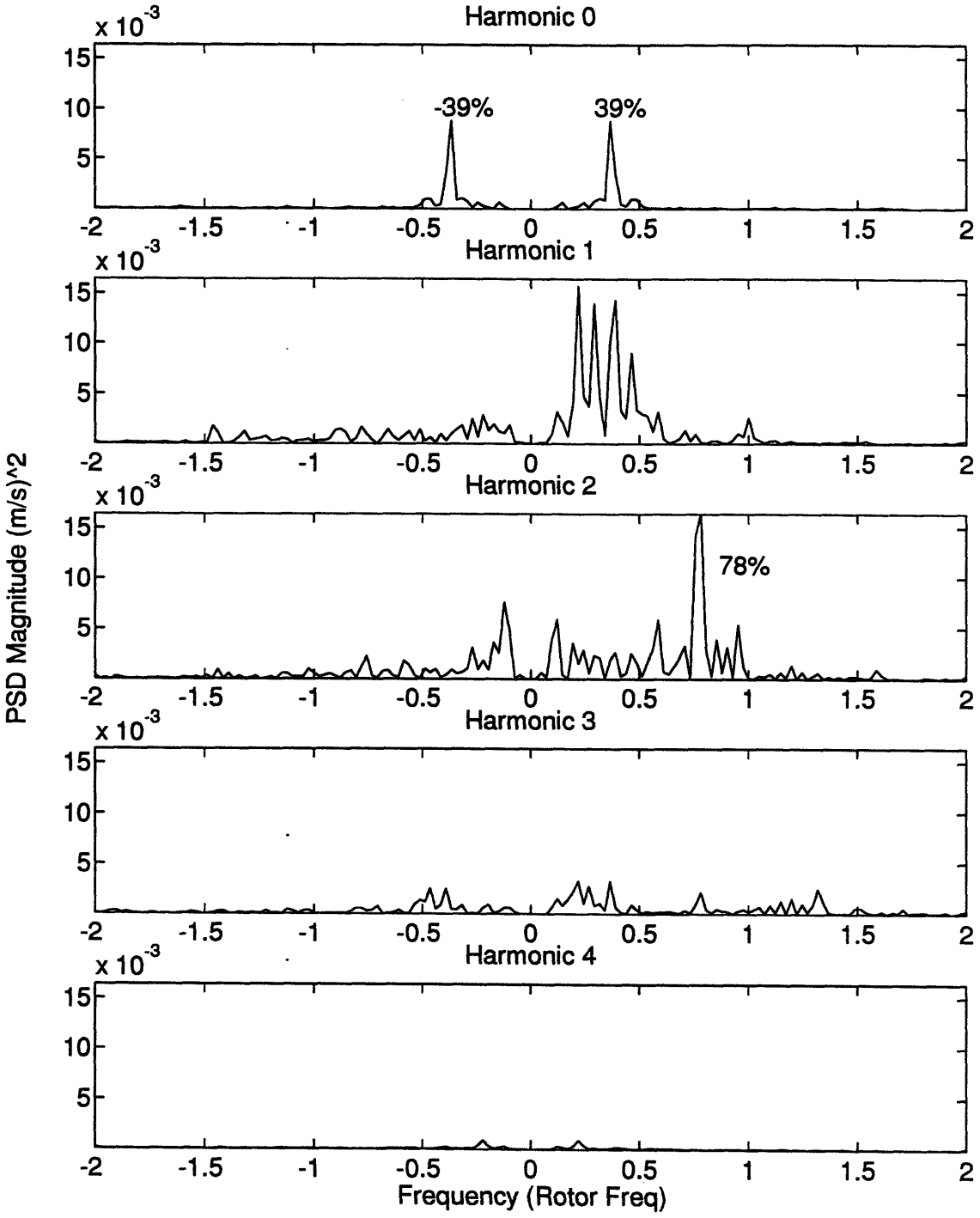

Figure 4.21 PSD's of SFHC prior to stall of measurements in Figure 4.23. Note the peaks at ± 39% of rotor frequency in the plot of PSD of the 0th spatial harmonic (axisymmetric mode).

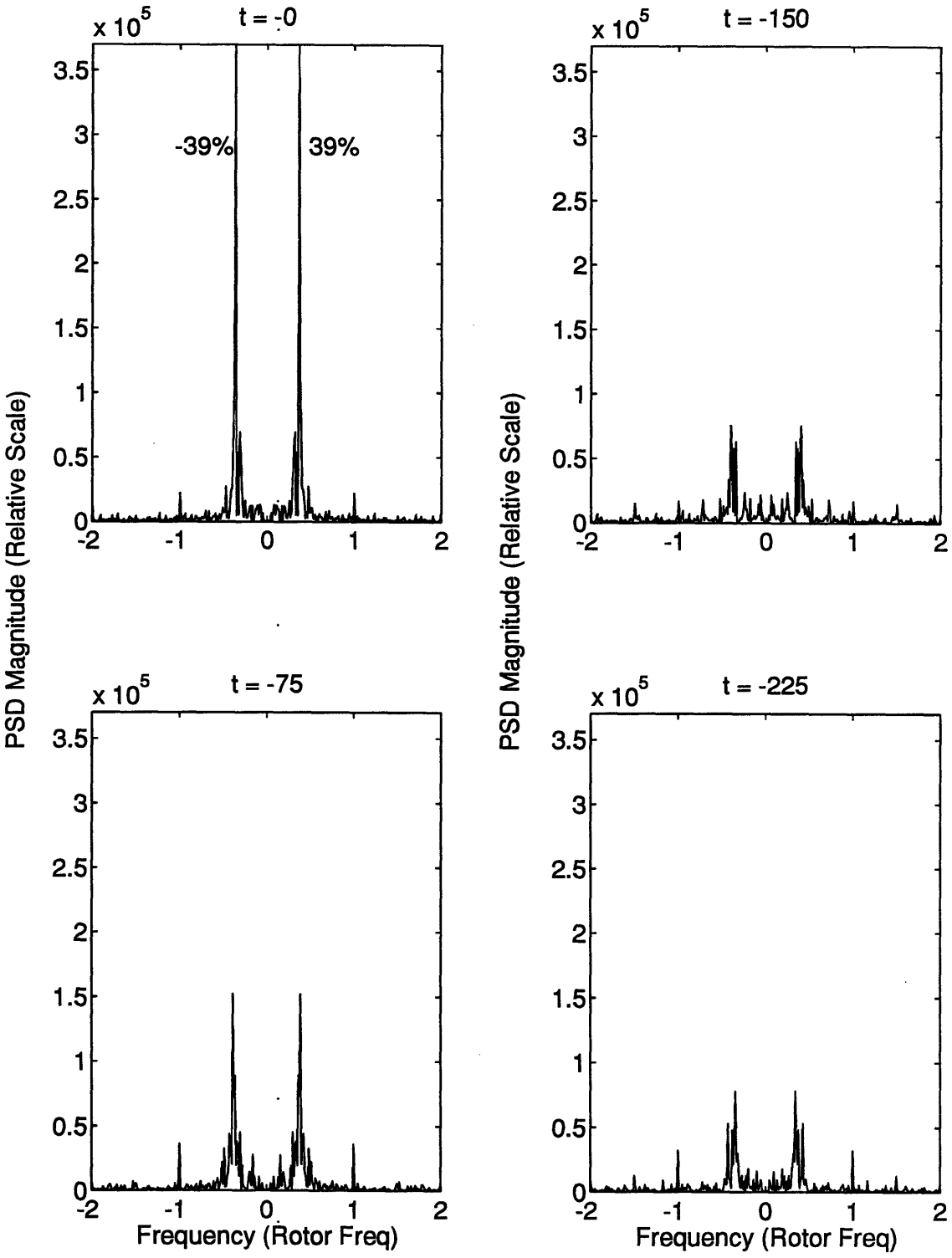

Figure 4.22 PSD's of the 0th spatial harmonic (axisymmetric mode) computed from casing static pressure traces at the compressor exit for sequential intervals up to point of stall (t = -0). Note the amplitude growth of the peaks at ±39% of rotor frequency.

CHAPTER FIVE

EFFECTS OF ROTATING DISTORTION ON COMPRESSORS

5.1 Introduction

When subjected to an upstream rotating distortion, the stability of a compressor may be severely degraded compared to that with upstream uniform flow. Such situation can occur when an upstream compressor or a fan goes into rotating stall in a multi-spool engine. Because of this, there is an interest in understanding the reasons behind the loss of compressor stability with rotating distortion. In this chapter, observations are made on the link between the loss of stability caused by an upstream rotating distortion and the disturbance structure(s) present in the natural stall inception of a compressor.

5.2 Background

The hypothesis that the loss of stability of a compressor subjected to an upstream rotating distortion is directly related to the unsteady disturbance structures was presented by Longley et al. [19] They suggested that loss of stability of a compressor can be attributed to the resonant response created by an interaction occurs between the upstream rotating distortion (forcing) and the natural eigenmode (modal wave or spike) of the compressor. In other words, the stability of a compressor may be degraded when the rotational speed of the distortion corresponds to a speed which excites a natural eigenmode (i.e. disturbance structure) of the compressor flowfield.

Longley et al. divided compressors into two types by their responses to rotating distortion: 1) a "dromedary" type which exhibits a single resonant peak in the plot of stability margin degradation versus distortion rotation speed (Figure 5.1), and 2) a "bactrian" type which exhibits double resonant peaks (Figures 5.2). The single resonant peak (roughly at 50% of rotor speed) of a dromedary compressor was attributed to the rotating distortion exciting a mode associated with a modal wave disturbance structure. The two resonant peaks of a bactrian compressor (lower speed peak roughly at 25% of rotor speed and higher speed peak roughly at 70% of rotor speed) were interpreted in [19] as excitation of two disturbances associated a modal wave and a spike, respectively. Longley et al. thus suggested that compressors which exhibit spike type disturbance during stall inception exhibit bactrian behavior, while compressors which exhibit modal wave type disturbance exhibit dromedary type behavior in the curve of stability loss versus distortion rotation speed.

5.3 Purpose of Chapter

The purpose of this chapter is to present some observations on recently collected data from ongoing experiments at General Electric Low Speed Compressor facility to examine the link between the disturbance structure(s) found in natural stall inception and the behavior of a compressor subjected to an upstream rotating distortion. The observation is made that in contrast to only dromedary behavior observed in [19], compressors which exhibit modal wave disturbance structure during natural stall inception can also exhibit bactrian behavior and show loss of stability at distortion speed of 70% of rotor speed.

5.4 Experimental Facility

The data to be described was collected from experiments at the GE Low Speed Research Compressor (LSRC). The compressor is a large-scale four stage low speed compressor (5 feet diameter). A schematic of the facility is shown in Figure 3.1. In its current configuration, the compressor has a constant cross sectional area and a hub-to-tip ratio of 0.85. A distortion screen, when used, is mounted 1.5 compressor radii upstream of the IGVs. The present distortion screen, which covers a 120° sector of the annulus, generates a square-wave-like total pressure distortion of 1.2 times the dynamic head based on the mean inlet velocity.

During the experiments, the compressor underwent two sets of modifications. The original configuration (Compressor 1) had a modern commercial design compressor blading with an IGV stagger angle of 4°. The configuration after a first set of modifications (Compressor 2) had the rotors and stators of Compressor 1 but the IGV's were removed. The third configuration (Compressor 3) had the rotors of Compressor 1, but had different stators and IGV's. The overall pressure rise characteristics of the three configurations are shown in Figure 5.3.

5.4.1 Instrumentation

Time resolved data were acquired using a circumferential array of hot-wire anemometers mounted 0.2 chords upstream of the first stage rotor. For Compressor 1, a circumferential array of 4 hot-wire anemometers spaced 90° apart was used. An array of 8 hot-wire anemometers spaced 45° apart was

used for Compressor 2 and Compressor 3. For Compressor 3, an additional array of 8 hot-wire anemometers was placed downstream of the first stage rotor. Measurements shown were made at radial immersion of 20% of span from the casing.

5.5 Observations

5.5.1 Natural Stall Inception

For all three configurations of the compressor, the observed disturbance was a modal wave. The velocity traces upstream of the first stage rotor during natural stall inception of Compressor 1 are shown in Figure 5.4. The wave-like characteristics of a modal wave type disturbance is evident visually. The PSD's of the spatial Fourier harmonics coefficients (SFHC) confirm that the second mode traveling at 28% of rotor speed becomes unstable (Figure 5.5).

Velocity traces upstream of the first stage rotor for Compressor 2 are shown in Figure 5.6. Again, the disturbance structure appears to be a modal wave. The PSD's of SFHC show that a first mode traveling at 32% of rotor speed is most unstable (Figure 5.7).

Velocity traces downstream of the first stage rotor for Compressor 3 are shown in Figure 5.8. The PSD's of SHFC show that the first mode traveling at 40% of rotor speed is most unstable (Figure 5.9).

5.5.2 Forced Response Behavior

While all the compressors display modal wave type disturbance during

stall inception, the compressors all have a peak in loss of stability near 70% of rotor speed. The plot of stability loss versus distortion screen rotation speed for the three compressors is shown in Figure 5.10. Compressor 1 shows peaks roughly at 35% and at 70% of rotor speed. Compressor 3 shows a broad peak at roughly 45% of rotor speed and a sharp peak at 70%. Compressor 2 has just a single broad peak at 70% of rotor speed.

5.5.3 Weak Disturbance Structure

All of the compressors display resonant peaks at 70% of rotor speed in the plot of loss of stability versus distortion rotation speed. The arguments in [19] imply that all the compressors have an instability onset associated with a spike type disturbance. To determine if spikes are indeed propagating around the annulus, the cross-correlation method developed in Chapter 2 is used to detect the presence of spikes. Only Compressor 3 had the instrumentation at the proper location to detect short wavelength disturbance, and the results are shown in Figure 5.11. There is no evidence of a short wavelength disturbance propagating near 70% of rotor speed. Thus there is no evidence for a spike type disturbance in the natural stall inception process.

5.6 Summary

It is demonstrated that compressors can exhibit a modal wave disturbance and yet exhibit increased loss in stability near 70% of rotor speed. This is a different behavior from that observed in [19]. All three compressors tested exhibited modal wave disturbances with no evidence of spikes. However, peaks near 70% of rotor speed are observed in all three

configurations in the curve of stability margin loss versus distortion rotation speed. One suggestion is that these compressors exhibit modal waves in the natural configuration but have a spike mode which is excited when the distortion screen generates a forcing at 70% of rotor speed.

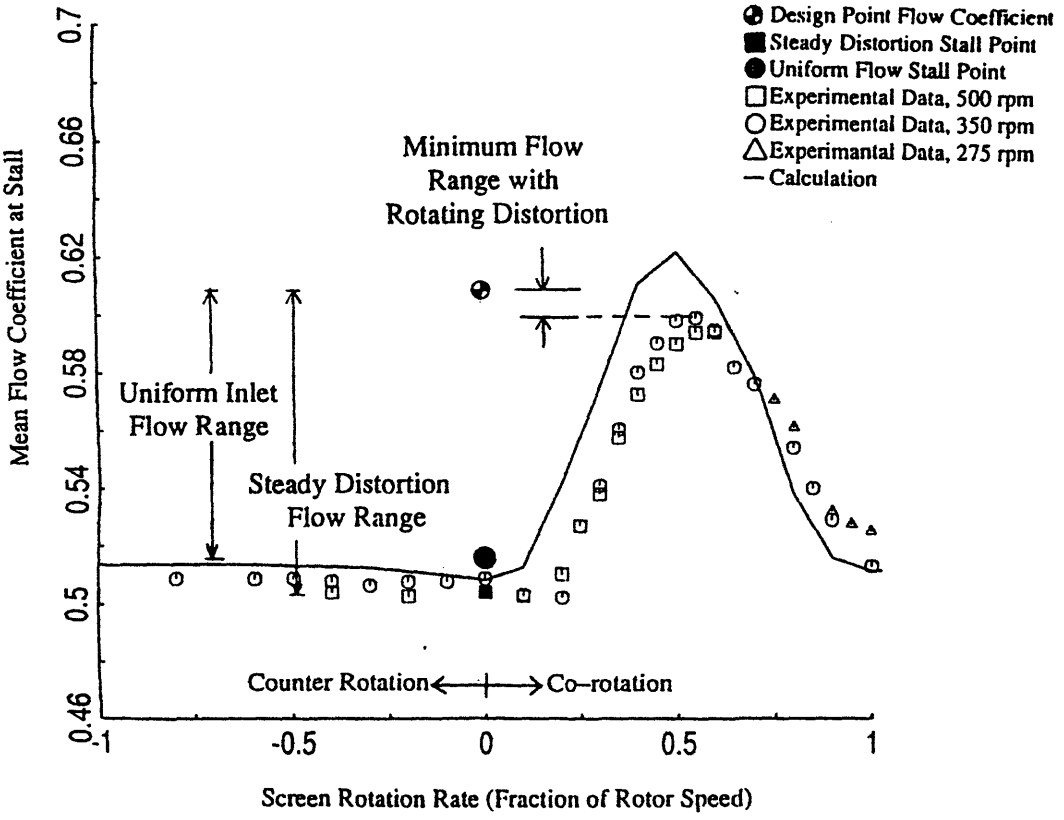

Figure 5.1 Flow coefficient at stall versus distortion rotation rate for a dromedary compressor [19]. (Compressor B in [19])

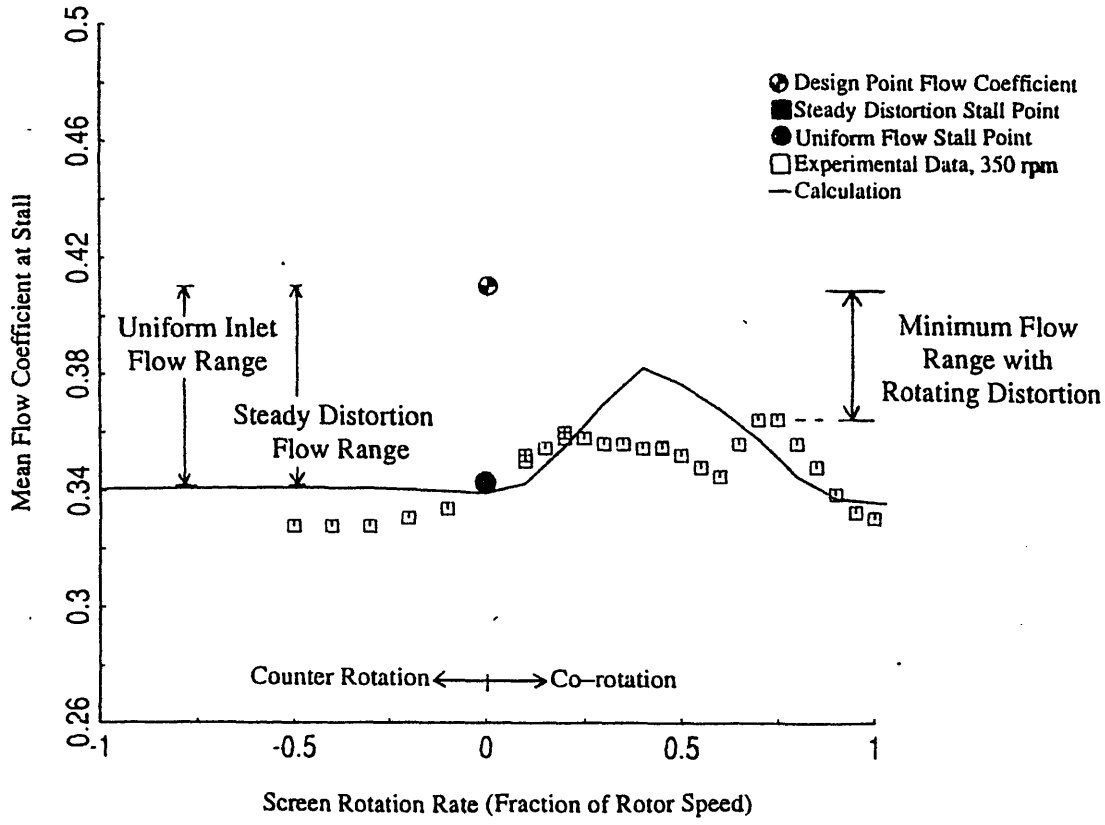

Figure 5.2 Flow coefficient at stall versus distortion rotation rate for a bactrian compressor [19]. (Compressor C in [19])

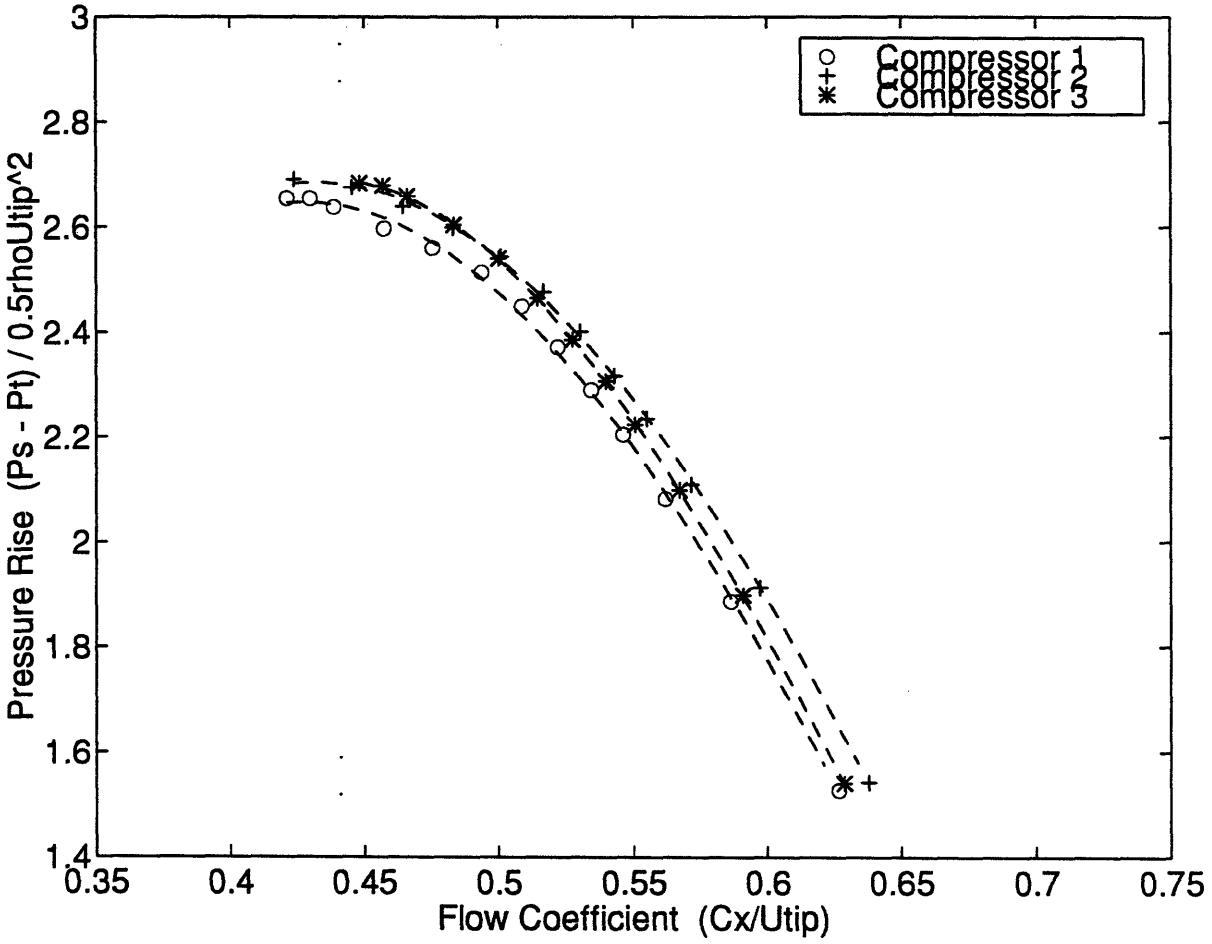

Figure 5.3 Overall total-to-static pressure rise characteristics

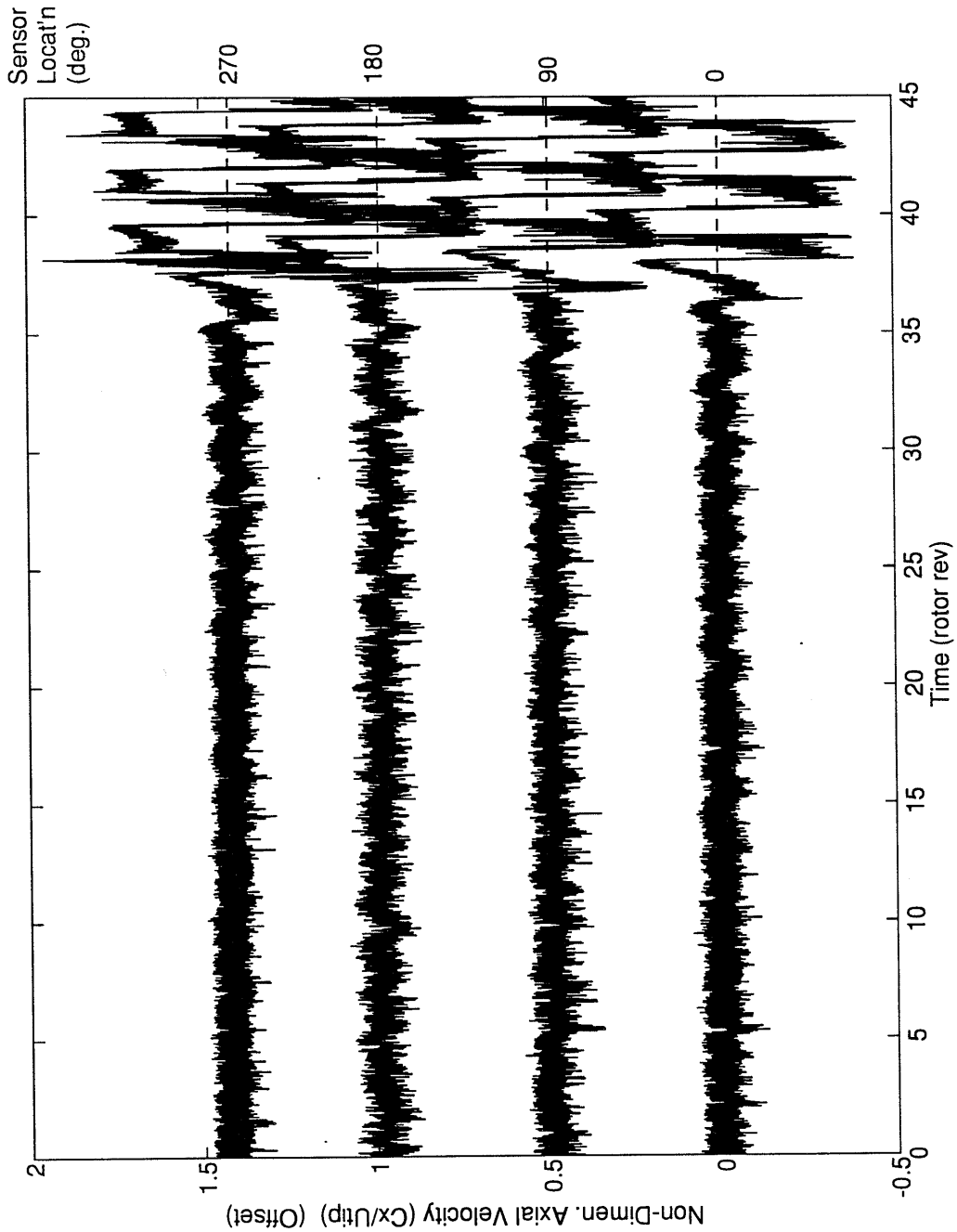

Figure 5.4 Hot-wire velocity traces near the tip at 1st stage rotor inlet for Compressor 1.

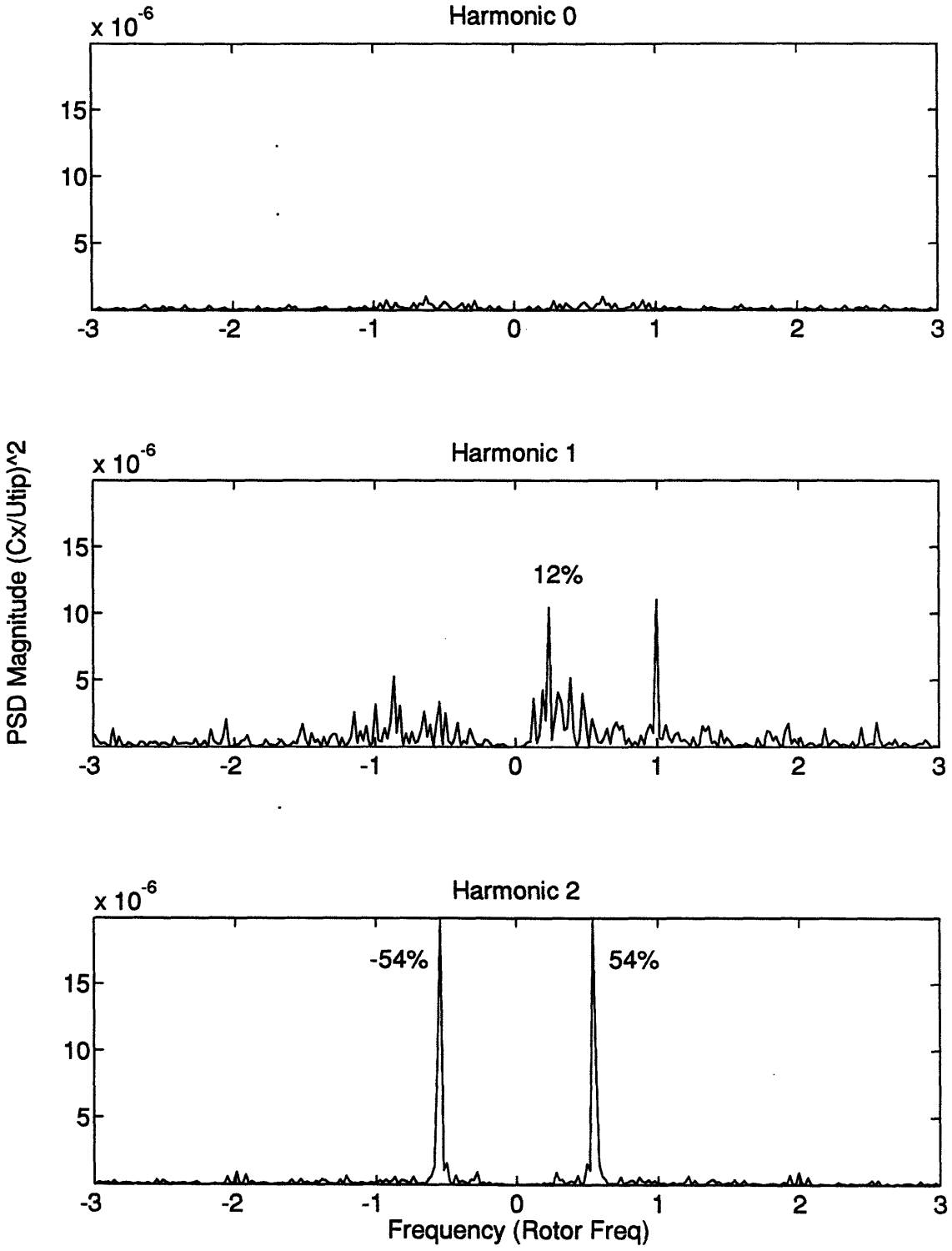

Figure 5.5 PSD's of SFHC prior to stall of measurements in Figure 5.4. Note the peak at ±54% of rotor frequency (propagation rate of ±28% of rotor speed) in the PSD of the 2nd spatial harmonic. The direction of the 2nd harmonic cannot be determined because the PSD is computed using only 4 sensors.

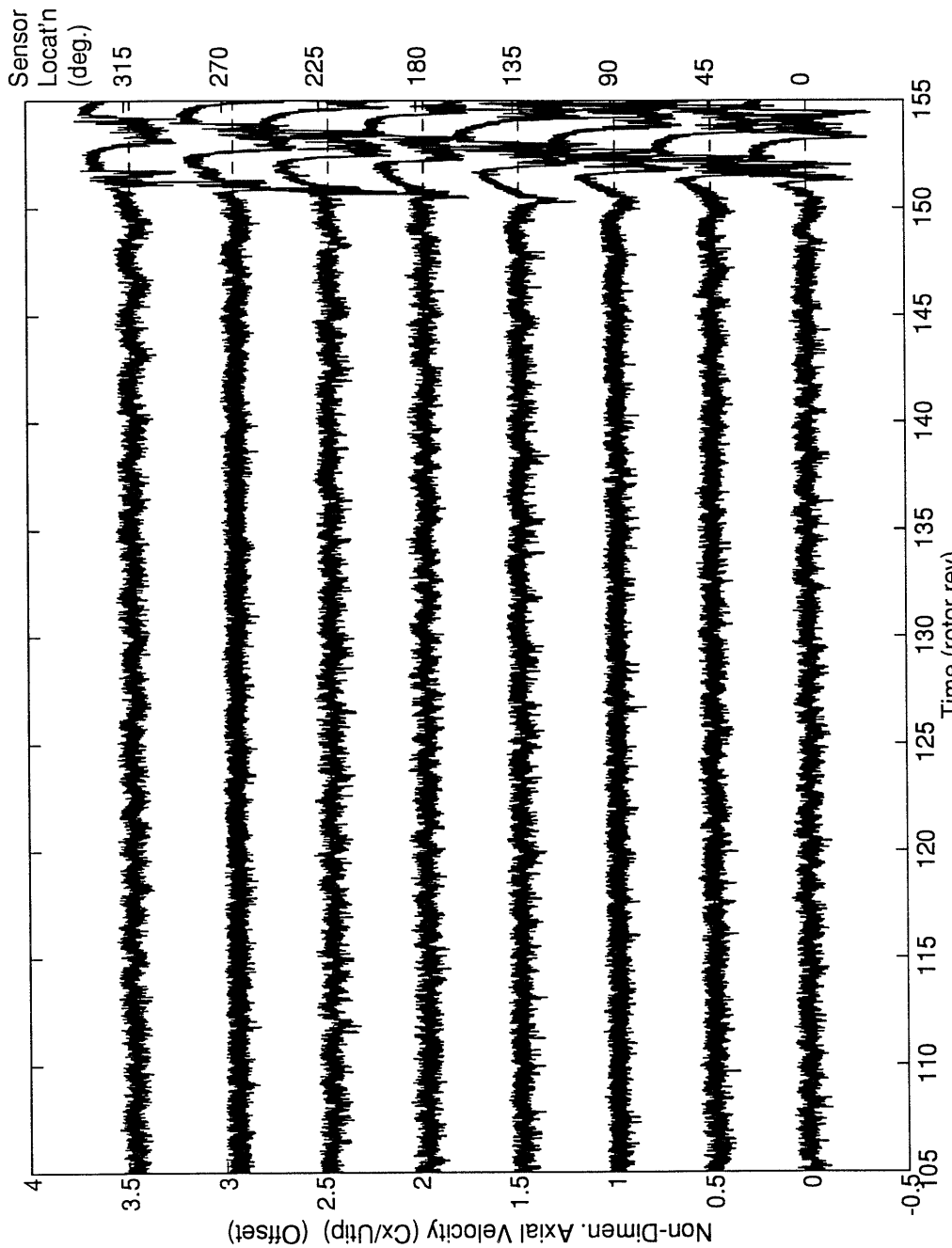

Figure 5.6 Hot-wire velocity traces near the tip at 1st stage rotor inlet for Compressor 2.

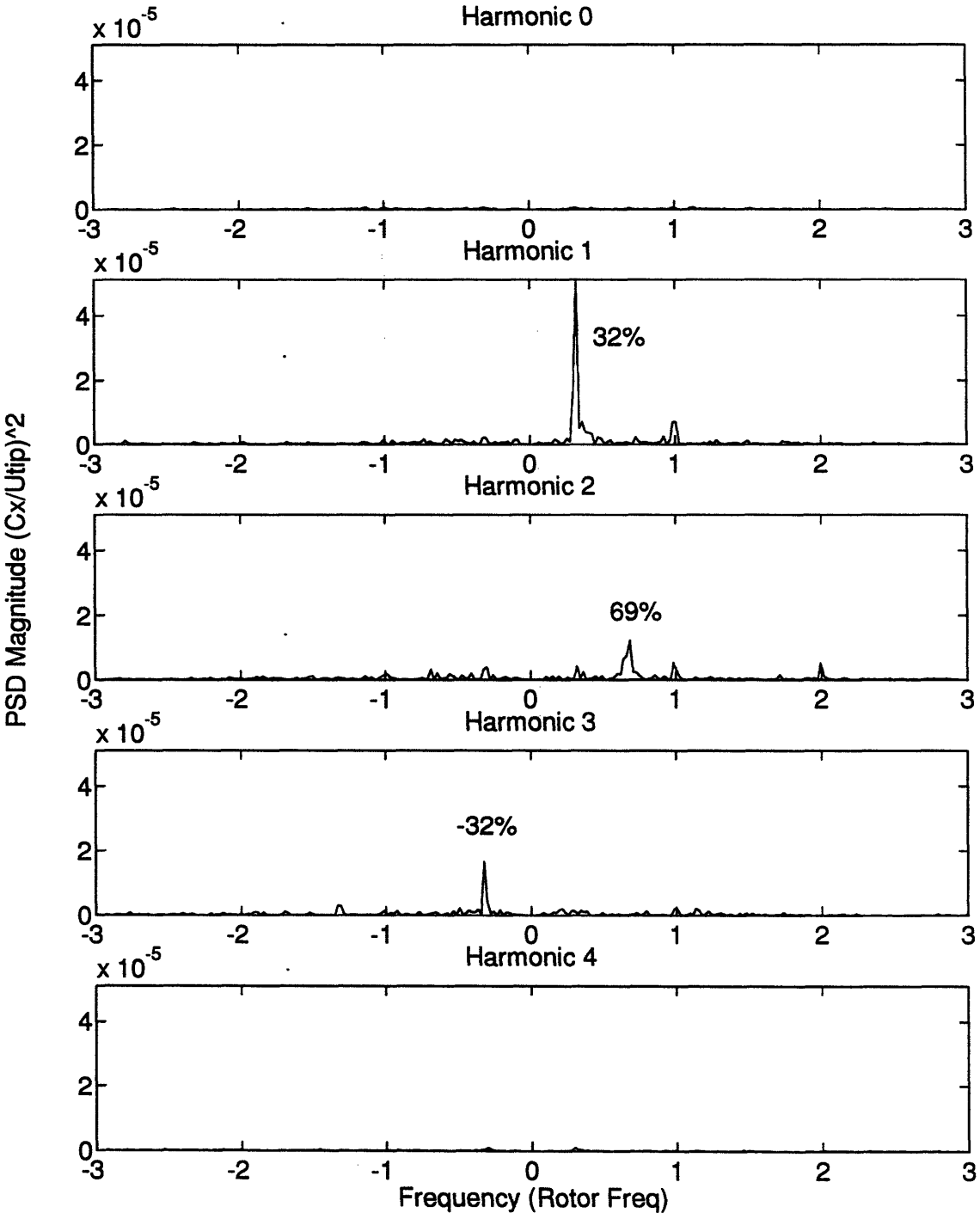

Figure 5.7 PSD's of SFHC prior to stall of measurements in Figure 5.6. Note the peak at 32% of rotor speed in the PSD of the 1st spatial harmonic.

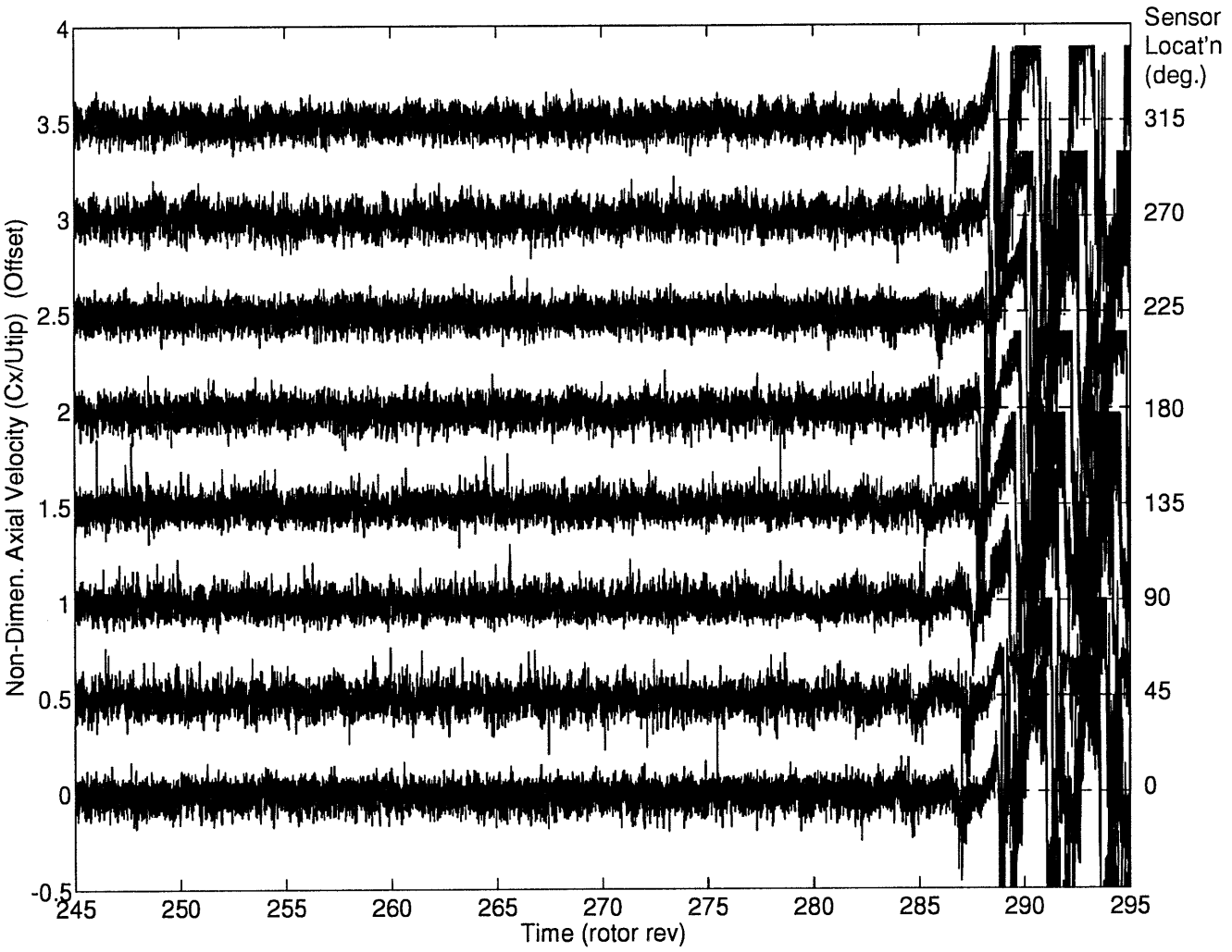

Figure 5.8 Hot-wire velocity traces near the tip at 1st stage rotor exit for Compressor 3.

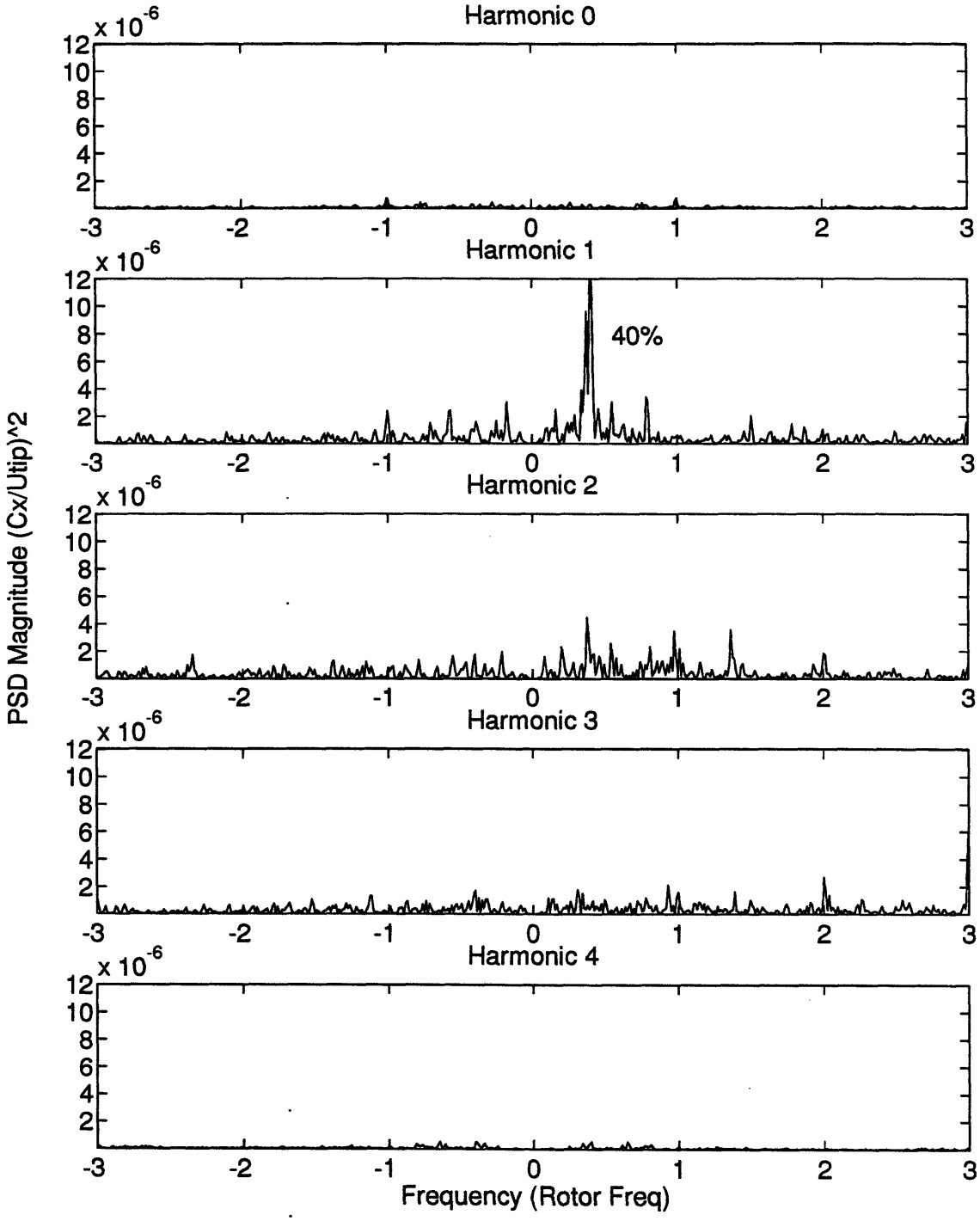

Figure 5.9 PSD's of SFHC prior to stall of measurements in Figure 5.8. Note the peak at 40% of rotor speed in the PSD of the 1st spatial harmonic.

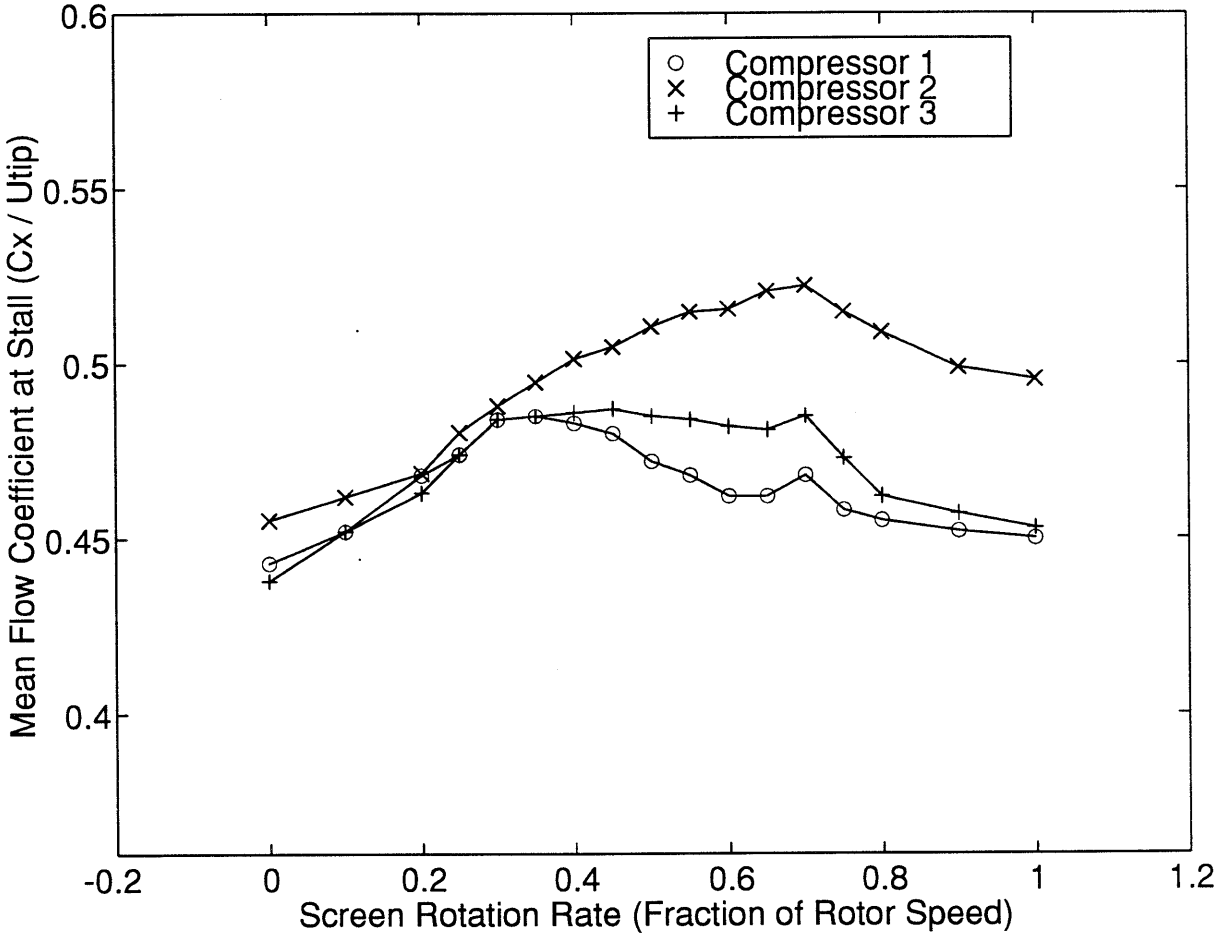

Figure 5.10 Flow coefficient at stall versus distortion rotation rate for a Compressor 1, 2, and 3. Note that each compressor shows at peak at 70% of rotor speed.

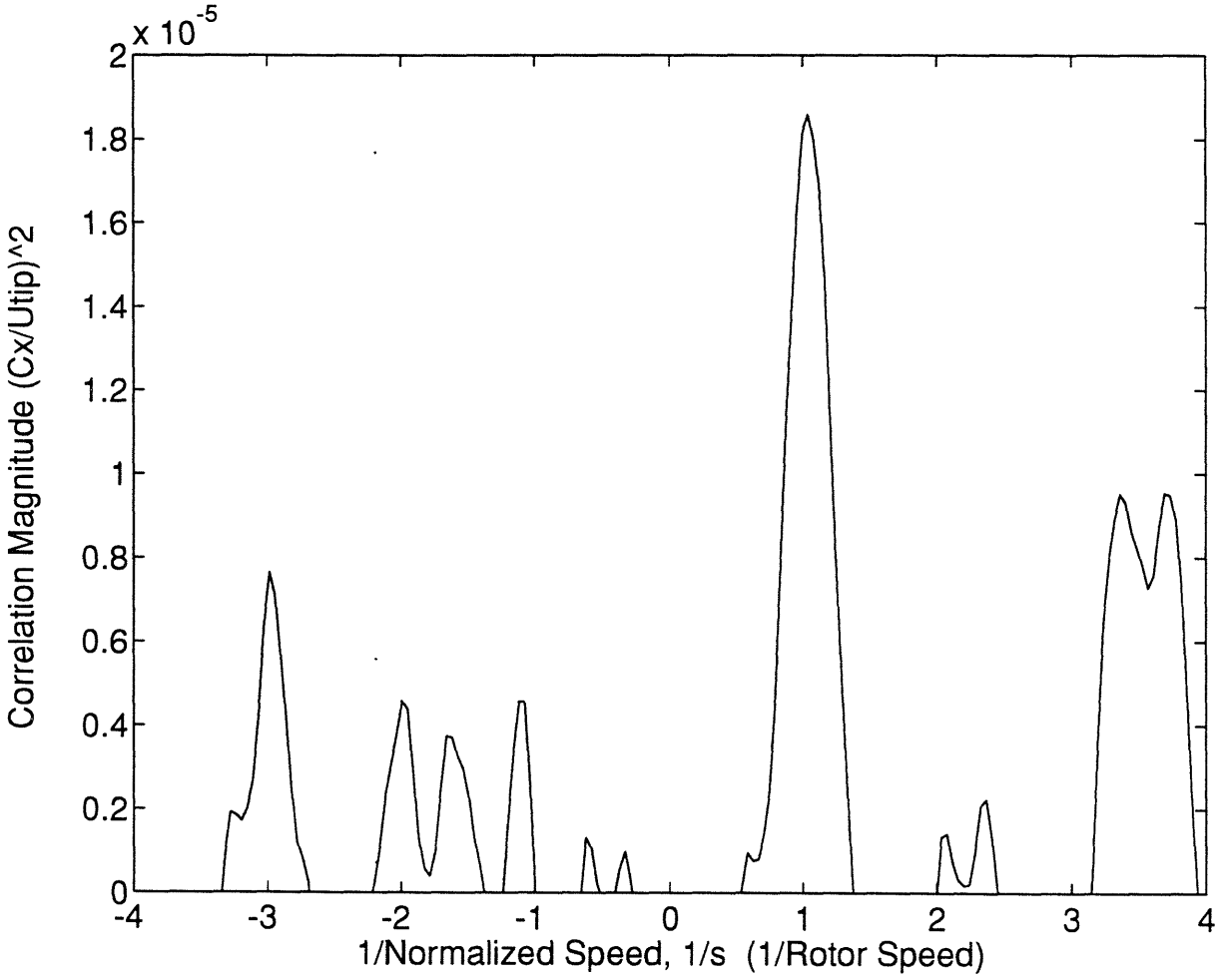

Figure 5.11 Cross-correlation of measurements in Figure 5.8 prior to stall.

CHAPTER SIX

CONCLUSIONS AND RECOMMENDATIONS

6.1 Summary and Conclusions

An experimental investigation was carried out on unsteady disturbance structures and their behavior at different operating conditions in several multi-stage compressors. To examine whether a precursor can be associated with a spike type disturbance structure, a new method of detecting spikes based on cross-correlations was developed. The method was then used to re-examine previous spike type stall inception data. Experiments were carried out on the MIT Three Stage compressor to examine if spike type disturbances develop under compressor operating conditions of higher relative first stage pressure rise and/or active control. Finally, observations were made on forced response behavior of compressors from recently collected data from ongoing experiments at General Electric Low Speed Research Compressor facility.

The conclusions of this study are:

1) Precursors associated with short-length scale disturbances (spikes) can exist in both low speed and high speed compressors. The spike precursor can be detected by cross-correlating measurements of spatially adjacent sensors, which produces a correlation peak at the time delay corresponding to the propagation rate of a spike.

2) The precursor is detectable on the low speed E^3 compressor up to 350 rotor revolutions prior to stall if cross-correlations are applied to pressure transducer measurements at first stage rotor exit.

3) The precursor is detectable on the high speed Viper compressor up to 350 and 100 rotor revolutions prior to stall for 81% and 83% of corrected speed, respectively. The cross-correlations are applied to pressure transducer measurements at first stage rotor inlet. At 98% of corrected speed, no spike precursor could be detected.

4) The precursor is associated with formation and decay of spikes as the compressor approaches stall. The spikes rarely travel beyond 1/2 rotor revolution before decaying. As the compressor approaches stall, the rate of formation and decay of spikes increase, causing the cross-correlation precursor to grow.

5) The maximum perturbation amplitude and circumferential size of the spikes (roughly $\Delta P/0.5\rho U_{tip}^2 = 0.1$ and 2 blade pitches, respectively for the E^3 compressor) remain relatively constant regardless of how close the compressor is to stall. Slight stage mismatching is thought to be responsible for setting these parameters as stable flow in the downstream stages stops the growth of the spikes. Stall occurs when the flow in the downstream stages becomes unstable and cannot prevent a spike from growing into a rotating stall cell.

6) When subjected to a rotating distortion, compressors which exhibit dominant modal wave disturbance structure in the natural stall inception process can display a resonant response thought to be associated with spike mode (i.e. resonant peak at 70% of rotor speed in the plot of loss of stability versus screen rotation) as well as a resonant response associated with a modal wave. It is suggested that on such compressors, the mode associated with a spike is not excited during natural stall inception but is excited when the distortion screen is rotating near 70% of rotor speed.

7) An actively controlled compressor can develop an acoustic disturbance when the compressor operates in the unstable region of the characteristics map (positive overall pressure rise slope). The instability in the MIT Three

Stage compressor while operating under active control is likely caused by a growing acoustic disturbance. No evidence of short wavelength disturbances is found while the compressor operates under active control.

6.2 Issues to Be Resolved

The origin of the short length-scale disturbance (spike) is unknown, and the biggest question surrounding a spike is still how and why it develops. For near term experimental research, some recommendations which may offer further insights to the spike type disturbance structure are presented in the following:

1) Mismatch a compressor which exhibits modal wave disturbance structure when matched. The compressor will then operate with a locally unstable flow in the first stage. Under these conditions, the 2-D modal waves, which must axially extend all the way through the compressor, will be suppressed. Only local disturbances will be allowed to develop since only the flow in first stage will be destabilized. If spikes develop under these conditions, it will demonstrate that the stability of the first stage governs whether a compressor shows modal wave or spike type disturbances during stall inception.

2) Make detailed measurements of a spike using an axial array of casing static pressure transducers at the first stage rotor. With such an array, it may be possible to map the pressure distribution near the tips of the blade passages. Since it is a highly localized disturbance (with circumferental extent of 1-2 blade pitches and radially confined to the tip), a spike may be an instability associated with a flow breakdown in the blade passage. Detailed measurements will show whether flow breakdown in the blade passage is a condition which leads to the formation of a spike.

3) Review of the compressor characteristics to determine the correct parameters for the formation of spikes. There is now data for several spike

type stall inception compressors, and it will be productive to see if they share any similar characteristics. Of particular interests are the pressure rise characteristics since they govern the stability of the compressor and the stages. A spike may be sensitive to various pressure rise characteristics, including the overall pressure rise, the individual stage pressure rises, and even the radial pressure rise distribution. The radial pressure rise distribution seems important to the development of a spike because of its 3-D nature. It may be difficult to experimentally measure the radial static pressure rise distribution, and computational methods may have to be used to estimate the distribution from blade geometry.

4) Determine if a resonant peak at 70% of rotor speed in the plot of loss of stability versus distortion rotation speed is associated with a spike type stall inception for a compressor which exhibits modal wave type natural stall inception. A way to experimentally assess this is to rotate the distortion screen at 70% of rotor speed and look for spikes amid the random noise generated by the screen. Nevertheless, it may be still be possible to detect spikes using the casing static pressure transducers even when a rotating distortion screen is present as demonstrated by [12] (Figure 6.1).

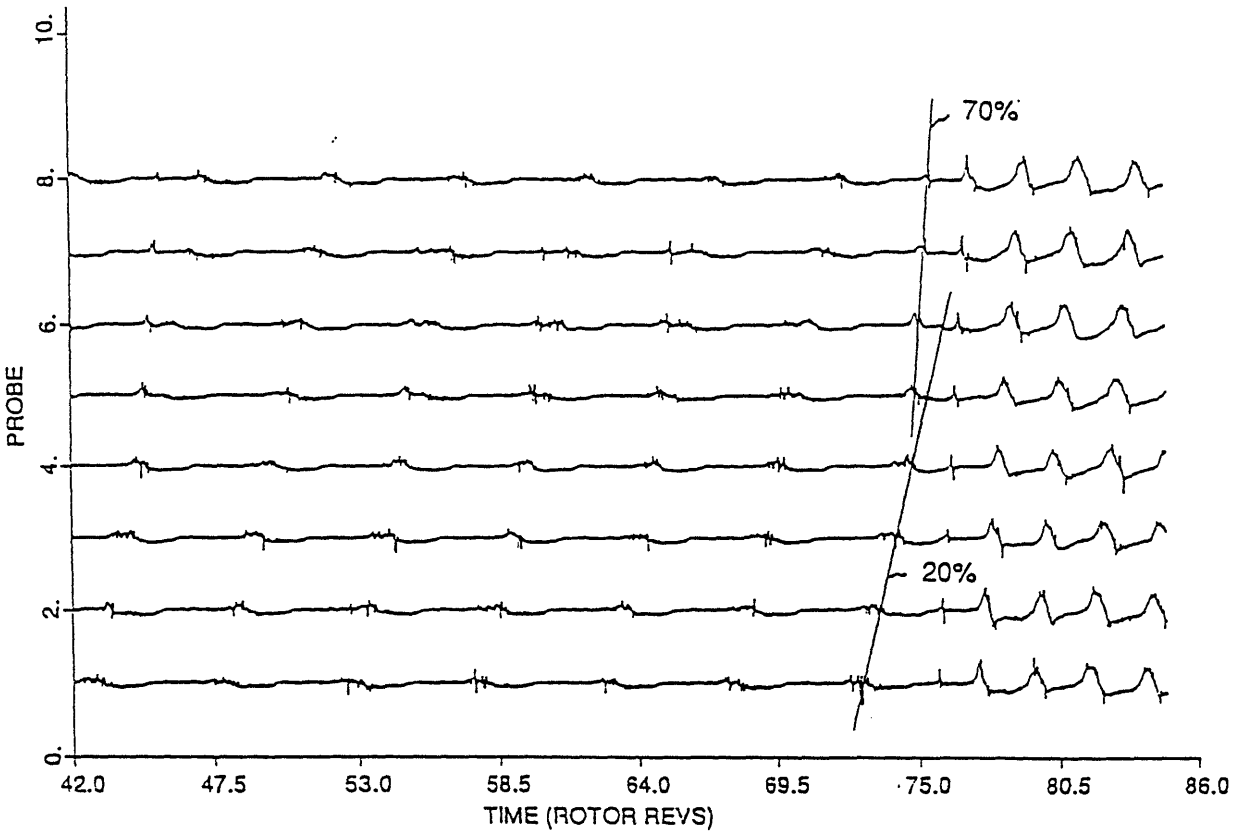

Figure 6.1 Casing static pressure traces at 1st stage rotor inlet during stall inception with an upstream distortion rotating at 20% of rotor speed. A guideline shows that the presence of a spike type disturbance can be detected amid the noise generated by a rotating distortion screen.

REFERENCES

1. Emmons, H.W., Pearson, C.E., and Grant, H.P., "Compressor Surge and Stall Propagation", Transactions of the ASME, Vol. 79, pp. 455-469, April 1955.

2. Day, I.J., "Stall Inception in Axial Flow Compressors", ASME Paper 91-GT-86, 1991.

3. Garnier, V.H., "Experimental Investigation of Rotating Waves as a Rotating Stall Inception Indication in Compressors", M.S. Thesis, MIT Dept. of Aeronautics and Astronautics, May 1988.

4. Day, I.J., Freeman, C., "The Unstable Behavior of Low and High Speed Compressors", ASME Paper 93-GT-26, 1993.

5. Day, I.J., "Active Suppression of Rotation Stall and Surge in Axial Compressors", Transactions of the ASME, Vol. 115, pp. 40-47, January 1993.

6. Paduano, J.D., "Active Control of Rotating Stall in Axial Compressors", MIT GTL Report No. 208, March 1992.

7. Haynes, J.M., "Active Control of Rotating Stall in a Three-Stage Axial Compressor", MIT GTL Report No. 218, June 1993.

8. Gysling, D.L., "Dynamic Control of Rotating Stall in Axial Flow Compressors Using Aeromechanical Feedback", Ph.D. Thesis, MIT Dept. of Aeronautics and Astronautics, August 1993.

9. Lavrich, P.L., "Time Resolved Measurements of Rotating Stall in Axial Flow Compressors", MIT GTL Report No. 194, August 1988.

10. Moore, F.K., Greitzer, E.M., "A Theory of Post Stall Transients in Axial Compression Systems Part I - Development of Equations", Journal of Engineering for Gas Turbines and Power, Vol. 108, January 1986, pp. 68-76.

11. McDougall, N.M., "Stall Inception in Axial Compressors", Ph.D. Thesis, Cambridge University, Dept. of Engineering, 1988.

12. Silkowski, P.D., "Measurements of Rotor Stalling in a Matched and Mismatched Multistage Compressor", MIT GTL Internal Report, August 1992.

13. Hendricks, G.J., Gysling, D.L., "A Theoretical Study of Sensor-Actuator Schemes for Rotating Stall Control", AIAA Paper 92-3486, 1992.

14. Eastland, A.H.J., "Investigation of Compressor Performance in Rotating Stall", MIT GTL Report No. 164, June 1982.

15. Gamache, R.N., "Axial Compressor Reversed Flow Performance", Ph.D. Thesis, MIT Dept. of Aeronautics and Astronautics, May 1985.

16. Day, I.J., personal communication, 1993.

17. Weigl, H.J., personal communication, 1993.

18. Marble, F.E., personal communication, 1994.

19. Longley, J.P., Shin, H.W., Plumley, R.E., Silkowski, P.D., Day, I.J., Greitzer, E.M., Tan, C.S., Wisler, D.C., "Effects of Rotating Inlet Distortion on Multistage Compressor Stability", Submitted to ASME Journal of Turbomachinery.

20. Wisler, D.C., "Core Compressor Exit Stage Study", Volume IV, Data and Performance Report for the Best Stage Configuration, NASA CR 165357, April 1981.

4958-43